Linearity Analysis and Enhancement Techniques for the Base-Collector Capacitance Dominated Distortion in Bipolar Amplifiers

J.M.M. van der Meulen

Technische Universiteit Delft

Delft University of Technology

Challenge the future

Linearity Analysis and Enhancement Techniques for the Base-Collector Capacitance Dominated Distortion in Bipolar Amplifiers

by

J.M.M. van der Meulen

in partial fulfillment of the requirements for the degree of

Master of Science
in Electrical Engineering

at the Delft University of Technology,
to be defended publicly on Thursday October 29, 2015 at 1:00 PM.

Supervisor:	ir. Michel Groenewegen,	NXP Semiconductors,	Daily supervisor
Thesis committee:	dr.ing. Mark van der Heijden,	NXP Semiconductors,	Supervisor
	ir. Paul Mattheijssen,	NXP Semiconductors,	Supervisor
	prof.dr.ir. Wouter Serdijn,	TU Delft,	External member
	prof.dr.ing. Leo de Vreede,	TU Delft,	Supervisor

This thesis is confidential and cannot be made public until October 29, 2020.

An electronic version of this thesis is available at `http://repository.tudelft.nl/`.

ABSTRACT

SiGe bipolar amplifiers are getting more competitive in terms of noise figure to GaAs amplifiers. However, the linearity of these amplifiers is still limited in view of these GaAs implementations.

In order to address and overcome these linearity limitations, this thesis report will start demonstrating that the linearity of SiGe bipolar amplifiers for base stations applications is limited by the base-collector charge related distortion. More specifically, it will be shown that in a CE-stage, the C_{bc} distortion tends to limit the linearity when the exponential distortion has been canceled. Using cross-coupled capacitive C_{bc} compensation, the OIP3 of the CE-stage can be still improved when all other transistor properties are close to ideal. However, once the base-emitter capacitances are added to the transistor model description, this linearity improvement vanishes again.

Traditionally, people overcome C_{bc} related constraints in a CE-stage by moving to a cascode configuration. However, it will be shown that in a cascode configuration the C_{bc} of the CB-stage becomes the limiting linearity factor, again under the assumption that exponential induced distortion of the CE-stage has been effectively canceled. To overcome the C_{bc} distortion in the cascode configuration, 3 different techniques have been developed in this report.

The first technique, a dedicated out-of-band matching has been proposed to cancel C_{bc} distortion. However, when considering the complete cascode lineup, it proves that the out-of-band currents from the CE-stage interfere with this C_{bc} compensation. Different methods have been proposed for cancellation of these currents, but only the use of an intermediate transformer between the CE- and CB-stage seems to be the most promising option.

The second technique developed aims for passive in-band C_{bc} compensation. A compensation circuit containing a series combination of an inductor, a resistor and a multiplied copy of the C_{bc} capacitance can give exact compensation to C_{bc} distortion in a limited frequency band, however it proves to be quite sensitive to device parasitics.

The last technique studied is active C_{bc} compensation. By sensing the currents in the base of the CB-stage, the nonlinear C_{bc} currents could be injected into the circuit with opposite phase, creating a much more linear amplifier. However, practical implementations also need to be stable to avoid oscillation. Adding stabilizing elements in the base of the CB-stage connection increases interactions between the C_{bc} of the CB-stage and the stabilization network. Due to IM3 currents from the CE-stage and phase deviations between these currents and the IM3 current from the C_{bc} of the CB-stage, the OIP3 will not increase when the Mextram model has been used.

Although many linearization techniques have been developed and extensively studied, improvements are still needed to come to more practical, robust and product proven linearity enhancement techniques. Consequently, in the concluding chapter clear recommendations are given for future research followed by the overall conclusions of this thesis work.

ACKNOWLEDGMENTS

"If I have seen further, it is by standing on the shoulders of giants."

- Isaac Newton

First and foremost I want to thank ir. Michel Groenewegen, for his great work as my supervisor at NXP Semiconductors. His patience, practical knowledge and detailed view really attributed a lot to my thesis work. His dedication to this thesis project can hardly be underestimated. His quick feedback and willingness to answer almost all questions whenever you ask them really helped to speed up my thesis project.

I also want to thank prof.dr.ing. Leo de Vreede, for his work as my supervisor at TU Delft. His extreme high knowledge has helped me a lot during this project. Although he has been tough on me on several occasions, he always showed his believe in me. He always kept my motivation high, whether intended or unintended. His curiosity is contagious, making him one of the best supervisors a student can imagine.

My thanks also goes to dr.ing. Mark van der Heijden and ir. Paul Mattheijssen, my other supervisors from NXP Semiconductors. Although more from a distance, their assistance in making this thesis really helped to get the thesis to a higher level.

I want to thank ing. Marco Pelk and my fellow student Marco D'Avino for their great work on the measurements done for this report. They saved me a lot of time, time that could be invested in the theoretical background of my thesis. I also want to thank Francis Belen for his work on the layout, saving me a lot of time.

Lastly I want to thank all the people who made me the person I am. I want to mention the Bredase Waterscouting Titus Brandsma, which provided me with the skills needed for cooperation and who helped me to relax even during the most stressful moments of my thesis. I also want to mention my great sisters, who have always been there for me, whenever I needed their help or just for a nice evening with nice food and good company. But most importantly I want to mention my parents, whose love, caring, support and advice have been of invaluable importance to me. I would not have reached where I am now without their help. They are the shoulders, enabling me to see further than I could possibly dream of without their help.

Jordi van der Meulen
Nijmegen, October 2015

CONTENTS

List of Figures

List of Tables

1

INTRODUCTION

The worldwide use of wireless communication is growing. Economic development in so-called third world countries pushes the demand for more cellular communication devices. These devices require base stations for communication. These base stations share many transceivers and should be able to cover a large land area.

Due to many mobile devices in a cell transmitting towards base stations, the linearity of the base station becomes very important. The first active building block of the receiver end is the low noise amplifier (LNA). In this master of science thesis, the linearity of the bipolar based LNAs for base station applications will be evaluated. Since base stations LNAs have a significantly higher DC power budget than in handset applications, their upper limitation on linearity will be the nonlinear base-collector capacitance (C_{bc}) [1], rather than their exponential behavior. Therefore the goal of this thesis is to improve the linearity of base station LNAs by finding new compensation schemes for the C_{bc} capacitance induced distortion.

1.1. LNAS FOR BASE STATIONS

In typical base stations, two LNAs are used: one in the top unit of the base station, to amplify the incoming signal and another amplifier at the ground level, to compensate for the losses that are caused by the coaxial cable between the top and ground unit (Figure 1.1 [1]).

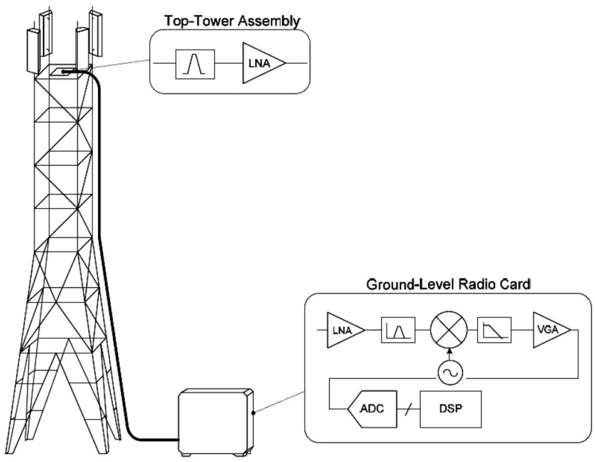

Figure 1.1: Overview of a base station [1]

Most base stations have multiple transceivers to improve the coverage and throughput. This means that while one transceiver is receiving a signal, another transceiver can be transmitting. With nonlinearities in the receiver, the strong transmit signal can mix to the frequency of the weak to be received signal causing interference. By making the receiver more linear, this effect can be minimized. Therefore, more linear receivers can tolerate stronger nearby signals. Since stronger signals are allowed, a larger coverage area is possible for more linear base stations, lowering the amount of base stations needed. Alternatively, the requirements on the TX/RX filtering in the base station can be more relaxed, allowing form factor reduction and cost savings.

1.2. DEVICE TECHNOLOGIES FOR LNAS

Historically there are multiple device technologies available to use for LNA design. Two types of transistors are most commonly used: the High Electron Mobility Transistor (HEMT) and the Heterojunction Bipolar Transistor (HBT). An overview of these devices can be seen in Table 1.1 [2].

Table 1.1: HEMT devices versus HBT devices [2]

Merit Parameter	**HEMT**	**HBT**	**Conclusion**
f_t	M	H	HBT has the highest speed
f_{max}	H	L	HEMT has the highest frequency
Noise figure	L	H	HEMT has the lowest noise
$IP3/P_{dc}$	M	H	HBT gives the best IP3 for low power consumption

HEMT devices are a special kind of JFET devices that feature a small channel length, large saturation current and large transconductance [3]. These characteristics give HEMT devices an excellent low noise and an increased frequency handling capability. The most important disadvantage of HEMT devices is their implementation material, gallium-arsenide (GaAs). Most modern applications are based on silicon for cost and integration reasons, as such excluding the use of HEMT devices.

HBT devices are a special kind of bipolar devices that use bandgap engineering in the emitter base-junction, resulting in higher Early voltages and lower base resistance [2] and transit time, yielding higher current gain, cutoff frequencies, and improved noise performance. When compared to HEMT devices, HBT devices can have better cutoff frequencies, but the noise performance of HBT devices tends to be worse. There are two popular implementations for HBTs, namely: gallium-arsenide (GaAs) and silicon-germanium (SiGe). GaAs has different velocity saturation for its electrons, resulting in a more linear behavior of the base-collector capacitance, allowing lower distortion levels. SiGe devices with high current gain ($\beta \gg 100$) can provide comparable noise figures as GaAs based devices. Since SiGe technology offers cost and integration advantages, the aim is to implement these base station LNA circuits also in SiGe, while overcoming the linearity penalty (compared to GaAs) that seems to be related to SiGe technology.

1.3. LINEARITY IN SIGE BIPOLAR AMPLIFIERS

Studies done so far on linearity of SiGe bipolar amplifiers focused on the exponential distortion of the bipolar transistor. The exponential distortion can be addressed in several ways. E.g. the multi-tanh method uses a doublet to shape the transfer function of the amplifier [4]. By shaping the transfer function, a more constant transconductance can be achieved, making the amplifier more linear. Implicit IM3 cancellation uses a local feedback inductor to improve the linearity of the amplifier [5]. Using in-band and out-of-band compensation techniques, the exponential distortion can be canceled. These methods also account for the nonlinear diffusion capacitance of the bipolar transistor. Note that the out-of-band matching technique for exponential distortion makes use of out-of-band terminations to linearize the bipolar amplifier, tending to provide more design freedom [6]. Lastly, increasing the bias current also helps to improve the linearity of the bipolar transistor.

Whatever method is used to improve the linearity of the SiGe bipolar transistor, all known methods do not address the distortion introduced by the depletion capacitance of the base-collector junction (C_{bc}). Consequently, as [1] demonstrates, in practical circuits the linearity is ultimately limited by the C_{bc} capacitance of the transistor. Therefore the goal of this report is to find techniques to improve the linearity of the base-collector capacitance.

1.4. THESIS ORGANIZATION

This thesis will start with an overview of the analysis techniques used to study nonlinearity in Chapter 2. The chapter will start with a discussion based on the power series representation. Using a one-tone excitation and a two-tone excitation the main problem of nonlinearity will be explained. Based on these results, the definitions and figures of merit used for quantifying nonlinearity in this report will be discussed. Then the drawbacks of memory effects in relationship with a power series representation will be discussed. To overcome the problem with power series repressentation due to memory effects, the Volterra analysis will be addressed. The chapter will end with a discussion of cascaded and differential circuits and their importance for linearity.

The thesis will continue in Chapter 3 with evaluating the nonlinearity in the CE-stage using a Gummel-Poon model. By applying the theory of out-of-band matching for exponential distortion as discussed by [6], the main linearity constraints will be examined. This examination will show that the C_{bc} capacitance is the limiting factor for the linearity in the CE-stage. To cancel the effects on linearity of the C_{bc} capacitance, the cross-coupled design will be studied. The effect of the different nonlinear contributions of the CE-stage in the cross-coupled design will be examined.

In Chapter 4 the nonlinearities in the CB-stage are considered. Just as for the CE-stage, the Gummel-Poon model is used to study the effects of the different nonlinear components in the CB-stage. The linearity performance of the CB-stage will be studied for current driven and voltage driven conditions. Next, the CB-stage and CE-stage are combined to create a cascode amplifier. Again, the resulting linearity has been studied using the Gummel-Poon model. This chapter shows that in a cascode amplifier, the C_{bc} is again the limiting factor for linearity, as such the characteristics of C_{bc} distortion will also be discussed in this chapter.

Chapter 5 up to 7 provide different methods to compensate the C_{bc} distortion in the cascode amplifier. In Chapter 5 an out-of-band matching network is proposed to achieve C_{bc} compensation. This chapter also explains the difficulties when applying out-of-band matching for C_{bc} distortion and provides several methods to overcome these difficulties.

In Chapter 6 a passive in-band C_{bc} compensation is presented. Based on Volterra analysis and simulation results, a test chip for passive in-band C_{bc} compensation is designed, which has been implemented in QUBiC4Xi technology.

In Chapter 7 an active C_{bc} compensation technique is proposed. Using a Gummel-Poon model, the different nonlinear elements of the cascode transistor have been individually enabled or disabled and their influence on the overall active C_{bc} compensation evaluated. In addition, various topologies for implementing the actual active compensation are proposed and discussed.

The report will finish with conclusions and recommendations in Chapter 8.

2

GENERAL BACKGROUND OF NONLINEARITY

Since this thesis report is about nonlinearity in bipolar amplifiers, this chapter will start with introducing the concept of nonlinearity. The definitions used in this report will be examined and the different kinds of analyses will be discussed. Also cascaded and differential circuits will be discussed.

A linear circuit is a circuit in which the superposition principle is valid [7]. For amplifiers, this means that the output signal can have a different output and phase compared to the input, but never a different frequency. Since there are no different frequencies in the output signal, the output signal is a linearly scaled copy of the input signal. On the other hand, output signals of a nonlinear amplifier contain many different frequencies, so these signals are not a scaled copy of the input signal.

There are two kinds of nonlinearities: strong nonlinearities and weak nonlinearities [7]. Strong nonlinearities occur when the circuit is driven with very large signals. These signals are limited by supply voltages and currents and by the operating mode of the transistor. When the signals exceed these limits, the circuit clips. For instance, in a bipolar transistor this is the case when the transistor is set into saturation due to high voltages.

Weak nonlinearities are due to the curved relationships in the device [8]. The most well-known weak nonlinearity in the bipolar transistor is the curved relationship between base-emitter voltage and collector current. However, also internal components of the device can be nonlinear. For instance, the C_{bc} of the bipolar transistor has a curved relationship with the base-collector voltage and with the collector current.

This chapter will introduce the concept of nonlinearity. In Section 2.1 the power series representation of nonlinearity will be discussed. Based on this discussion, definitions concerning nonlinearity will be given in Section 2.2. The power series representation is not valid when memory effects are present in the system. Volterra analysis is valid in this situation. Therefore, Section 2.3 will discuss memory effects and the Volterra analysis. Most systems consist of a cascade of circuits. The linearity of these cascaded circuits will be discussed in Section 2.4. The chapter will end with a discussion on differential circuits in Section 2.5.

2.1. POWER SERIES REPRESENTATION OF NONLINEARITY

Nonlinear memoryless circuits can be described by using the power or Taylor series representation [9]. In the Taylor analysis, a function is described around a certain point. For the function Y(X), the function can be described around the point X=i with the following Taylor analysis [10]:

$$Y(X) = Y(i) + \frac{dY(i)}{dX}(X-i) + \frac{1}{2!}\frac{d^2Y(i)}{dX^2}(X-i)^2 + \frac{1}{3!}\frac{d^3Y(i)}{dX^3}(X-i)^3 + ... \tag{2.1}$$

The AC signal variant of Equation (2.1) is [11]:

$$y(x) = a_1 x + a_2 x^2 + a_3 x^3 + ... \tag{2.2}$$

where a_1, a_2, a_3,..., represent the Taylor coefficients. An example of the power series representation will be shown, using Figure 2.1.

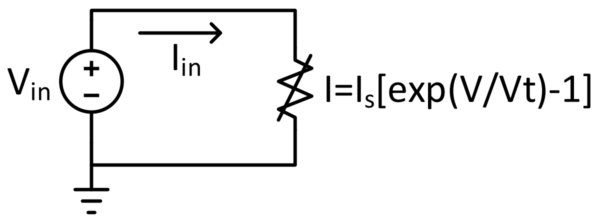

Figure 2.1: A nonlinear resistor

The resistor shown in Figure 2.1 is driven by a voltage source. $V_{in} = V_{bias} + v_{in}$, in which the V_{bias} is the DC-bias voltage and v_{in} is the AC-voltage. The current I_{in} can be described by the following equation:

$$I_{in} = I_s\left[e^{V_{bias}/V_t} - 1\right] + \frac{I_s e^{V_{bias}/V_t}}{V_t}(V_{in} - V_{bias}) + \frac{I_s e^{V_{bias}/V_t}}{2V_t^2}(V_{in} - V_{bias})^2 + \frac{I_s e^{V_{bias}/V_t}}{6V_t^3}(V_{in} - V_{bias})^3 + ...[A] \quad (2.3)$$

where $V_t = kT/q$ is the thermal voltage, k is Boltzmann's constant $(1.38x10^{-23}J/K)$, T is the temperature in kelvin, q is the elementary charge $(1.60x10^{-19}C)$ and I_s is the saturation current.

The term $V_{in} - V_{bias}$ can also be noted as v_{in}, since it only contains the AC signal. Also the DC constant $I_s e^{V_{bias}/V_t}$ can be simplified to $I_{in,DC}$. This simplifies Equation (2.3) to:

$$I_{in} = I_{in,DC} + \frac{I_{in,DC}}{V_t}v_{in} + \frac{I_{in,DC}}{2V_t^2}v_{in}^2 + \frac{I_{in,DC}}{6V_t^3}v_{in}^3 + ...[A] \quad (2.4)$$

2.1.1. ONE-TONE EXCITATION

When a nonlinear system is excited with a sinusoid, the nonlinear behavior will cause harmonics in the frequency domain. When Equation (2.2) is excited with $x = A\cos(2\pi f t)$, where A is the amplitude, f is the fundamental frequency and t is time, the following equation for $Y(t)$ is found [11]:

$$y(t) = \frac{a_2 A^2}{2} + \left(a_1 A + \frac{3a_3 A^3}{4}\right)\cos(2\pi f t) + \frac{a_2 A^2}{2}\cos(2\pi \cdot (2f) \cdot t) + \frac{a_3 A^3}{4}\cos(2\pi \cdot (3f) \cdot t) + ... \quad (2.5)$$

From this equation it can be concluded that not only the fundamental frequency f is created, but also signals at the frequencies $2f$ and $3f$, called harmonics. Also an extra DC-component is created, and the amplitude around the fundamental frequency is altered. Especially the effect on the amplitude of the fundamental frequency is devastating, since it influences the gain of the circuit, resulting in gain compression or expansion for higher input amplitudes [11]. The DC-term also gives a DC-shift [12], which might result in unwanted biasing conditions. The other tones can be filtered out, and most of the time only the $2f$ component is considered for nonlinearity, unless the circuit needs to be extremely wideband. The frequency domain due to these harmonics is shown in Figure 2.2.

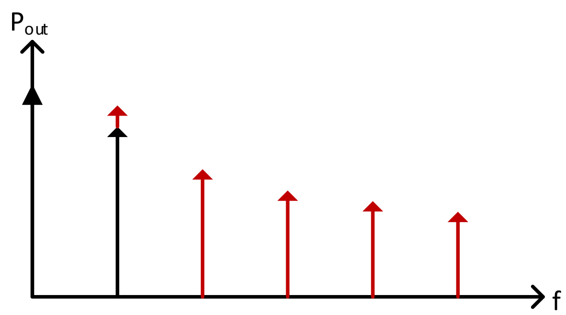

Figure 2.2: The frequency domain of a nonlinear function with a one-tone excitation

2.1.2. TWO-TONE EXCITATION

When the same nonlinear system is excited with two sinusoids, the nonlinear behavior will cause harmonics and intermodulation products in the frequency domain. When Equation (2.2) is excited with $x = A\cos(2\pi f_1 t) + A\cos(2\pi f_2 t)$, where A is the amplitude, f_1 and f_2 are the fundamental frequencies and t is time, the following equation for $Y(t)$ is found [13]:

$$y(t) = a_2A^2 + \left(a_1A + \frac{9}{4}a_3A^3\right)\cos(2\pi f_{1,2}t) + \frac{1}{2}A^2\cos(2\pi\cdot(2f_{1,2})\cdot t) + \frac{1}{4}a_3A^3\cos(2\pi\cdot(3f_{1,2})\cdot t) + a_2A^2\cos(2\pi\cdot(f_2 \pm f_1)\cdot t) + \frac{3}{4}a_3A^3\cos(2\pi\cdot(2f_{1,2} \pm f_{2,1})\cdot t) + \ldots \quad (2.6)$$

As can be seen, not only harmonics arise, but also nonlinear intermodulation products. The most important intermodulation products for this report are at the following frequencies:

- $|f_2 - f_1|$
- $f_1 + f_2$
- $2f_1 - f_2$
- $2f_2 - f_1$

Especially the last two intermodulation products are troublesome, since they are very close to the fundamental frequencies when f_1 and f_2 are relatively close in frequency. Therefore they cannot be filtered out. When interference occurs, the intermodulation products can corrupt wanted signals [11]. Therefore, these intermodulation products need to be kept as low as possible, which is the main subject of this report. In Figure 2.3 the frequency domain is given for the two-tone excitation.

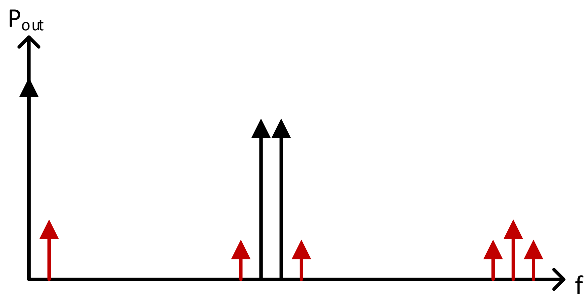

Figure 2.3: The frequency domain of a nonlinear function with a two-tone excitation

2.2. DEFINITIONS AND FIGURES OF MERIT FOR NONLINEARITY

As could be seen in Section 2.1, harmonics and intermodulation products are created when a nonlinear system is excited with a two-tone input signal. For simplicity, these harmonics and intermodulation products will be given a name. The following harmonics and intermodulation products are considered the most important for linearity:

- $2f_1$
- $2f_2$
- $|f_2 - f_1|$
- $f_1 + f_2$
- $2f_1 - f_2$
- $2f_2 - f_1$

For the definitions, the assumption will be that $f_1 < f_2$. The following definitions will be used:

- $HD2_{low}$ is the harmonic signal at the frequency $2f_1$
- $HD2_{high}$ is the harmonic signal at the frequency $2f_2$
- $IM2_{low}$ is the intermodulation signal at the frequency $|f_2 - f_1|$
- $IM2_{high}$ is the intermodulation signal at the frequency $f_1 + f_2$
- $IM3_{low}$ is the intermodulation signal at the frequency $2f_1 - f_2$
- $IM3_{high}$ is the intermodulation signal at the frequency $2f_2 - f_1$

In the literature, most of the time $IM2$ and $IM3$ get a slightly different definition. There, these numbers express the ratio between the amplitude of the signal at the fundamental frequency and the signal at the $IM2$ and $IM3$ frequency. When using the Taylor expansion in Equation (2.6), this would result in the following numbers [12]:

$$IM2 = \left|\frac{a_2}{a_1}\right| A \tag{2.7}$$

$$IM3 = \frac{3}{4}\left|\frac{a_3}{a_1}\right| A^2 \tag{2.8}$$

As can be seen, these measures of linearity contain one main drawback: they include the amplitude of the input signal. To have a linearity qualification that is not amplitude dependent, another measure or linearity has been considered.

As seen in Equation (2.6), the IM3 components have a cubic (to the power 3) relationship with the input amplitude. For small-signals, the fundamental tone increases linearly with the amplitude, depending solely on $a_1 A$. If these magnitudes are extrapolated, they will cross at a certain input and output signal level. At a certain input and output signal level, the IM3 component will be as large as the fundamental tone. This point is called the third order intercept point (IP3), and the concept of it can be seen in Figure 2.4 [13]. There are two ways to express IP3. The input third order intercept point (IIP3) is defined as the input power at which the IM3 component and fundamental tone would cross, if they remain their cubic and linear relationship with amplitude. The output third order intercept point is defined as the output power at which the IM3 component and fundamental tone would cross, if they keep their cubic and linear relationship with amplitude.

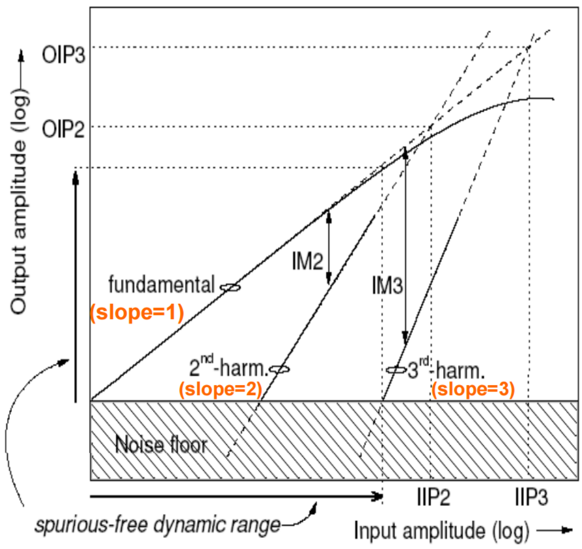

Figure 2.4: The definition of the third order intercept point. Courtesy L.C.N. de Vreede [13]

The formula for IIP3 can be found by equating the IM3 term $(\frac{3}{4}a_3A^3)$ and the fundamental term (a_1A)

and solve this for the amplitude A. Since IIP3 is defined as the input power and OIP3 as the output power where the IM3 component and fundamental component cross, the only difference between IIP3 and OIP3 is the gain a_1. Therefore, the following equations can be found for IIP3 [11] and OIP3:

$$IIP3 = \sqrt{\frac{4}{3}\left|\frac{a_1}{a_3}\right|} \tag{2.9}$$

$$OIP3 = \sqrt{\frac{4}{3}\left|\frac{a_1^3}{a_3}\right|} \tag{2.10}$$

Just as there is an $IM3_{low}$ and an $IM3_{high}$, there is also a $IP3_{low}$ and $IP3_{high}$. For the $IP3_{low}$ the $IM3_{low}$ component has been used to determine the IP3 point, while for the $IP3_{high}$ the $IM3_{high}$ component has been used. If in this report $IP3_{low}$ or $IP3_{high}$ are not specified, but only $IP3$ is used, then the $IP3_{low}$ and $IP3_{high}$ have the same or comparable results.

IP3 is a measure of small signal nonlinearity and therefore a measure of weak distortion. For strong distortion, another measure is used. As shown in Section 2.1, at large signals the gain of the amplifier will be changed by the factor $\frac{9}{4}a_3A^3$. This results in gain expansion or compression. The linearity performance due to this expansion or compression is measured with the P_{1dB} point. The P_{1dB} point is the output power at which the gain of the amplifier deviates 1dB from the small signal gain, as can be seen in Figure 2.5 [13]. In

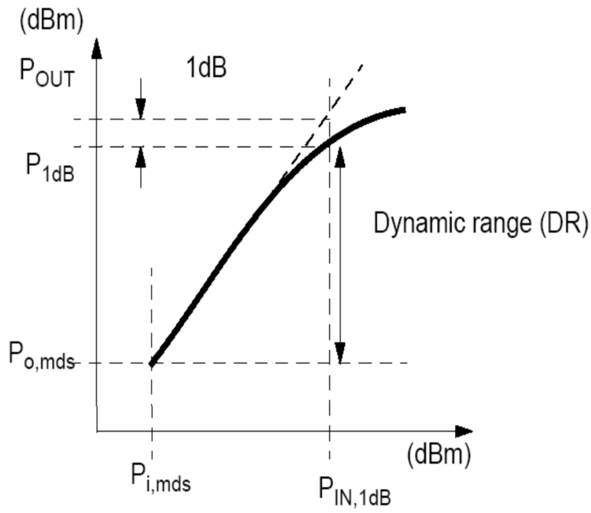

Figure 2.5: The definition of P_{1dB} point. Courtesy L.C.N. de Vreede [13]

this report the main focus will be on IP3 and not on P_{1dB}. The goal is to increase the IP3 performance and not the P_{1dB} performance.

2.3. MEMORY EFFECTS AND VOLTERRA ANALYSIS

The power series analysis in Section 2.1 has one basic assumption: the output signal at a specific time moment can be described fully in terms of the input signal at that specific time moment. However, once capacitances and inductances are added, this is not the case, due to the voltage-current relationship in these components. As an example the circuit of Figure 2.1 will be expanded with a capacitor. Figure 2.6 displays the new circuit.

The input current can now be described as:

$$I_{in}(V(t)) = I_s\left(e^{V(t)/V_t} - 1\right) + C\frac{d}{dt}V(t)[A] \tag{2.11}$$

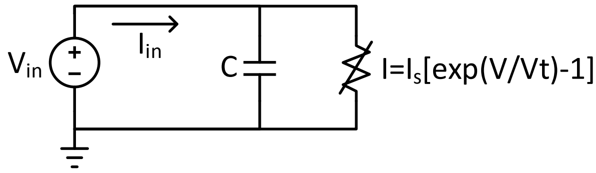

Figure 2.6: A nonlinear resistor with a linear capacitor

When doing the Taylor analysis around point V_{bias}, calculating the DC-term is still easy:

$$I_{in,DC} = I_{in}(V_{bias}) = I_s\left(e^{V_{bias}/V_t} - 1\right)[A] \tag{2.12}$$

However, calculating the first order term becomes troublesome:

$$a_1 = \frac{dI_{in}(V_{bias})}{dV(t)} = \frac{d}{dV(t)}\left(I_s e^{V(t)/V_t} + C\frac{d}{dt}V(t)\right) = \frac{I_{in,DC}}{V_t} + \frac{d}{dV(t)}C\frac{d}{dt}V(t)[A/V] \tag{2.13}$$

As can be seen, the first part of this equation is solved with ease, since $I_s\left(e^{V(t)/V_t} - 1\right)$ can be differentiated to $V(t)$ without a problem. However, for the capacitor, the first derivation is with respect to time. Therefore, $V(t)$ needs to be filled in. For now, a one-tone signal is assumed, so $V(t) = A\cos(2\pi f t)$. Then the derivative becomes:

$$\frac{d}{dV(t)}C\frac{d}{dt}V(t) = \frac{d}{dV(t)}C\frac{d}{dt}A\cos(2\pi f t) = -\frac{d}{dV(t)}CA\cdot 2\pi f\sin(2\pi f t) \tag{2.14}$$

Since $V(t)$ is already assigned, a derivation to $V(t)$ is not possible anymore at this point. Mathematically this would give an answer, but that answer does not provide useful insight, since no correct derivation to $V(t)$ could be done.

The time-dependency in the capacitances and inductances is called the memory effect and it is the main reason why Taylor series analysis doesn't work for these kind of circuits [12]. In order to get a good prediction for IP3, Volterra series analysis can be used [12].

Volterra series analysis is a way to calculate small signal linearity. In Volterra analysis, the output can be described as a function of different input functions, as in the following equation [12]:

$$y(t) = H_1[x(t)] + H_2[x(t)] + H_3[x(t)] + ...H_n[x(t)] + ... \tag{2.15}$$

In this equation, H_n is the Volterra operator, which can be calculated with the following equation [12]:

$$H_n[x(t)] = \int_{-\infty}^{+\infty} ... \int_{-\infty}^{+\infty} h_n(\tau_1, \tau_2, ..., \tau_n)x(t-\tau_1)x(t-\tau_2)...x(t-\tau_n)d\tau_1 d\tau_2...d\tau_n \tag{2.16}$$

where $h_n(\tau_1, \tau_2, ...\tau_n)$ is the n-th order Volterra kernel. Most of the time the Volterra kernel will be calculated in the frequency domain by means of a Laplace transform, resulting in the Volterra kernel $H_n(s_1, s_2, ..., s_n)$.

Volterra kernels can be used to calculate the IIP3 of the system. The IIP3 of the system is, expressed in Volterra kernels [12]:

$$IIP3_{low} = \sqrt{\frac{4}{3}\left|\frac{H_1(s_1)}{H_3(s_1, s_1, -s_2)}\right|} \tag{2.17}$$

$$IIP3_{high} = \sqrt{\frac{4}{3}\left|\frac{H_1(s_2)}{H_3(s_2, s_2, -s_1)}\right|} \tag{2.18}$$

where $s_1 < s_2$. Since the difference between IIP3 and OIP3 is determined by the linear gain, the following equations for OIP3 can be found:

$$OIP3_{low} = \sqrt{\frac{4}{3}\left|\frac{H_1(s_1)}{H_3(s_1,s_1,-s_2)}\right|} \cdot H_1(s_1) \tag{2.19}$$

$$OIP3_{high} = \sqrt{\frac{4}{3}\left|\frac{H_1(s_2)}{H_3(s_2,s_2,-s_1)}\right|} \cdot H_1(s_2) \tag{2.20}$$

As can be seen, the differences between $IP3_{low}$ and $IP3_{high}$ occur in circuits with memory, since the Volterra kernels are frequency dependent. For the Taylor analysis, no frequency dependent parts are present, making the $IP3_{low}$ and $IP3_{high}$ the same quantity.

Calculation of the Volterra kernels is an iterative process, which can result in extensive equations. This report will not go into the details of explaining the calculations of the Volterra kernels. The calculation of Volterra kernels can be found in great detail in the book “Distortion Analysis of Analog Integrated Circuits” of Piet Wambacq and Willy Sansen [12]. Appendix A will contain Volterra analyses done for this report, which are also examples of the techniques described by [12].

2.4. CASCADED CIRCUITS

Most systems include a cascade of circuits. The performance, in terms of noise and nonlinearity, can be expressed in terms of the performance of the individual circuits. Figure 2.7 shows a cascaded system [13]. For

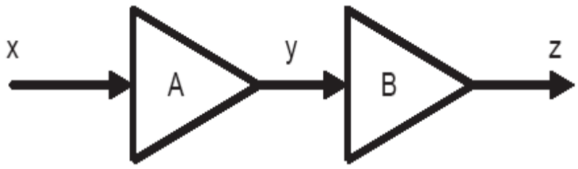

Figure 2.7: A cascaded system. Courtesy L.C.N. de Vreede [13]

the calculation of the IIP3 of the cascaded system, the memory effects are ignored for simplicity. The transfers of the separate system blocks can then be described by the following equations [13]:

$$y(t) = a_1 x(t) + a_2 x^2(t) + a_3 x^3(t) + ... \tag{2.21}$$

$$z(t) = b_1 y(t) + b_2 y^2(t) + b_3 y^3(t) + ... \tag{2.22}$$

Now the IIP3 can be determined by the following equations [13]:

$$IIP3_{cas} = \sqrt{\frac{4}{3}\left|\frac{a_1 b_1}{a_1^3 b_3 + 2a_1 a_2 b_2 + a_3 b_1}\right|} \tag{2.23}$$

$$IIP3^2_{cas} = \left[\frac{1}{IIP3^2_A} + \frac{a_1^2}{IIP3^2_B} + \frac{3a_2 b_2}{2b_1}\right]^{-1} \tag{2.24}$$

Equation (2.24) shows that if the first stage has a high linear gain (a_1), the $IIP3_{cas}$ becomes dependent on the linearity of the second stage [1].

The noise figure can be calculated using Friis formula [14]:

$$F = F_a + \frac{F_b - 1}{G_a} \tag{2.25}$$

where F is the noise figure of the cascaded system, F_a is the noise figure of the first stage, F_b is the noise figure of the second stage and G_a is the gain of the first stage. If the gain of the first stage is large, the noise figure will be dominated by the noise figure of the first stage.

Since the noise figure is dominated by the noise figure of the first stage and the linearity is dominated by the linearity of the second stage, the focus of this report can go fully to linearity, since a two-stage design makes the design in terms of noise/linearity optimization more or less orthogonal.

2.5. DIFFERENTIAL CIRCUITS

In differential circuits, signals are composed out of common mode and differential mode signals. Differential mode signals are opposite in phase, and when they meet at an intermediate node, they will cancel each other resulting in a differential "virtual ground". Common mode signals have the same phase and add up when they meet on such an intermediate node.

Consequently, if the input of a differential circuit is V_{in}, the signals running through each branch are $-V_{in}/2$ and $+V_{in}/2$. At common mode points, they cancel each other due to their opposite signs. In second order Volterra kernels, the signals get squared, as can be seen in Section 2.3. Therefore, the second order voltages depend on $(-V_{in})^2$ and V_{in}^2, which have the same sign. On common mode points, the sum of these signals add up. This means that common mode impedances only affect the second order signals. More generally, all even order signals are affected by the common mode impedances, while odd order signals are not. This can be used to provide second order shorts at the input and output of the amplifier [1]. It can also be used to get out-of-band cancellation [6].

3

NONLINEARITY IN THE CE-STAGE

In amplifiers, the first stage is most of the time a common emitter (CE) stage. This is because of the relatively large gain compared to the common collector (CC) stage, which does not have voltage-gain, and the common base (CB) stage, which does not have current-gain [8]. Since the CE-stage is used in almost all amplifiers, it is useful to examine the linearity of the CE-stage.

There are a few major sources of nonlinearity in the bipolar transistor. The most important nonlinearities for this thesis report are shown in Figure 3.1. The I_c current is characterized by exponential nonlinearity, as

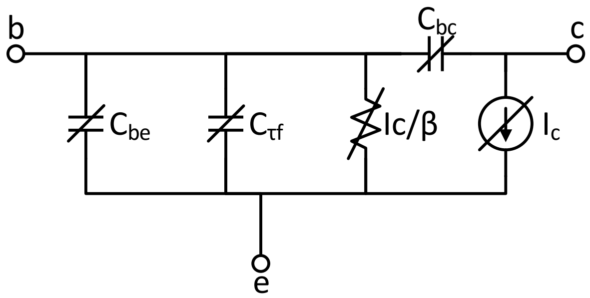

Figure 3.1: Nonlinear contributions in the CE-stage

described in Section 3.1. The base current I_c/β can be modeled as a nonlinear conductor. $C_{\tau f}$ represents the diffusion capacitance that is present due to the transit time τ_f. The linearity degradation due to the τ_f capacitance will be discussed in Section 3.2. C_{be} and C_{bc} are the depletion capacitances present in the transistor. The effect of these capacitances will be discussed in Section 3.3 and Section 3.4. The avalanche effect is not discussed in this thesis report and therefore it is not included in Figure 3.1.

To identify the regions of nonlinearity for the QUBiC4Xi BNA HV device, the circuit in Figure 3.2 has been used, as described by [15]. In this figure, R_1 and R_2 are chosen such that the input and output are matched, while keeping the gain above 10dB. The results can be seen in Figure 3.3. In this figure, 3 important regions can be identified [6].

1. The exponential distortion. For lower currents, where the I_c is under the peak f_t current [6], the exponential distortion of the bipolar transistor dominates. As will be shown in Section 3.1, the V_{ce} voltage has no influence on the linearity in this region.

2. The C_{bc} and τ_f region. In this region, the nonlinearity due to the depletion capacitance C_{bc} and the nonlinear effects in the transit time τ_f becomes dominant. This is the case for higher I_c currents. Although this thesis report is mainly about the C_{bc} distortion, this high current region will not be explicitly discussed in this thesis report. In this region of operation, the f_t rolls of steeply, since the bias current I_c is above the I_c@peak f_t [6]. In high linearity applications, with the exception of the power amplifier in high power operation, the device always operates at lower currents. To accomplish higher

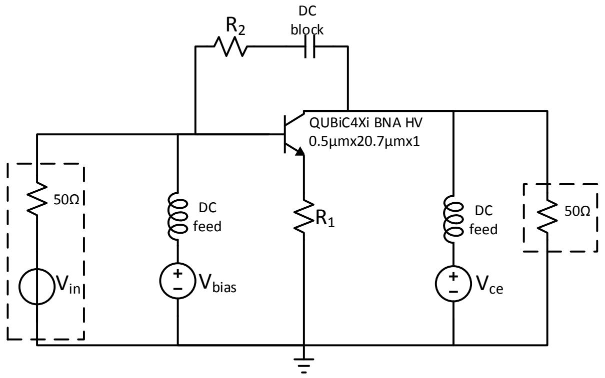

Figure 3.2: Circuit used to characterize the QUBiC4Xi BNA HV device

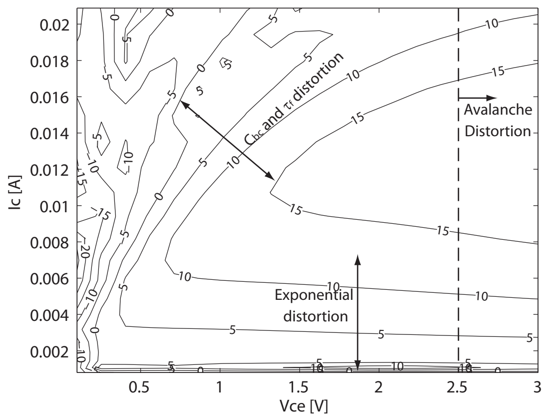

Figure 3.3: OIP3 contours in dBm of the 0.5μm x 20.7μm x 1 QUBiC4Xi BNA HV device

currents in the circuit, devices are placed in parallel. Since the transistor is not biased in this region, but in the first region, the distortion present due to the C_{bc} tends to be less dominant compared to the distortion from the exponential I_c-V_{be} characteristic. The importance of τ_f and C_{bc} will be explained in more detail in Section 3.2 and Section 3.4.

3. The avalanche region. Above the BV_{CEO} of the device, avalanche effects occur [3]. The BV_{CEO} of the QUBiC4Xi BNA HV transistor is 2.5V [16]. This region is avoided in almost any design and therefore avalanche is not considered in this thesis report.

This chapter will discuss the different contributions to the nonlinearity of the CE-stage. The discussion will be based on the Gummel-Poon model [17]. In Section 3.1 the exponential distortion will be discussed. Since exponential distortion is a dominant source of nonlinearity, out-of-band matching, as presented by [6], will be discussed. In Section 3.2 the transit time τ_f will be added to the Gummel-Poon model. This section will show how the τ_f influences the distortion and how this influence can be reduced. In Section 3.3 the same will be done for the C_{je} parameter, representing the nonlinear depletion capacitance in the base-emitter junction. This section will show how this capacitance influences the out-of-band matching conditions. Just as for the τ_f, this section will discuss how to minimize the influence of the C_{je} capacitance. Then the C_{jc} will be added in Section 3.4, representing the nonlinear depletion capacitance in the base-collector junction. This section will show that the nonlinearity resulting from this depletion capacitance interferes with the out-of-band cancellation, in a way not presented in [6]. Next the results using the Mextram model will be shown in Section 3.5, so the results of the Gummel-Poon analysis can be compared with those of the QUBiC4Xi BNA HV Mextram analysis. Gain compression will only be studied using the Mextram model, since the Mextram model incorporates more effects relevant for gain compression, like quasi-saturation, high injection etc. Cross-coupling is used for unilaterization of the C_{bc} capacitance [18]. To demonstrate how this influences linearity, Section 3.6 will discuss cross-coupling. The chapter will end with conclusions in Section 3.7.

3.1. EXPONENTIAL DISTORTION IN THE CE-STAGE

As has been shown in Figure 3.3, the nonlinear contribution of the exponential distortion is dominant when the transistor has a bias current I_c below the I_c at peak f_t. Exponential distortion is described by the exponential relationship between the base-emitter voltage (V_{be}) and the collector current I_c:

$$I_c = I_s\left(e^{\frac{V_{be}}{V_t}} - 1\right)[A] \tag{3.1}$$

where I_s is the saturation current and V_t is the thermal voltage, described by $\frac{kT}{q}$ where k is Boltzmann's constant ($1.38 \cdot 10^{-23} J/K$), T is the temperature measured in kelvin and q is the elementary charge ($1.6 \cdot 10^{-19} C$). This function can be seen when plotting the I_c current versus the V_{be} voltage for the transistor, as shown in Figure 3.4.

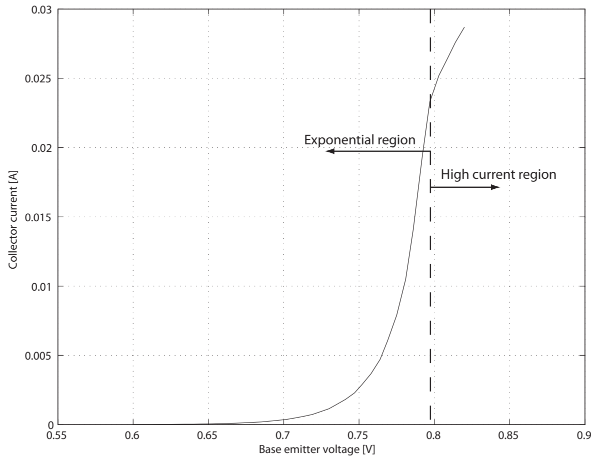

Figure 3.4: The I_c-V_{be} relation for the QUBiC4Xi BNA HV 0.5μm x 20.7μ x 1 transistor

To study the influence of the exponential distortion in the CE-stage, a simple Taylor analysis is performed on the circuit shown in Figure 3.5. In this circuit, only the forward current gain β is included in the Gummel-Poon model, which is very high for the QUBiC4Xi process [16]. This results in the Gummel-Poon model as described by Section 3.1.

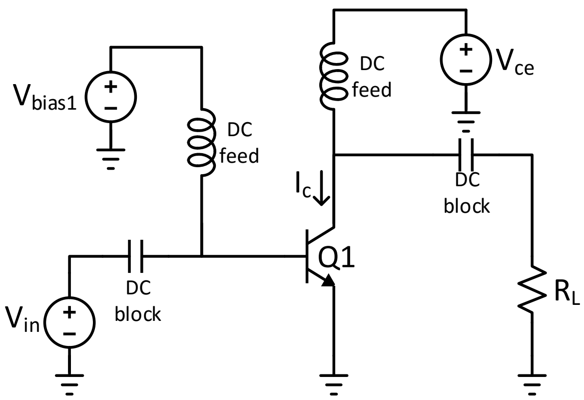

Figure 3.5: The circuit used for analysis of the exponential distortion

Since this circuit is voltage driven, the input resistance r_π plays no role in this analysis. The small-signal

Table 3.1: The Gummel-Poon model for studying exponential distortion

Parameter	Description	Value
β	Forward current gain	2000
I_s	Saturation current	0.5fA
A	Area transistor	1

Taylor analysis gives the following equation for the AC collector current [6]:

$$i_c = \frac{I_{c,bias}}{V_t} v_{in} + \frac{I_{c,bias}}{2V_t^2} v_{in}^2 + \frac{I_{c,bias}}{6V_t^3} v_{in}^3 + ...[A] \tag{3.2}$$

where $I_{c,bias}$ is the DC collector current and V_t is the thermal voltage. Using Equation (2.10), the OIP3 of the system can be calculated:

$$OIP3 = \sqrt{\frac{4}{3}\left|\frac{a_1^3}{a_3}\right|} = \sqrt{\frac{4}{3}\left|\frac{\left(\frac{I_{c,bias}}{V_t}\right)^3}{\frac{I_{c,bias}}{6V_t^3}}\right|} = \sqrt{8}I_{c,bias}[A] \tag{3.3}$$

The circuit shown in Figure 3.5 can also be simulated, using the Gummel-Poon model and using the Mextram model. In these simulations, the biasing voltage V_{bias1} has been changed, such that the bias current $I_{c,bias}$ increases. The simulation frequencies that have been used for the two-tone simulation are 1.795GHz and 1.805GHz. Both simulations have been done in Figure 3.6. For higher currents, the results for the Mextram

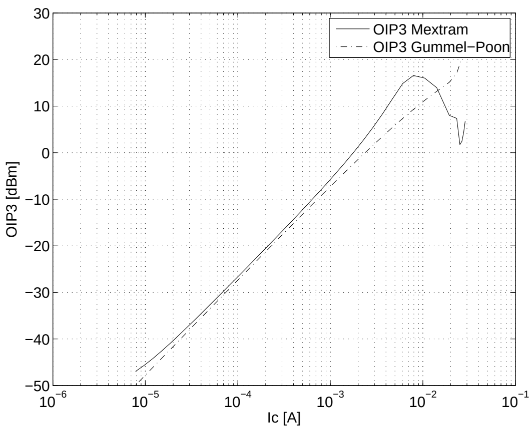

Figure 3.6: OIP3 versus $I_{c,bias}$ for the Gummel-Poon model and for the Mextram model of the QUBiC4Xi 0.5μm x 20.7μm x 1

model start to divert from those for the Gummel-Poon model. First this happens under influence of the base and emitter resistances present in the system. The cause of this effect will be discussed later on in this section. For even higher currents, high-current effects like the Kirk effect start to play a dominant role, making the OIP3 irregular.

3.1.1. OUT-OF-BAND MATCHING

To compensate for the exponential distortion, out-of-band matching is used, as described in [6]. Out-of-band matching provides design orthogonality between gain, noise and impedance matching, since the linearization is done by adjusting the out-of-band signals [6]. Out-of-band matching works by indirect mixing of the IM3 component. The IM2 and HD2 components produced in the circuit mix to the IM3 frequency, as illustrated in Figure 3.7 [19].

To cancel the exponential distortion in a wideband system, the following equation has to be made zero [6]:

$$\varepsilon(\Delta s, 2s) = g_{m,3}\left[\frac{2}{3}F(\Delta s) + \frac{1}{3}F(2s)\right] \tag{3.4}$$

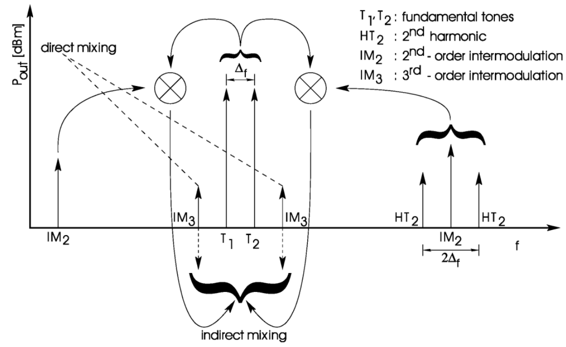

Figure 3.7: The principle of out-of-band matching [19].

where ε describes the second order contribution to the IM3 and $g_{m,3}$ is the third order Taylor component of the exponential distortion. In this system, $s_1 = j2\pi f_1$, $s_2 = j2\pi f_2$ with $f_1 < f_2$ being the fundamental frequencies. It is assumed that $s_1 \approx s_2 \approx s$, $s_2 - s_1 = \Delta s$. F is described by the following equation [6]:

$$F(s) \approx \frac{1 - 2g_m\left(\frac{Z_b}{\beta} + Z_e\right) + s\left[\left(C_{je} - 2\tau_f g_m\right)(Z_b + Z_e) + C_{bc}Z_b\left(1 - 2g_m Z_e\right)\right]}{1 + g_m\left(\frac{Z_b}{\beta} + Z_e\right) + s\left[\left(C_{je} + \tau_f g_m\right)(Z_b + Z_e) + C_{bc}Z_b\left(1 + g_m Z_e\right)\right]} \tag{3.5}$$

where g_m is the first order Taylor component of the exponential distortion, also known as the transconductance gain, Z_b is the base impedance, β is the forward current gain, Z_e is the emitter impedance, C_{je} is the base-emitter depletion capacitance, τ_f is the forward transit time and C_{bc} is the base-collector depletion capacitance. In this analysis it is assumed that the C_{je} and C_{bc} capacitances are completely linear and that the load impedance at Δs and $2s$ is zero [6]. To get perfect IM3 cancellation, ε has to be made zero, which can be done by making $F(s)$ zero for $s = \Delta s$ and $s = 2s$.

For the current analysis, only the exponential distortion is present. The nonlinear behavior of transit time τ_f and the depletion capacitance C_{je} and C_{bc} themselves haven't been added yet. Therefore Equation (3.5) simplifies to the following equation:

$$F(s) \approx \frac{1 - 2g_m\left(\frac{Z_b}{\beta} + Z_e\right)}{1 + g_m\left(\frac{Z_b}{\beta} + Z_e\right)} \tag{3.6}$$

Making F zero for this equation can be done for an infinite amount of Z_b and Z_e combinations, but for clarity purposes, two cases will be studied. In the first case, Z_b will be made zero and Z_e will be used for the IM3 cancellation of the exponential distortion. This is called emitter tuning. In the second case, Z_e will be made zero and Z_b will be used for the IM3 cancellation of the exponential distortion. This is called base tuning. Both cases will be studied. For emitter tuning a sensitivity analysis has been done, which will also be presented.

EMITTER TUNING

For emitter tuning, Z_b is shorted for the out-of-band frequencies. Therefore, Equation (3.6) simplifies to the following equation:

$$F(s) \approx \frac{1 - 2g_m Z_e}{1 + g_m Z_e} \tag{3.7}$$

To make this equation zero, the following must hold:

$$Z_e = \frac{1}{2 \cdot g_m} [\Omega] \tag{3.8}$$

So an out-of-band resistor needs to be applied for cancellation of the exponential IM3 distortion. In Chapter 2 it has been shown that differential circuits make it easier to apply out-of-band impedances, since the even harmonics are common-mode signals. Therefore, the circuit shown in Figure 3.10 has been used. Throughout this chapter, this circuit will be used to examine emitter tuning. In this analysis, the models for

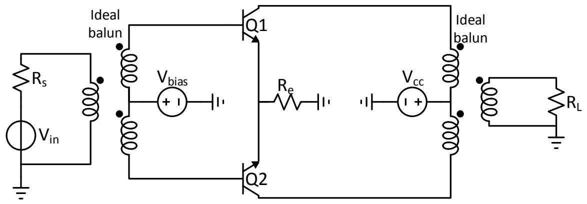

Figure 3.8: Differential CE-stage with emitter tuning for exponential IM3 cancellation

Table 3.2: Simulation values for studying emitter tuning

Parameter	Description	Value
I_c	Collector current	80mA
T_{in}	Turns ratio input balun	2:3
T_{out}	Turns ratio output balun	5:4
V_{cc}	Supply voltage	2.5V
R_s	Source impedance	50Ω
R_L	Load impedance	50Ω
P_{in}	Input power for each tone	-40dBm
f_c	The center frequency	1.8GHz
Δf	Tone spacing	10MHz

Q1 and Q2 will be changed to study the effects of the different nonlinearity contributions in the device. The other values are fixed and can be found in Table 3.2.

In a differential circuit, the IM2 and HD2 currents going through Z_e double. In order to maintain the same IM2 and HD2 voltages, the impedance Z_e needs to be halved, resulting in the following condition:

$$Z_e = \frac{1}{4 \cdot g_m} [\Omega] \tag{3.9}$$

Z_e has been implemented using the resistor R_e. Since $g_m = \frac{I_c}{V_t}$, the bias current also influences the IM3 cancellation of the exponential distortion. Two simulations have been done. In the first simulation, only R_e has been swept. In the second simulation, I_c and R_e have been swept. The Gummel-Poon parameters for the Q1 and Q2 transistors are given in Table 3.3. The results can be seen in Figure 3.9. The optima for OIP3

Table 3.3: Gummel-Poon parameters for studying emitter tuning

Parameter	Description	Value
β	Forward current gain	2000
I_s	Saturation current	0.5fA
A	Area transistor	25

occurs exactly for the resistor value predicted by Equation (3.12). The relation between I_c and R_e is also as predicted. As can be seen, the OIP3 peaks to 85 dBm, making it a perfect cancellation.

BASE TUNING

For base tuning Z_e is shorted for the out-of-band frequencies. Again, Equation (3.6) simplifies:

$$F(s) \approx \frac{1 - 2g_m \cdot \frac{Z_b}{\beta}}{1 + g_m \cdot \frac{Z_b}{\beta}} \tag{3.10}$$

To make this equation zero, the following must hold:

$$Z_b = \frac{\beta}{2 \cdot g_m} [\Omega] \tag{3.11}$$

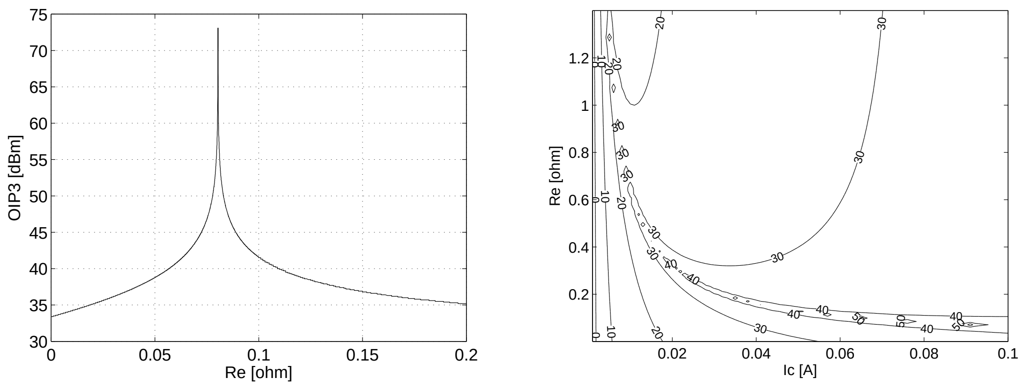

(a) R_e sweep, I_c=80mA (b) R_e and I_c sweep

Figure 3.9: OIP3 versus R_e and OIP3 contours in the I_c-R_e plane for emitter tuning

So again an out-of-band resistor needs to be applied for cancellation of the exponential IM3 distortion. In Chapter 2 it has been shown that differential circuits make it easier to apply out-of-band impedances, since the even harmonics are common-mode signals. Therefore, the circuit shown in Figure 3.10 has been used. In

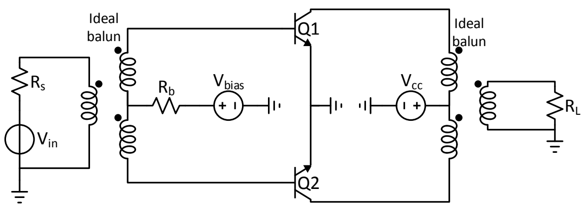

Figure 3.10: Differential CE-stage with base tuning for exponential IM3 cancellation

a differential circuit, the IM2 and HD2 currents going through Z_b double. In order to maintain the same IM2 and HD2 voltages, the impedance Z_b needs to be halved, resulting in the following condition:

$$Z_b = \frac{\beta}{4 \cdot g_m} [\Omega] \tag{3.12}$$

Z_b has been implemented using the resistor R_b. The bias has been chosen such that $I_{c,bias}$ = 80mA. Again, two simulations have been done. In the first simulation, only R_b has been swept. In the second simulation, I_c and R_b have been swept. The Gummel-Poon parameters are the same as for emitter tuning and can be found in Table 3.3. The results can be seen in Figure 3.11. Again, the results match with the theory.

In this thesis report, base tuning will not be used. There are three reasons to use emitter tuning instead of base tuning:

1. Wideband behavior. When capacitances are added to the model, wideband behavior becomes more important. As demonstrated by [6], base tuning is not as wideband as emitter tuning. Although [6] presents solutions to circumvent this problem, wideband behavior can already be established by using emitter tuning.

2. C_{bc} out-of-band matching. This report is ultimately about the nonlinearity of C_{bc} capacitance. The nonlinear C_{bc} capacitance is not influenced by IM2 and HD2 products at the emitter. It is affected by the IM2 and HD2 products at the base. By using emitter tuning, these products are shorted, simplifying the analysis for the nonlinear C_{bc} capacitance.

3. β variation. The current amplification factor β plays an important role in base tuning. Data provided by NXP shows that the β of QUBiC4Xi BNA HV devices spreads a lot. In Figure 3.12 a histogram is shown of the measured β values over 5985 devices. As can be seen, the β spreads a lot, from 1500 up to 3300.

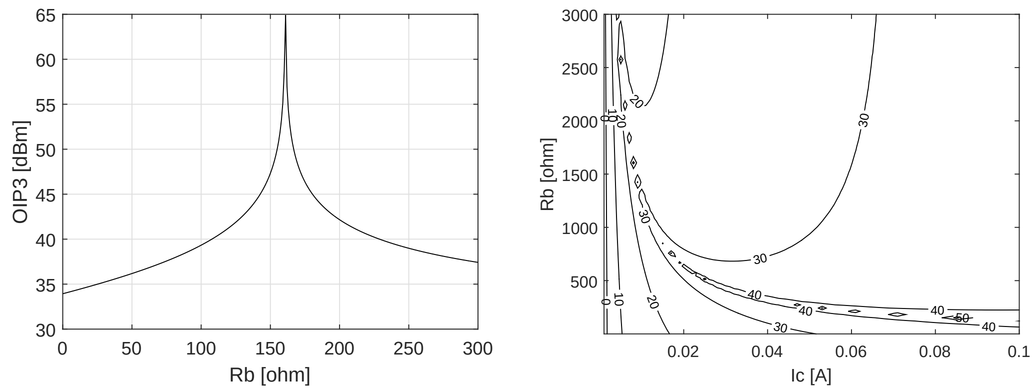

(a) R_b sweep, I_c=80mA (b) R_b and I_c sweep

Figure 3.11: OIP3 versus R_b and OIP3 contours in the I_c-R_b plane for base tuning

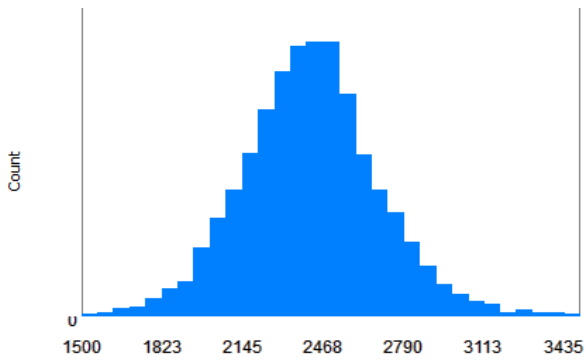

Figure 3.12: β variation in QUBiC4Xi BNA HV devices. Courtesy K. Oldenziel

SENSITIVITY OF EMITTER TUNING

Emitter tuning gives the following equation for cancellation:

$$Z_e = \frac{1}{4 \cdot g_m} [\Omega] \tag{3.13}$$

where g_m can be expressed as:

$$g_m = \frac{I_c}{V_t} = \frac{I_c \cdot q}{k \cdot T} [S] \tag{3.14}$$

where I_c is the DC bias collector current, q is the elementary charge, k is Boltzmann's constant ($1.38 \cdot 10^{-23} J/K$) and T is the temperature in kelvin. Up to now, the temperature, supply voltage and resistances have been considered fixed. The temperature has been fixed at $25°C$. From the equations, 3 cases can be found for process, voltage and temperature (PVT) variation. Due to the temperature dependency, the temperature is expected to influence the emitter tuning. Due to voltage and process variation the collector current may shift and therefore the collector current can also influence the emitter tuning. Due to process variation the resistor value can also shift, influencing the emitter tuning.

To study the effects of PVT variation, 3 simulations have been done. In the first simulation, the temperature has been swept from $-40°C$ up to $120°C$. In the second simulation a Monte Carlo analysis with 1000 samples has been done. In this simulation, the collector current I_c will have a Gaussian distribution, with a standard deviation of 5%. In the last simulation a Monte Carlo analysis with 1000 samples has been done. In this simulation, the resistor R_e will have a Gaussian distribution, with a standard deviation of 5%. The results are given in Figure 3.13. As can be seen, the OIP3 varies a lot due to temperature dependency. This means that the only way to make this compensation work for temperature is to have a resistor that compensates for the temperature, so a PTAT resistor. Variations in the I_c current or R_e resistor have the same effect. They both lower the OIP3 significantly. This thesis report will not have a big emphasis on PVT variation. However, it

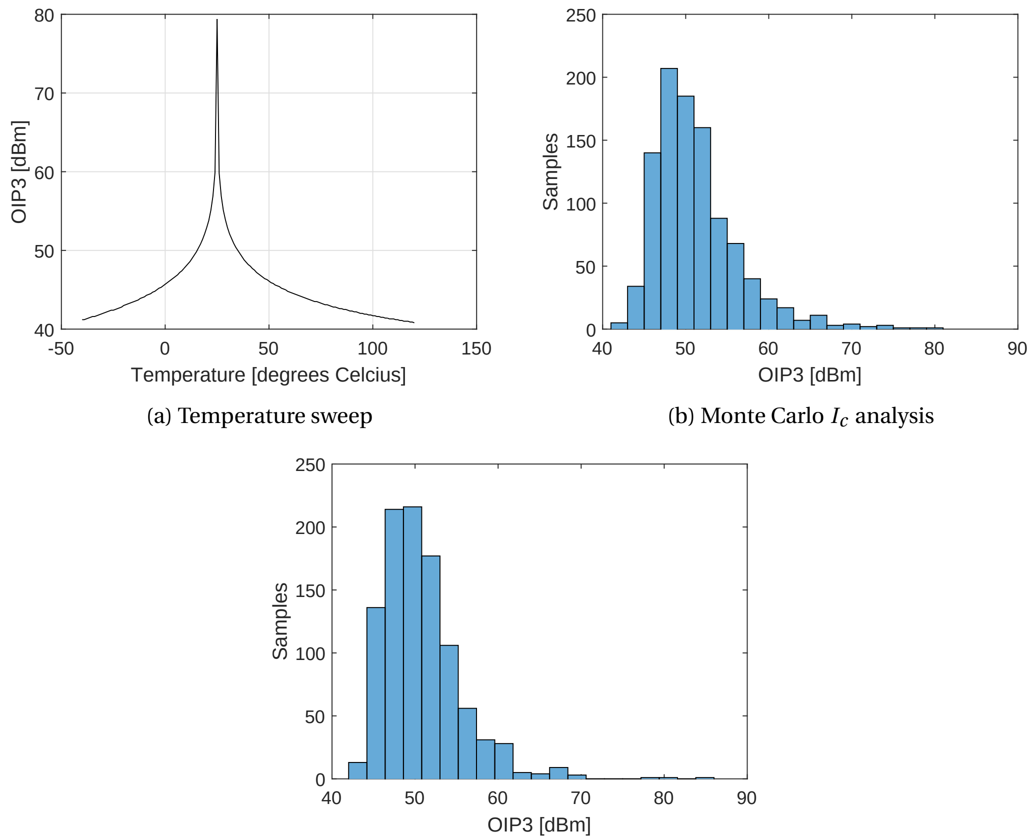

(a) Temperature sweep

(b) Monte Carlo I_c analysis

(c) Monte Carlo R_e analysis

Figure 3.13: Sensitivity analysis of emitter tuning

is important to bear in mind that out-of-band matching for exponential distortion does not provide perfect OIP3 cancellation due to PVT variation.

3.2. TRANSIT TIME τ_f IN THE CE-STAGE

In the previous section the IM3 components due to the exponential distortion have been canceled using out-of-band matching. The transit time τ_f is another major source of IM3 distortion and therefore it needs to be studied.

The transit time τ_f adds a nonlinear current, correlated with the exponential distortion. The transit time will manifest itself as a diffusion capacitance, with the following value:

$$C_{\tau_f} = \tau_f \frac{d}{dV_{be}} I_c [F] \tag{3.15}$$

In [6], this diffusion capacitance is included in the analysis, and a solution is provided. For that solution Equation (3.5) has to be studied again. When emitter tuning is used, Z_b is zero. C_{bc} and C_{je} are not included yet. This means that Equation (3.5) simplifies to the following equation:

$$F(s) \approx \frac{1 - 2g_m Z_e + s \cdot -2\tau_f g_m Z_e}{1 + g_m Z_e + s \cdot \tau_f g_m Z_e} \tag{3.16}$$

Making this equation zero results in the following solution for Z_e:

$$Z_e = \frac{1}{2g_m + s \cdot 2\tau_f g_m} [\Omega] \tag{3.17}$$

This is a parallel combination of a resistor with the value $\frac{1}{2g_m}$ and a capacitor with the value $2\tau_f g_m$. To implement this, a differential structure has been chosen, shown in Figure 3.14. Again, in the differential

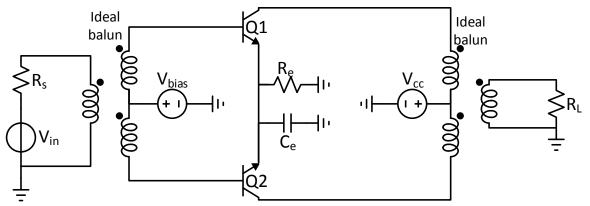

Figure 3.14: Differential CE-stage with emitter tuning for exponential distortion and τ_f distortion

structure the IM2 and HD2 currents are twice as large, so the impedance Z_e needs to be halved. This means that the resistor value changes to $\frac{1}{4g_m}$ and the capacitor values changes to $4\tau_f g_m$. Two simulations have been done. In the first, the resistor value and the collector current are kept constant. The C_e capacitance is swept. In the second simulation, the resistor value R_e and capacitor value C_e are swept and OIP3 contours are given. The Gummel-Poon parameters can be found in Table 3.4. The simulation results can be found in Figure 3.15. As can be seen, a clear optimum exists for the OIP3. Also in the C_e-R_e plane this optimum is visible. Again

Table 3.4: Gummel-Poon parameters for studying emitter tuning

Parameter	Description	Value
β	Forward current gain	2000
I_s	Saturation current	0.5fA
τ_f	Transit time	13ps
A	Area transistor	25

the OIP3 peaks up to 85dBm, suggesting perfect cancellation. Therefore, the τ_f does not pose a problem for the OIP3 as long as it is linearized.

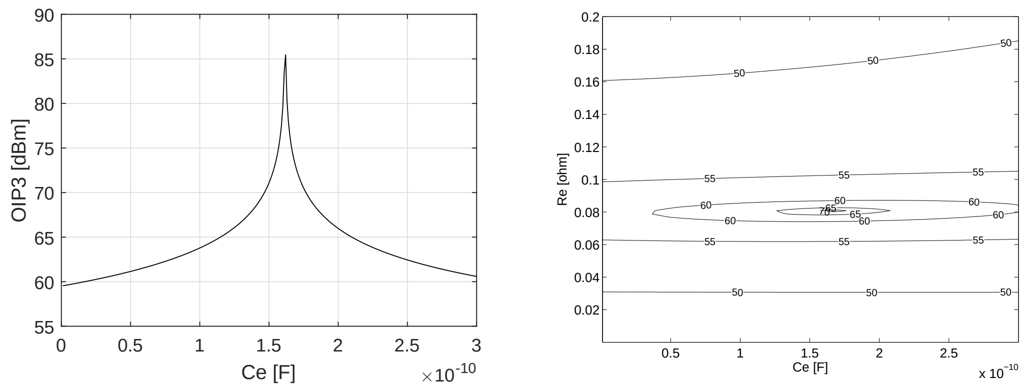

(a) C_e sweep, I_c=80mA (b) R_e and C_e sweep

Figure 3.15: OIP3 versus C_e and OIP3 contours in the C_e-R_e plane for emitter tuning

3.3. DEPLETION CAPACITANCE C_{je}

The depletion capacitance C_{je} is a nonlinear capacitance in the base-emitter junction of the bipolar transistor. In [6] this capacitance is assumed to be linear. Since the depletion capacitance C_{je} is at the input of the transistor, the voltage swing on it is small. In normal amplifiers, the base-emitter junction is also in forward, making the depletion capacitance rather small. Therefore it will also be assumed to be linear in this analysis.

With the base impedance Z_b still shorted and the C_{bc} capacitance still zero, Equation (3.5) simplifies to the following equation:

$$F(s) \approx \frac{1 - 2g_m Z_e + s\left(C_{je} - 2\tau_f g_m\right) Z_e}{1 + g_m Z_e + s\left(C_{je} + \tau_f g_m\right) Z_e} \tag{3.18}$$

Making this equation zero results in the following solution for Z_e:

$$Z_e = \frac{1}{2g_m + s \cdot (2\tau_f g_m - C_{je})} [\Omega] \tag{3.19}$$

Again, this is a parallel combination of a resistor and a capacitor. The resistor has a value of $\frac{1}{2g_m}$ and the capacitor has a value of $2\tau_f g_m - C_{je}$. This means that the C_{je} capacitance lowers the value needed for the compensation capacitor. The same circuit has been used as in Section 3.2. Two simulations have been done. In the first, the resistor value and the collector current are kept constant. The C_e capacitance is swept. In the second simulation, the resistor value R_e and capacitor value C_e are swept and OIP3 contours are given. The Gummel-Poon parameters can be found in Table 3.5. The simulation results can be found in Figure 3.16. As can be seen, the optimal value for C_e shifted to the left. The OIP3 also decreased, suggesting that the

Table 3.5: Gummel-Poon parameters for studying emitter tuning

Parameter	Description	Value
β	Forward current gain	2000
I_s	Saturation current	0.5fA
τ_f	Transit time	13ps
C_{je0}	Zero-bias base-emitter depletion capacitance	0.12 pF
V_{je}	Built-in voltage of the base-emitter junction	0.7V
m_{je}	Grading coefficient of the base-emitter junction	1/3
A	Area transistor	25

nonlinearity of the C_{je} cannot be fully disregarded.

If the C_e would be disregarded, the τ_f and C_{je} distortion will decrease the OIP3. However, an R_e-I_c

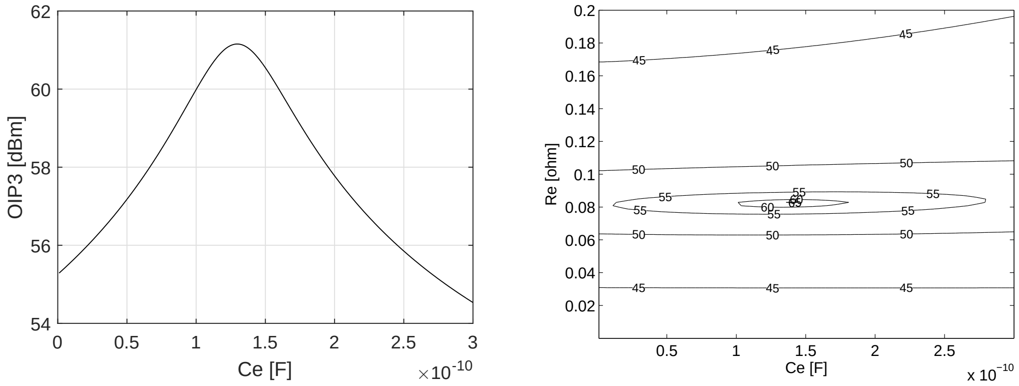

(a) C_e sweep, I_c=80mA

(b) R_e and C_e sweep

Figure 3.16: OIP3 versus C_e and OIP3 contours in the C_e-R_e plane for emitter tuning

sweep can still be done, to see whether the OIP3 contours still show the same characteristics as in Section 3.1. The results of this simulation is shown in Figure 3.17. As can be seen, the OIP3 contours have the same

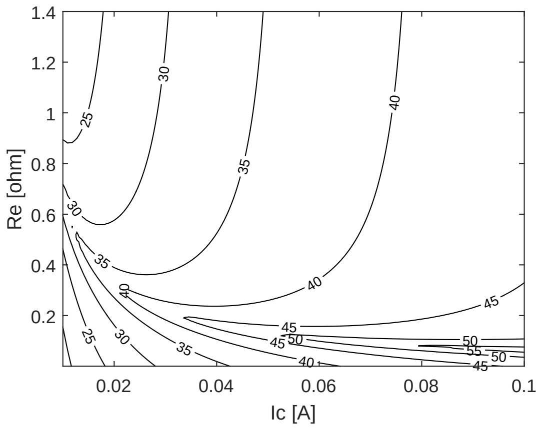

Figure 3.17: Constant OIP3 contours in the R_e-I_c plane

characteristics. This means that exponential distortion is still dominant. It also means that emitter tuning is indeed wideband, else the IM3 improvements wouldn't be found.

3.4. DEPLETION CAPACITANCE C_{jc}

The C_{jc} variable is part of the equation for the base-collector capacitance C_{bc}. This C_{bc} can be modeled using the Gummel-Poon model by the following equation [17]:

$$C_{bc}(V_{cb}) = \frac{C_{jc}}{\left(1 + \frac{V_{cb}}{V_{jc}}\right)^{m_{jc}}} [F] \tag{3.20}$$

where V_{cb} is collector-base voltage, C_{jc} is the capacitance value for zero bias conditions, V_{jc} is the built-in voltage of the base-collector junction and m_{jc} is the grading coefficient of the base-collector junction. In Figure 3.18 the C_{bc} versus V_{cb} has been plotted for the QUBiC4Xi BNA HV 0.5μm x 20.7μm x 1 device.

In [6], the C_{bc} is assumed to be linear. For the C_{je} capacitance this is a fair assumption, since the voltage swing on the C_{je} capacitance is low. However, the C_{bc} is connected to the output, which delivers a large voltage swing. Therefore, it cannot always be assumed that C_{bc} is linear.

To test whether the C_{bc} is limiting linearity, emitter tuning has been used. Again a R_e-I_c sweep is

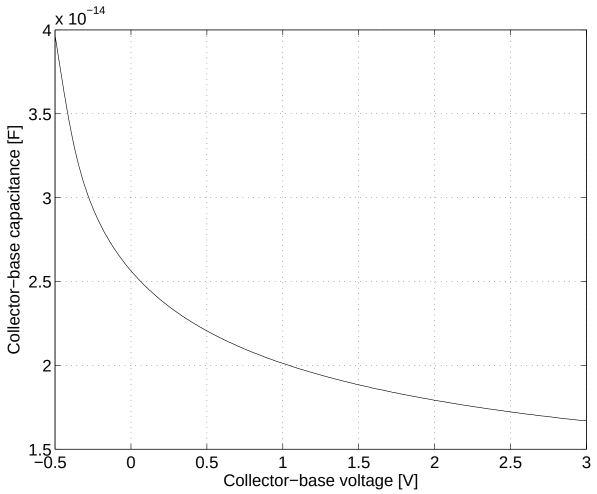

Figure 3.18: C_{bc} vs V_{cb} characteristisc for the QUBiC4Xi BNA HV 0.5μm x 20.7μm x 1 transistor

done. Also the R_e has been swept, keeping I_c constant at 80mA. The Gummel-Poon parameters are shown in Table 3.6. The simulation results are given in Figure 3.19.

Table 3.6: Gummel-Poon parameters for studying emitter tuning

Parameter	**Description**	**Value**
β	Forward current gain	2000
I_s	Saturation current	0.5fA
τ_f	Transit time	13ps
C_{je0}	Zero-bias base-emitter depletion capacitance	0.12 pF
C_{jc}	Zero-bias base-collector depletion capacitance	26fF
V_{je} & V_{jc}	Built-in voltage of the base-emitter and base-collector junction	0.7V
m_{je} & m_{jc}	Grading coefficient of the base-emitter and base-collector junction	1/3
A	Area transistor	25

As can be seen, a plateau in OIP3 is reached around 40dBm. For higher currents, the OIP3 doesn't increase. Also the R_e doesn't give cancellation anymore, suggesting that the exponential distortion is much less dominant at higher currents. This shows that the assumption, that C_{bc} is linear, is not valid for the higher current regions.

Up to now, for wideband cancellation, a capacitance in the emitter has been used. Therefore another contour plot has been made with the OIP3 plotted in the C_e-R_e plane. The results are given in Figure 3.20.

The results do show an optimum for OIP3. However, this optimum requires a negative resistance. The optimum also doesn't correspond with the optimum found using Equation (3.5). The explanation for this optimum is not fully understood yet. It is likely that the IM3 components of the exponential distortion and the IM3 components of the C_{bc} distortion cancel each other due to phase and amplitude shifts in the CE-stage. Since the phase and amplitude of the C_{bc} is depending on the voltage swing, the optimum would differ for different bias-voltage and load impedances. The exponential distortion depends on the I_c current, suggesting that the optimum is also influenced by the current. Since the cancellation has many dependencies, it is uncertain whether this OIP3 cancellation can be found in all situations.

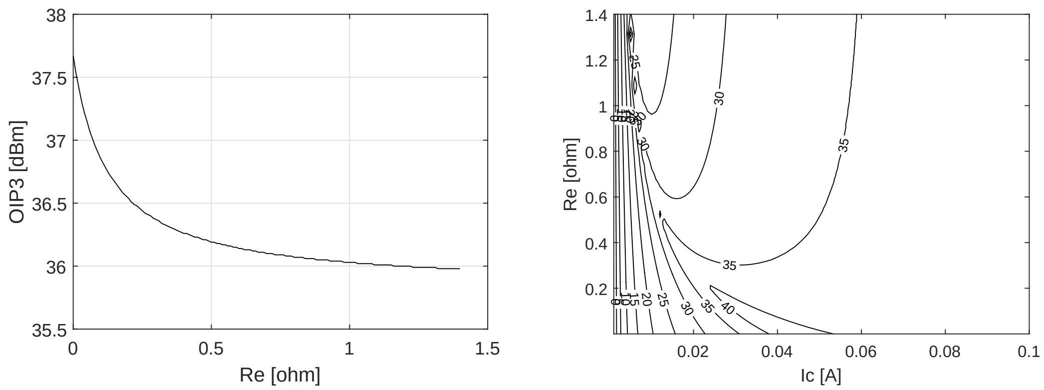

(a) R_e sweep, I_c=80mA

(b) R_e and I_c sweep

Figure 3.19: OIP3 versus R_e and OIP3 contours in the I_c-R_e plane for emitter tuning

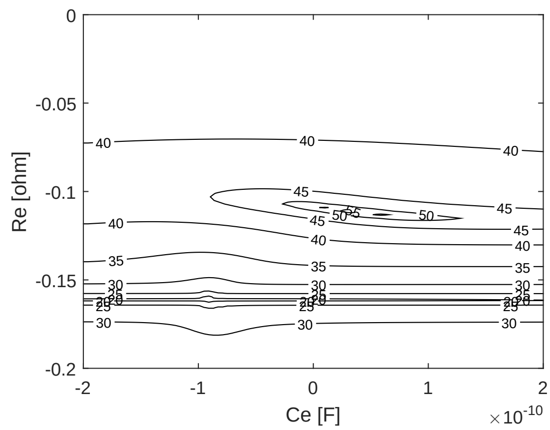

Figure 3.20: Constant OIP3 contours in the R_e-C_e plane

3.5. CE-STAGE MODELED USING THE MEXTRAM MODEL

In the previous sections, the influence of the different nonlinear sources in the CE-stage has been examined with the Gummel-Poon model. In this section the linearity of the CE-stage will be studied for the Mextram model.

The Mextram model and Gummel-Poon model differ in several ways. The most important difference for this analysis is the current dependency of the C_{bc} capacitance [20]. In this thesis report, this current dependency is ignored, but it is important to bear in mind that the current dependency is likely to affect the linearity of the C_{bc} capacitance.

In previous sections the complete Gummel-Poon model hasn't been used. This has not been done, since this Gummel-Poon model is not available for the QUBiC4Xi BNA HV transistor. Since the nonlinear sources are the main point of interest, only those have been included in the model. The Mextram model is complete, and therefore out-of-band matching can be affected by base- and emitter-resistances in the model.

This section, focusing on the linearity performance that can be obtained with the Mextram model, will start with an examination of the strong distortion of the fundamental component being determined by the P_{1dB} point. Using loadline analysis, a choice is made for the turns ratio of the output balun. After this analysis, the weak nonlinearity will be studied.

3.5.1. GAIN COMPRESSION USING THE MEXTRAM MODEL

To get the highest P_{1dB}, the V_{cc} voltage is chosen as high as possible. For QUBiC4Xi BNA HV transistors, the BV_{CEO} is 2.5V. The bias current I_c is 80mA. When using these numbers, a load of 31Ω single ended would give a good loadline in terms of achievable output power. A turns ratio of 5:4 is chosen. With a load resistance of 50Ω, this results in a resistance of 78Ω at the output, which is approximately 39Ω for each branch. QUBiC4Xi BNA HV 0.5μm x 20.7μm x 25 transistors are used. The circuit topology is shown in Figure 3.10. The resistor has been shorted for this analysis. The resulting loadline on the collector of one of the transistors is shown in Figure 3.21a. The resulting performance for P_{1dB} can be seen in Figure 3.21b. As can be seen, the P_{1dB} is

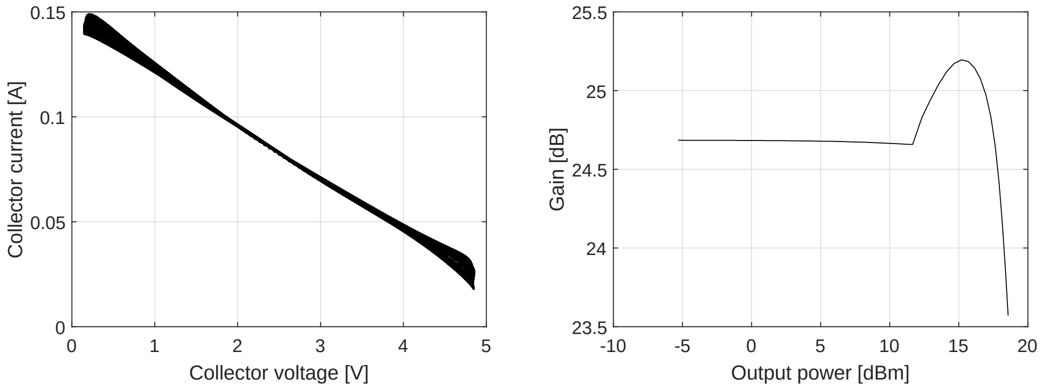

(a) Loadline (b) P_{1dB}

Figure 3.21: The loadline and P_{1dB} point for the differential CE-stage

17.5dBm.

3.5.2. WEAK NONLINEARITY IN THE CE-STAGE WHEN USING THE MEXTRAM MODEL

For weak nonlinearity, the OIP3 has been simulated again. Emitter tuning is used to cancel the exponential distortion. Two simulations have been done. In the first simulation, only R_e has been added, and an I_c-R_e sweep has been done. In the second simulation, R_e and C_e have been added and swept while I_c = 80mA. The results can be seen in Figure 3.22.

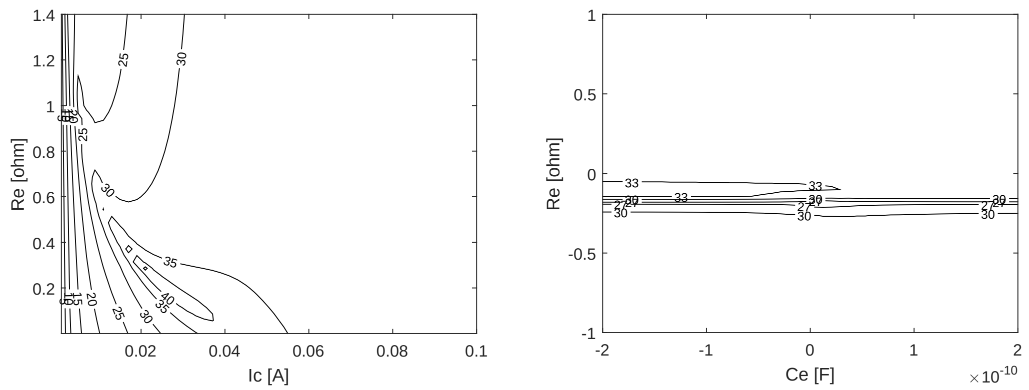

(a) R_e-I_c plane (b) R_e-C_e plane

Figure 3.22: Constant OIP3 contours in the R_e-I_c plane and in the R_e-C_e plane

As can be seen, the OIP3 is again limited. The maximum OIP3 is between 30 and 40dBm. When looking at the R_e-C_e plane, it can be concluded that no clear optimal combination exists. In Section 3.4 an optimum did exist. However, as has been pointed out, this optimum is dependent on many variables, including load and biasing conditions. Also no current dependency of the C_{bc} is present in Section 3.4, decreasing complexity and makes it more likely that an optimal combination for R_e and C_e is possible.

3.6. CROSS-COUPLING THE CE-STAGE

Since the C_{bc} dominates for higher currents, the C_{bc} needs to be addressed. The C_{bc} does not only affect linearity, but also the gain, by creating a feedback path in the device. To address this problem, unilaterization using cross-coupled capacitances has been proposed by [18]. When nonlinear C_{bc} capacitances are used in the cross-coupled feedback, OIP3 compensation might also be possible. Therefore this section will discuss cross-coupling in the CE-stage.

The circuit used for cross-coupling is given in Figure 3.23. In the first simulation, the Gummel-Poon

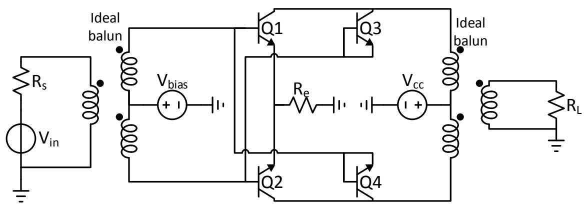

Figure 3.23: Circuit with cross-coupled C_{bc} capacitances

model has been used. The emitter resistance is set to $\frac{1}{4g_m}\Omega$, which should give perfect IM3 cancellation of the exponential distortion as discussed in Section 3.1. The models for Q1, Q2, Q3 and Q4 will be adapted throughout this section. The simulation values for the other components can be found in Table 3.2. In Table 3.7 the Gummel-Poon parameters are given. The variable x gives the relative area between the compensation transistors Q3 and Q4 and the transistors of the CE-stage Q1 and Q2. This relative area has been swept. Since cross-coupled design should give unilaterization, the S_{12} and OIP3 have been plotted. The results can be seen in Figure 3.24.

Table 3.7: Gummel-Poon parameters for studying cross-coupling

Parameter	Description	Value
β	Forward current gain	2000
I_s	Saturation current	0.5fA
C_{jc}	Zero-bias base-collector depletion capacitance	26fF
V_{jc}	Built-in voltage of the base-collector junction	0.7V
m_{jc}	Grading coefficient of the base-collector junction	1/3
A	Area transistor Q1 and Q2	25
A_{com}	Area transistor Q3 and Q4	$x \cdot 25$

For a relative area of 1, the S_{12} drops significantly to -75dB, while it was around -37dB. The current going through the cross-coupled transistors counteracts the current going through the C_{bc}. Therefore, no IM3 current due to the C_{bc} is present at the input. However, at the output the C_{bc} current has doubled. The IM3 current does the same thing. It is not present anymore at the input for $x = 1$, but it has doubled at the output. When the relative scaling is increased, the C_{bc} current entering the input changes in phase. This current is amplified by the transistor, compensating the IM3 currents at the output. Therefore, an OIP3 maximum exists at a relative scaling of 1.05.

In this section, the Gummel-Poon model will be expanded to see whether the unilaterization still works and whether the OIP3 still peaks when τ_f and C_{je} are added. When this is done, the emitter tuning is adapted to see whether an optimum can be reached for a certain combination for C_e and R_e, just as in Section 3.4. In the end, the Gummel-Poon model will be replaced by the Mextram model and the emitter tuning will be tested again.

3.6.1. ADDING τ_f TO THE GUMMEL-POON MODEL

In Section 3.2, the τ_f variable has added some nonlinearity when C_e has been kept zero. However, in Section 3.4, the C_{bc} capacitance has been shown to be the limiting factor for IM3. Therefore, it is expected

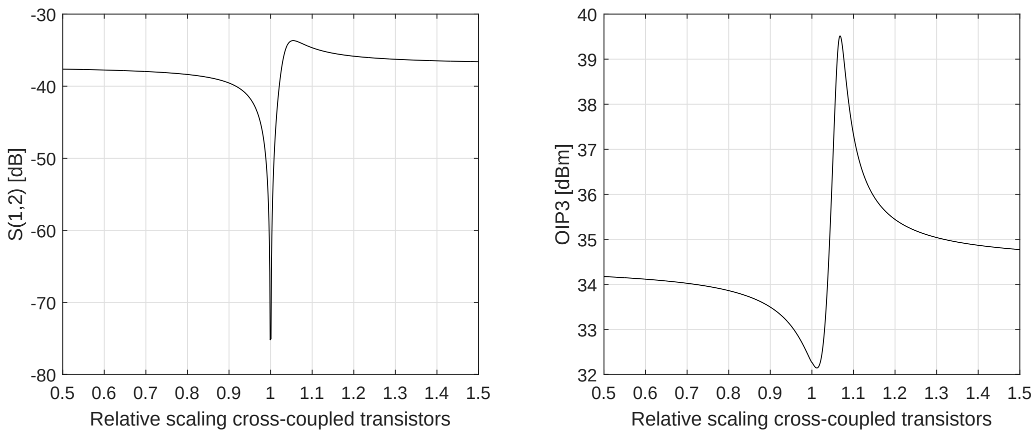

(a) S_{12} (b) OIP3

Figure 3.24: S_{12} and OIP3 versus the relative area of the compensation transistors

that the nonlinearity of τ_f does not influence the cross-coupling in the CE-stage.

The model used in the simulations has been given in Table 3.8. The simulation results are shown in Figure 3.25.

Table 3.8: Gummel-Poon parameters for studying cross-coupling

Parameter	Description	Value
β	Forward current gain	2000
I_s	Saturation current	0.5fA
τ_f	Transit time	12ps
C_{jc}	Zero-bias base-collector depletion capacitance	26fF
V_{jc}	Built-in voltage of the base-collector junction	0.7V
m_{jc}	Grading coefficient of the base-collector junction	1/3
A	Area transistor Q1 and Q2	25
A_{com}	Area transistor Q3 and Q4	$x \cdot 25$

The simulation results show that the S_{12} still profits from the cross-coupled design. However, the OIP3 does not seem to profit from the cross-coupling. Although the OIP3 is just as high as in Figure 3.24b, the OIP3 doesn't show a sharp peak anymore. The high values for the OIP3 can be explained as a result from the linear diffusion capacitance due to τ_f. This capacitance lowers the voltage swing at the input, positively influencing the OIP3 of the C_{bc} capacitance. However, the cancellation mechanism, in which the IM3 currents from the cross-coupling are amplified doesn't work anymore, since the diffusion capacitance adds extra phase to those currents. Therefore, no optimum can be reached anymore.

3.6.2. ADDING C_{je} TO THE GUMMEL-POON MODEL

Since τ_f increased the OIP3 by lowering the voltage swing at the input, adding C_{je} is expected to give the same effect. Again, no cancellation point should be found since the IM3 currents get a phase shift in the amplifier. The Gummel-Poon parameters are given in Table 3.9. The simulation results are shown in Figure 3.26.

As expected, the cross-coupling still provides unilaterization. However, the OIP3 did not improve under influence of the C_{je}. This suggests that the voltage swing at the output is more influential on the C_{bc} capacitance in this case.

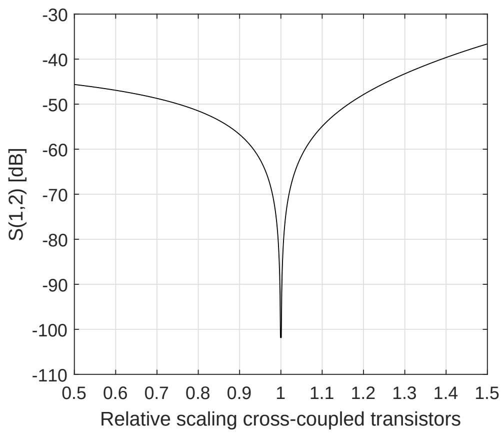

(a) S_{12}

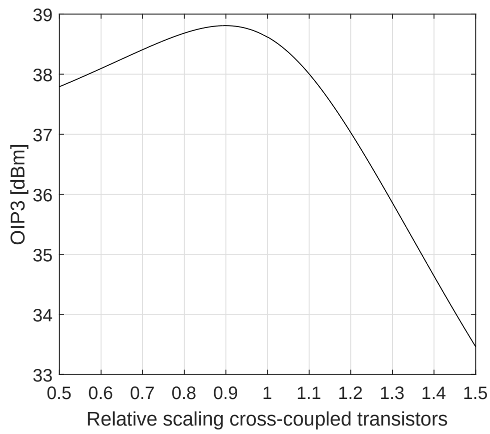

(b) OIP3

Figure 3.25: S_{12} and OIP3 versus the relative area of the compensation transistors

Table 3.9: Gummel-Poon parameters for studying cross-coupling

Parameter	Description	Value
β	Forward current gain	2000
I_s	Saturation current	0.5fA
τ_f	Transit time	12ps
C_{je0}	Zero-bias base-emitter depletion capacitance	0.12pF
C_{jc}	Zero-bias base-collector depletion capacitance	26fF
V_{je} & V_{jc}	Built-in voltage of the base-emitter and base-collector junction	0.7V
m_{je} & m_{jc}	Grading coefficient of the base-emitter and base-collector junction	1/3
A	Area transistor Q1 and Q2	25
A_{com}	Area transistor Q3 and Q4	$x \cdot 25$

3.6.3. EMITTER TUNING

To see how the cross-coupling affects the emitter-tuning, an emitter capacitance has been added. Just as in Section 3.4, the R_e and C_e values have been swept and a plot with constant OIP3 contours has been made. During this simulation, the relative scaling of the compensation transistors has been set to 1, so the amplifier is unilateral. The results are shown in Figure 3.27. As can be seen, no optimum value can be found for OIP3.

3.6.4. CROSS-COUPLING USING THE MEXTRAM MODEL

In the Mextram model, the current dependency is included for the C_{bc} model. Therefore it is unsure whether the unilaterization still works. Therefore the relative scaling has been swept again to see whether the S_{12} still drops. Also the R_e and C_e have been swept again, while the scaling factor has been set to 1. The simulation results can be seen in Figure 3.28.

As can be seen, cross-coupling does not give as strong unilaterization as found previously for the Gummel-Poon model when using the Mextram model. There is an optimum however for a relative scaling of 0.95. The OIP3 still has no optimum, meaning that the cross-coupling did not help to address the problem of C_{bc} distortion.

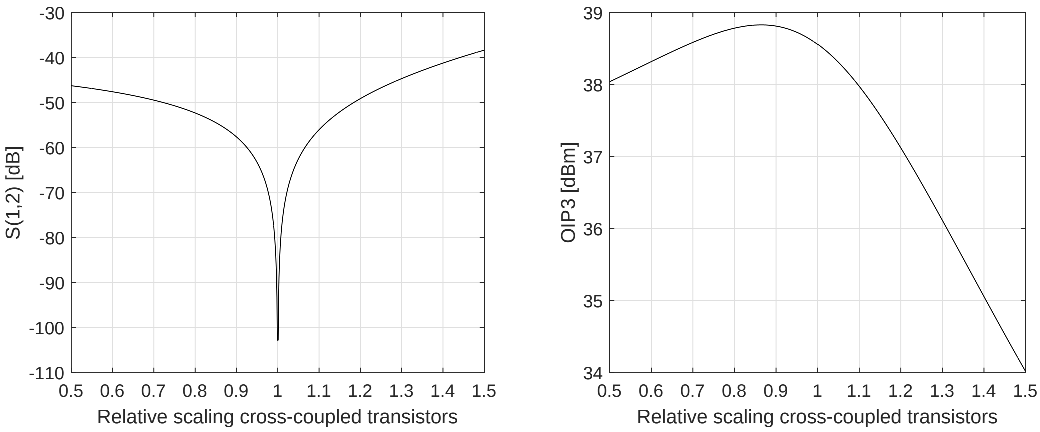

(a) S_{12} (b) OIP3

Figure 3.26: S_{12} and OIP3 versus the relative area of the compensation transistors

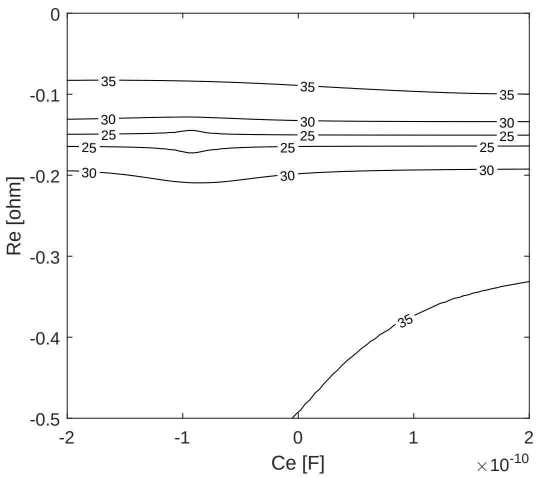

Figure 3.27: Constant OIP3 contours in the R_e-C_e plane

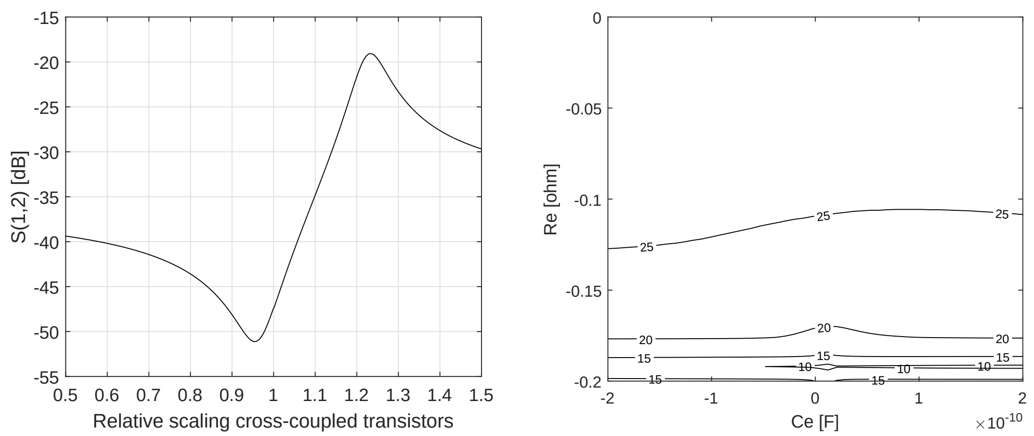

(a) S_{12} (b) OIP3 contours

Figure 3.28: S_{12} versus the relative area of the compensation transistors and the constant OIP3 contours in the R_e-C_e plane

3.7. CONCLUSIONS AND RECOMMENDATIONS

In this chapter, the linearity performance of the differential CE-stage has been studied. The different contributions to IM3 have been presented.

In Section 3.1 the exponential distortion has been discussed. It has shown that for higher I_c currents, the OIP3 due to the exponential distortion increases. However, above certain current levels the exponential distortion doesn't dominate linearity anymore, so increasing the I_c current only works up to a certain level. Out-of-band matching as presented by [6] has been discussed. There are two variants of out-of-band matching: emitter tuning and base tuning. Both have been discussed. Emitter tuning has been chosen for cancellation of the exponential distortion and a sensitivity analysis has been done. This analysis showed a large dependency on emitter resistance R_e, collector current I_c and the temperature.

In Section 3.2 the transit time τ_f has been added to the Gummel-Poon model. Based on [6] a formula for the emitter impedance has been derived. With a parallel combination of an emitter resistance R_e and capacitance C_e, perfect IM3 cancellation has been found again.

In Section 3.3 the depletion capacitance C_{je} has been added to the Gummel-Poon model. Again a formula for the emitter impedance has been derived. With a parallel combination of an emitter resistance R_e and capacitance C_e, high OIP3 numbers could be reached, but no perfect cancellation due to the nonlinear IM3 currents from the C_{je}. It has been demonstrated that emitter tuning has a wideband behavior, making C_e less necessary for reaching high OIP3 numbers.

In Section 3.4 the depletion capacitance C_{bc} has been added to the Gummel-Poon model. The IM3 currents from the C_{bc} capacitance are dominant at higher currents in the CE-stage. Optima have been found for the OIP3 when sweeping R_e and C_e, but these optima are not fully explained yet by analytical considerations.

In Section 3.5 the Gummel-Poon model has been replaced with the Mextram model. The correct loading has been derived for the CE-stage, resulting in a 5:4 output balun. It has been shown that for higher currents, the OIP3 reaches a maximum, where emitter tuning does not work anymore. Also with the addition of C_e, no optimum has been reached.

In Section 3.6, cross-coupling has been used to make the CE-stage unilateral and to see whether the OIP3 improves with cross-coupling. It has been shown that for the Gummel-Poon model, cross-coupling can provide very good unilaterization. However, when τ_f and C_{je} are added, no improvement in OIP3 could be reached. This is due to the effect τ_f and C_{je} have on the phase of the current from the cross-coupling at both the input and output. Like suggested in [1], this might be solved by adding resistive feedback. This resistive feedback also influences the phase of the C_{bc} currents and the cross-coupling currents. This might lead to a compensation of IM3 created by the C_{bc} capacitance. Emitter tuning has been used again to find optima, which have not been found.

4

NONLINEARITY IN THE CB-STAGE

In Chapter 3, the CE-stage has been discussed. It has been shown that in the CE-stage, the C_{bc} is the most dominant source of nonlinear distortion, if the exponential distortion is canceled. Another stage often used in bipolar amplifiers is the common-base (CB) stage. A very common combination is the cascode amplifier, in which the first stage is a CE-stage and the second stage is a CB-stage.

The cascode amplifier has several advantages over a single CE-stage amplifier. The CB-stage has a very low input impedance, neutralizing the C_{bc} capacitance of the CE-stage [8]. Also the CB-stage is more unilateral, making the whole amplifier more unilateral. Lastly the cascode amplifier can enable higher compression points, as will be discussed in this chapter.

In this chapter, the CB-stage will be studied in detail. First the CB-stage itself will be discussed in Section 4.1. In this section, the main characteristics of the CB-stage will be discussed, and the linearity performance will be tested. Secondly the cascode amplifier will be studied in Section 4.2. The linearity of the cascode amplifier will be tested in this section. In Section 4.3 the characteristics for the C_{bc} in the CB-stage will be discussed. This includes a simple model for Volterra analysis, and a study of anti-parallel C_{bc} capacitances. The chapter will end with conclusions in Section 4.4.

4.1. CB-STAGE

The CB-stage can be seen as a current-controlled current source (CCCS) [8]. Just like a CCCS, the output impedance of the CB-stage is high and the input impedance is low. The current gain of the CB-stage is close to 1. In this section, the nonlinear behavior of the CB-stage will be studied. More details on the linear characteristics of the CB-stage can be found in Section 7.5.

For the linearity analysis of the CB-stage, two situations will be studied. In the first situation, the CB-stage is voltage driven. In the second situation, the CB-stage is current driven. The CB-stage is very linear when it is current driven [6]. This section will show why the CB-stage is very linear in that situation. It will also demonstrate that the C_{bc} capacitance is the dominating nonlinearity in the CB-stage.

VOLTAGE DRIVEN VERSUS CURRENT DRIVEN

The OIP3 of the voltage driven CB-stage can be described by the following equation [6]:

$$OIP3_{CB,vd} \approx 2I_c\sqrt{2\left|\frac{(1+sR_sC_\pi)(1+2sR_sC_\pi)}{(1+sR_sC_{je})(1+2sR_sC_{je})}\right|}[A] \tag{4.1}$$

where I_c is the collector current, $s = j2\pi f$, where f is the center frequency, R_s is the source impedance, $C_\pi = C_{\tau_f} + C_{je}$, C_{τ_f} is the base-emitter diffusion capacitance and C_{je} is the base-emitter depletion capacitance. For this analysis, a narrowband system has been assumed. Also the C_{bc} has been ignored.

The OIP3 of the current driven CB-stage can be described by the following equation [6]:

$$OIP3_{CB,cd} \approx 2I_c\sqrt{\frac{R_s}{r_e}\left|\frac{1+sr_eC_\pi}{1+sR_sC_{je}}\right|}[A] \tag{4.2}$$

where $r_e = 1/g_m$ with g_m being the linear transconductance of the transistor.

The current driven situation occurs when $R_s \gg r_e$. Due to the higher bias current used for this thesis report, the g_m of the transistor is high, making the r_e low. Therefore, the CB-stage is current driven most of the time.

To verify whether a current driven CB-stage really performs better compared to a voltage driven CB-stage, two test setups have been made. In Figure 4.1 these circuits are shown.

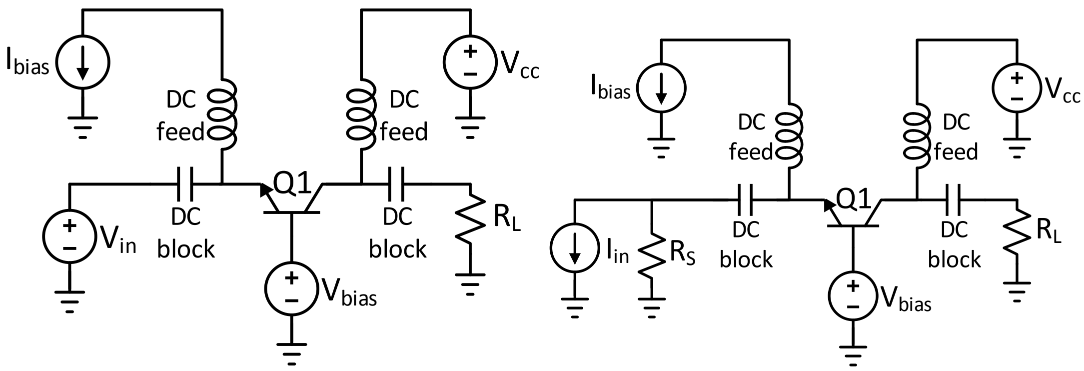

(a) Voltage driven (b) Current driven

Figure 4.1: Test circuits to compare voltage driven versus current driven CB-stages

The Q1 transistors have been implemented using a Gummel-Poon model and using a Mextram model. First the Gummel-Poon model will be studied. Just as in Chapter 3, the Gummel-Poon model will start with exponential distortion only, after which it will be expanded with the transit time τ_f, the depletion capacitance C_{je} and finally with the depletion capacitance C_{bc}. Then the Mextram model will replace the Gummel-Poon model. In all simulations, the biasing and applied signals remain the same. These conditions are given in Table 4.1.

The tone spacing has been kept constant. The center frequency will be swept from 1MHz to 60GHz. The f_t for the QUBiC4Xi BNA HV 0.5μm x 20.7μm x 25 is 50GHz when a bias current of 80mA is applied. The amplitudes of the tones have been chosen such that the IM3 currents are above the noise level, but the transistor is not in gain compression.

Table 4.1: Simulation conditions for studying the CB-stage

Parameter	**Description**	**Value**
I_{bias}	DC emitter current	80mA
V_{bias}	Base voltage	1.6V
V_{cc}	Supply voltage	3.3V
i_{in}	Amplitude of the input current for each tone	3mA
v_{in}	Amplitude of the input voltage for each tone	1mV
Δf	Tone spacing	1kHz
R_L	Load resistance	32Ω

For the current driven situation, $R_s = 500\Omega$. For the voltage driven situation $R_s = 0\Omega$, so Equation (4.1) simplifies to the following equation:

$$OIP3_{CB,vd} \approx \sqrt{8} I_c [A] \tag{4.3}$$

The OIP3 for the voltage driven CB-stage is the same as found for the CE-stage in Section 3.1.

4.1.1. EXPONENTIAL DISTORTION

When only the exponential distortion is present, the Equation (4.1) and Equation (4.2) simplify to the following equation:

$$OIP3_{CB,vd} \approx \sqrt{8} I_c [A] \tag{4.4}$$

$$OIP3_{CB,cd} \approx 2 I_c \sqrt{\frac{R_s}{r_e}} [A] \tag{4.5}$$

Since in the current driven CB-stage, R_s is 500Ω and r_e is $1/g_m$, the OIP3 is expected to be very high. The Gummel-Poon model for this simulation is given in Table 4.2. The simulation results can be seen in Figure 4.2.

Table 4.2: Gummel-Poon model for CB-stage with exponential distortion

Parameter	**Description**	**Value**
I_s	Saturation current	0.5fA
β	Forward current gain	2000
A	Area of the transistor	25
$f_{t@I_c=80mA}$	Cut off frequency	infinity

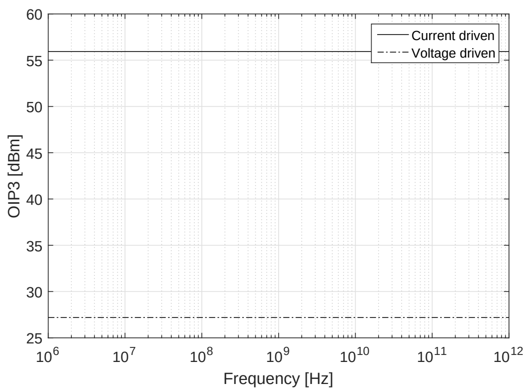

Figure 4.2: OIP3 versus frequency for a current driven and a voltage driven CB-stage modeled with only exponential distortion

The OIP3 is constant at 27dBm for the voltage driven CB-stage and 56dBm for the current driven CB-stage. As expected, the OIP3 is significantly higher for the current driven CB-stage. The OIP3 is not infinity due to the limited source impedance. The OIP3 of the voltage driven CB-stage is still rather high, which is due to the higher biasing current of 80mA.

4.1.2. ADDING τ_f

With addition of transit time τ_f, the diffusion capacitance C_{τ_f} is added to the equations. Since the equation for OIP3 of the voltage driven CB-stage is not dependent on the C_{τ_f}, it remains the same. Equation (4.2) describing the OIP3 for the current driven CB-stage simplifies to:

$$OIP3_{CB,cd} \approx 2 I_c \sqrt{\frac{R_s}{r_e} \left| 1 + s r_e C_{\tau_f} \right|} [A] \tag{4.6}$$

As can be seen, the OIP3 stays constant as long as $s r_e C_{\tau_f} \ll 1$. When $f = \frac{g_m}{2\pi C_{\tau_f}}$ [Hz], which is the f_t of this device, the OIP3 starts to increase. The Gummel-Poon model for the simulation with τ_f is given in Table 4.3.

Table 4.3: Gummel-Poon model for CB-stage with τ_f

Parameter	Description	Value
I_s	Saturation current	0.5fA
β	Forward current gain	2000
τ_f	Forward transit time	13ps
A	Area of the transistor	25
$f_{t@I_c=80mA}$	Cut off frequency	12GHz

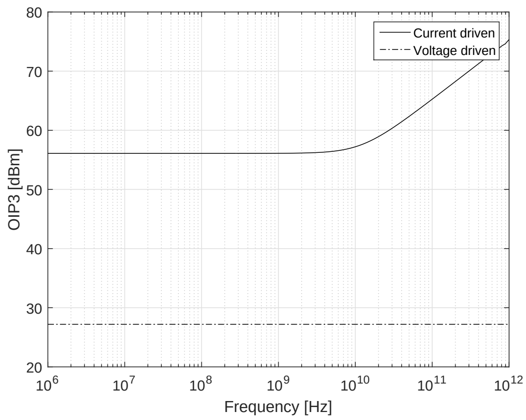

Figure 4.3: OIP3 versus frequency for a current driven and a voltage driven CB-stage with diffusion capacitance

The simulation results can be found in Figure 4.3.

As can be seen, the OIP3 is still high when the CB-stage is current driven. The OIP3 starts to increase around 10GHz, which corresponds to the theory, since the f_t of the device is 12GHz. The OIP3 of the voltage driven CB-stage is still 27dBm, suggesting that the exponential distortion is still dominant, as expected.

4.1.3. ADDING C_{je}

When the depletion capacitance C_{je} is added, the equation for the OIP3 stays the same for the voltage driven CB-stage. For the current driven situation, the OIP3 is described by Equation (4.2). According to this equation, the OIP3 starts to drop above the point $f = 1/(2\pi R_s C_{je})$. It stabilizes again around the f_t of the device. The Gummel-Poon model used for simulation has been given in Table 4.4. The simulation results can be found in Figure 4.4.

Table 4.4: Gummel-Poon model for CB-stage with C_{je}

Parameter	Description	Value
I_s	Saturation current	0.5fA
β	Forward current gain	2000
τ_f	Forward transit time	13ps
C_{je0}	Zero-bias base-emitter depletion capacitance	0.12pF
V_{je}	Built-in voltage of the base-emitter junction	0.7V
m_{je}	Grading coefficient of the base-emitter junction	1/3
A	Area of the transistor	25
$f_{t@I_c=80mA}$	Cut off frequency	11GHz

As can be seen, the OIP3 for the current driven CB-stage is still higher. As expected, it starts to roll off around 25MHz, which is the $1/(2\pi R_s C_\pi)$ frequency. The OIP3 settles around the f_t of the device. The OIP3 of the voltage driven CB-stage is still 27dBm, suggesting that it is still dominated by the exponential distortion.

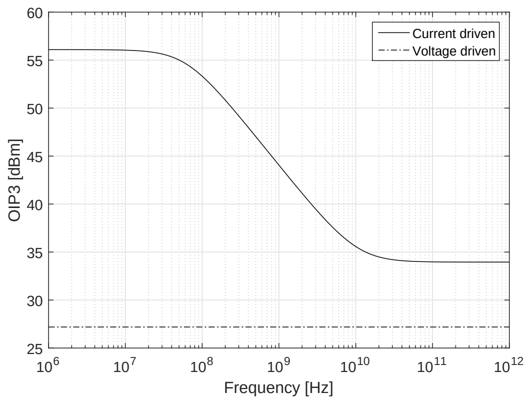

Figure 4.4: OIP3 versus frequency for a current driven and a voltage driven CB-stage with depletion capacitance C_{je}

4.1.4. ADDING C_{jc}

Just as in Section 3.4, the C_{jc} is the zero-bias base-collector capacitance. So when adding C_{jc}, C_{bc} distortion is expected. For the voltage driven CB-stage this does not have to strongly influence the OIP3, since the voltage driven CB-stage also has exponential distortion, tending to mask the additional C_{bc} distortion. For the current driven CB-stage, it is expected that the C_{bc} has more influence on the OIP3, since the exponential nonlinearity is low. For the voltage driven CB-stage, the C_{bc} distortion is expected to be dominant above the f_t of the device. The Gummel-Poon model used for the simulations is given in Table 4.5. The simulation results are given in Figure 4.5.

Table 4.5: Gummel-Poon model for CB-stage with C_{jc}

Parameter	Description	Value
I_s	Saturation current	0.5fA
β	Forward current gain	2000
τ_f	Forward transit time	13ps
C_{jc}	Zero-bias base-collector depletion capacitance	26fF
C_{je0}	Zero-bias base-emitter depletion capacitance	0.12pF
V_{je} & V_{jc}	Built-in voltage of the base-emitter and base-collector junction	0.7V
m_{je} & m_{jc}	Grading coefficient of the base-emitter and base-collector junction	1/3
A	Area of the transistor	25
$f_{t@I_c=80mA}$	Cut off frequency	11GHz

As expected, the OIP3 starts to drop at the f_t of the device for the voltage driven CB-stage. For the current driven CB-stage, the exponential distortion is very low, so the C_{bc} is dominant from lower frequencies onward. Also, the OIP3 starts to drop below 25MHz, so the drop in OIP3 cannot be attributed to the decreasing OIP3 due to C_{je}. Therefore, the C_{bc} distortion dominates the linearity for the current driven CB-stage.

4.1.5. CB-STAGE USING THE MEXTRAM MODEL

In this section, the Gummel-Poon model will be replaced by the Mextram model. The Mextram model is a more detailed model, influencing the OIP3. The f_t of the Mextram-modeled devices is at 50GHz. The simulations are shown in Figure 4.6.

As can be seen, the OIP3 of the current driven CB-stage is still better, although it is not so high as for the Gummel-Poon model. In the Gummel-Poon model used, the current gain β has been assumed to be constant. This constant β gives a high input impedance to the amplifier. However, in Mextram, the current gain is not only dependent on β and this results in a lowering of the input impedance of the transistor. For Equation (4.2) this would result in a decrease in the source impedance R_s. The OIP3 starts to decrease at higher frequencies due to the C_{bc}. The voltage driven CB-stage has a slightly better OIP3, due to the emitter

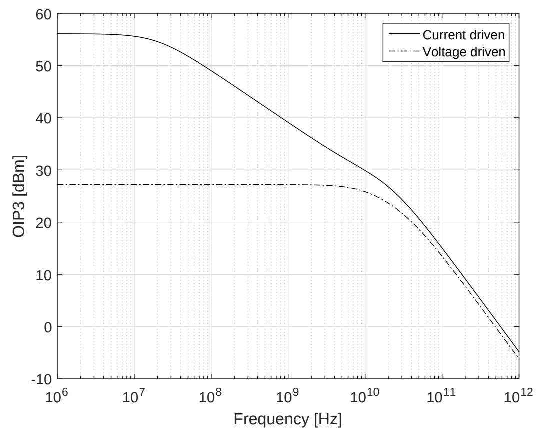

Figure 4.5: OIP3 versus frequency for a current driven and a voltage driven CB-stage with depletion capacitance C_{bc}

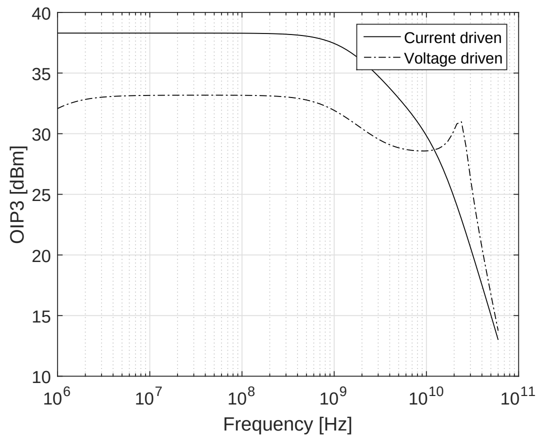

Figure 4.6: OIP3 versus frequency for a current driven and a voltage driven CB-stage using the Mextram model

resistance, increasing R_s. The nonlinear behavior of the voltage driven CB-stage at higher frequencies is not fully understood. It is believed that the exponential distortion and the C_{bc} distortion cancel each other shortly at 20GHz, but it is unknown where this mechanism comes from.

4.2. CASCODE AMPLIFIER

The cascode amplifier is commonly used for its improved frequency behavior, since it neutralizes the feedback effect of the C_{bc} capacitance of the CE-stage [8]. The cascode amplifier has as first stage a CE-stage, followed by the CB-stage. The differential cascode amplifier used in this section is shown in Figure 4.7. In the cascode amplifier, the CB-stage is driven by the CE-stage. The CE-stage has a high ohmic output, making the CB-stage current driven [8]. This should ensure that the contribution of the exponential distortion of the CB-stage in the cascode amplifier is small.

In this section, the linearity of the cascode amplifier will be examined. This analysis will start with the Gummel-Poon model. The Gummel-Poon model for the CE-stage includes the transit time τ_f and the depletion capacitances C_{je} and C_{bc} and is given in Table 4.5. The Gummel-Poon model of the CB-stage will be gradually expanded. First the exponent will be examined. Then the transit time τ_f and the depletion capacitance C_{je} are included. In the next step, the depletion capacitance C_{bc} will be included. Lastly all the Gummel-Poon models will be replaced by Mextram models. Gain compression will only be studied using the Mextram model, since the Mextram model incorporates more effects relevant for gain compression, like quasi-saturation, high injection etc. The simulation values used in this setup can be found in Table 4.6.

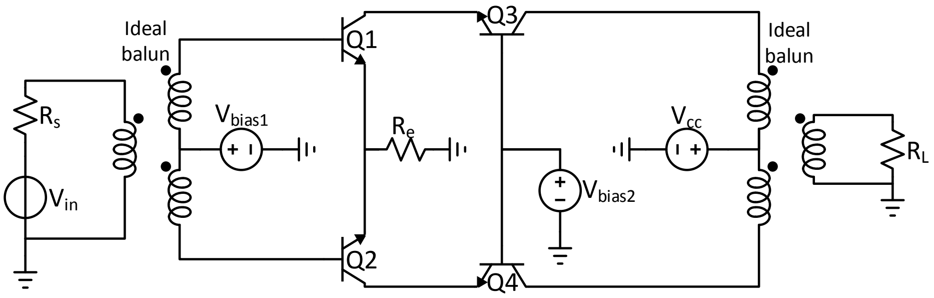

Figure 4.7: The differential cascode amplifier

Table 4.6: Simulation conditions for studying the cascode amplifier

Parameter	**Description**	**Value**
I_c	DC collector current	80mA
V_{bias}	Base voltage of the CB-stage	1.6V
V_{cc}	Supply voltage	3.3V
p_{rf}	Amplitude of the input power for each tone	-40dBm
f_c	Center frequency	1.8GHz
Δf	Tone spacing	1kHz
T_{in}	Turns ratio input balun	2:3
T_{out}	Turns ratio output balun	5:4

4.2.1. EXPONENTIAL DISTORTION

For the first simulation, only the exponential distortion is included in the Gummel-Poon model of the CB-stage. The output impedance of the CE-stage is high, so the CB-stage should be very linear. At the same time, the C_{bc} of the CE-stage should be neutralized, meaning that the exponential distortion of the CE-stage is dominant. To increase the OIP3, out-of-band matching has been used in the CE-stage, as described by [6]. Using an emitter resistance, emitter tuning has been used. Two simulations have been done. In the first simulation, the R_e has been swept, while I_c has been kept constant at 80mA. In the second simulation, the R_e and the I_c have been swept. A contour plot of the OIP3 has been made in the $R_e - I_c$ plane. The Gummel-Poon model of the CB-stage is given in Table 4.2. The simulation results are given in Figure 4.8.

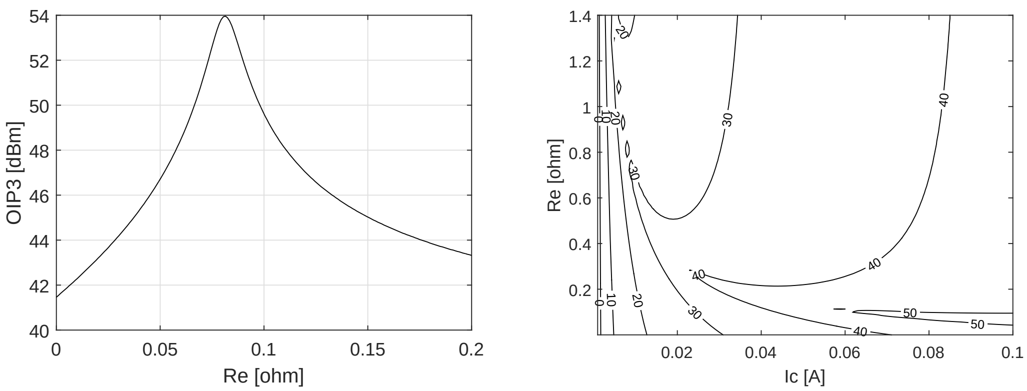

(a) R_e sweep, I_c=80mA

(b) R_e and I_c sweep

Figure 4.8: OIP3 versus R_e and OIP3 contours in the I_c-R_e plane for emitter tuning

When the results shown in Figure 4.8 are compared with those found in Figure 3.19 it becomes clear that the CB-stage significantly decreases the influence of the C_{bc} in the CE-stage. Like expected, the CB-stage does not add to the IM3, since it is current driven. The finite OIP3 is a result from the diffusion and depletion capacitances in the CE-stage. The diffusion capacitance can be counteracted by adding a capacitance in the emitter of the CE-stage or by correctly scaling the transistor [6]. However, later in this section it will be demonstrated that the diffusion and depletion capacitances in the CE-stage are not the dominating nonlinearities in the cascode amplifier, making the use of an emitter-capacitance not very effective.

4.2.2. ADDING τ_f AND C_{je}

In Section 4.1 it has become clear that the τ_f and C_{je} are not the dominating factors for OIP3 in the current driven CB-stage, but the C_{bc} is. Therefore, τ_f and C_{je} are added at the same time. Again, emitter tuning has been used to cancel the exponential distortion of the CE-stage. In Table 4.4 the Gummel-Poon model of the CB-stage has been given. The simulation results are shown in Figure 4.9.

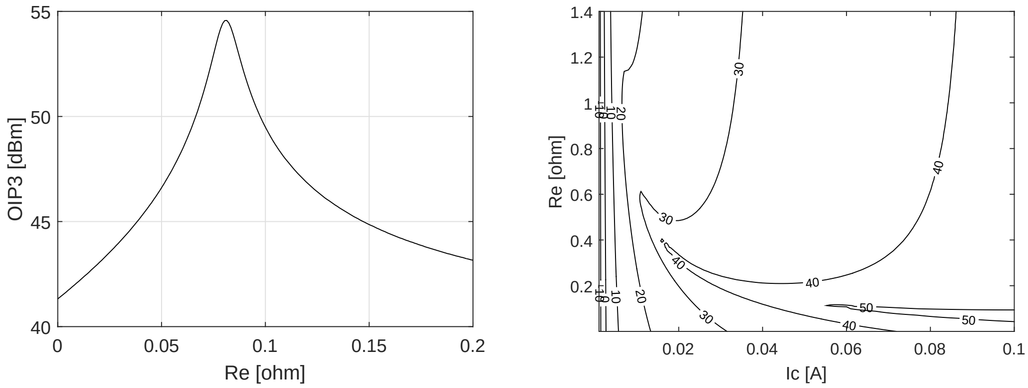

(a) R_e sweep, I_c=80mA (b) R_e and I_c sweep

Figure 4.9: OIP3 versus R_e and OIP3 contours in the I_c-R_e plane for emitter tuning

When comparing Figure 4.9 with Figure 4.8, it can be concluded that the results haven't changed. Again, due to the current driven conditions, the CB-stage is very linear. The diffusion and depletion capacitances of the CE-stage limit the OIP3 of the system.

4.2.3. ADDING C_{jc}

In Section 4.1, the C_{bc} has limited the OIP3 of the CB-stage for higher frequencies. Therefore, in this final step using the Gummel-Poon model, the C_{jc} variable is added to the Gummel-Poon model of the CB-stage. The complete Gummel-Poon model for the CB-stage can be found in Table 4.5. It is expected that the C_{bc} of the CB-stage limits the OIP3 when the exponential distortion of the CE-stage is canceled. The simulation results can be found in Figure 4.10.

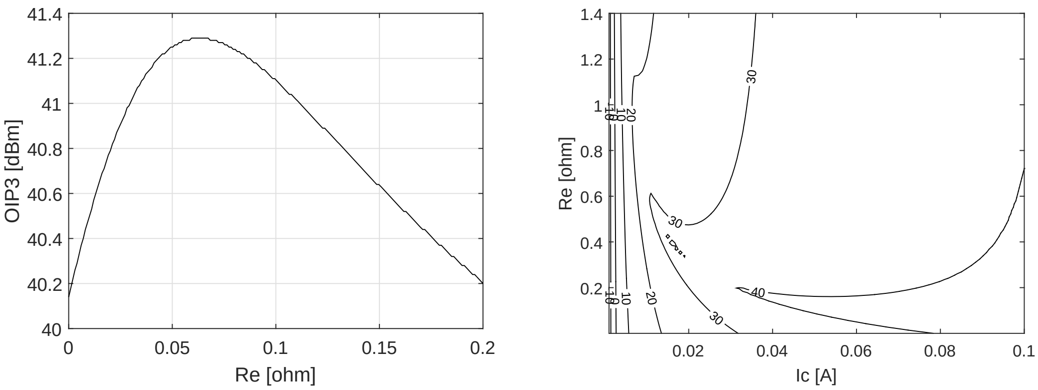

(a) R_e sweep, I_c=80mA (b) R_e and I_c sweep

Figure 4.10: OIP3 versus R_e and OIP3 contours in the I_c-R_e plane for emitter tuning

As can be seen, the OIP3 is limited to 41.3dBm. Even when the exponential distortion of the CE-stage has been canceled, the OIP3 is limited, showing that the C_{bc} of the CB-stage limits the OIP3 of the cascode amplifier when the exponential distortion is canceled.

4.2.4. CASCODE AMPLIFIER USING THE MEXTRAM MODEL

The cascode amplifier has been simulated using the Mextram model. The Mextram model is a more sophisticated model than the Gummel-Poon model. An important difference is the current dependency of the C_{bc} capacitance [20]. First strong nonlinearities will be discussed. Then the weak nonlinearities will be discussed.

GAIN COMPRESSION IN THE CASCODE AMPLIFIER

To prevent strong nonlinearities, the loadline needs to be chosen correctly. The bias voltage is 3.3V, which should prevent avalanche distortion in the CB-stage. The collector-emitter voltage V_{ce} of the CB-stage is 2.5V. The bias current is 80mA. Therefore a loadline of 31Ω single ended should give a good loadline in terms of achievable output power. This should result in a high P_{1dB}. The results can be found in Figure 4.11.

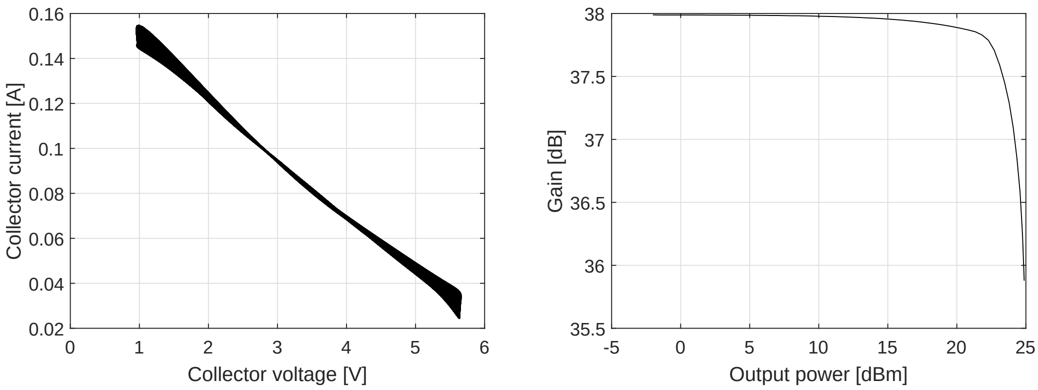

(a) Loadline (b) P_{1dB}

Figure 4.11: The loadline and P_{1dB} point for the differential cascode amplifier

The P_{1dB} of the system is at 24dBm, which is 6.5dB higher than the P_{1dB} of the differential CE-stage found in Chapter 3. A cascode amplifier can provide a higher P_{1dB} point than the CE-stage amplifier, if the supply voltage is increased. When this supply voltage is increased to ensure that the maximum allowable collector-emitter voltage of BV_{CEO} can be applied on the CB-stage, the cascode can deliver higher P_{1dB}. This is due to the decreased quasi-saturation present in the cascode amplifier. Quasi-saturation is induced at high currents by an internal voltage drop in the collector region, triggering a forward biased behavior inside the base-collector junction. This triggers charge accumulation in the base, reducing the collector current and therefore also reduces the current gain β of the device. In a CB-stage, the base is biased with a fixed voltage source. This voltage source will counteract the charge accumulation in the base, decreasing the effect of quasi-saturation. Therefore, the currents in a cascode amplifier can be higher, resulting in a higher P_{1dB}.

WEAK NONLINEARITIES IN THE CASCODE AMPLIFIER

To study the weak nonlinearities in the cascode amplifier, the OIP3 has been simulated. Emitter tuning has been used to cancel the exponential distortion. Two simulations have been done. In the first simulation, the current has been kept constant at 80mA, while the R_e has been swept. In the second simulation, both I_c and R_e have been swept and a contour plot of the OIP3 has been made. The results are shown in Figure 4.12.

As can be seen, the exponential distortion of the CE-stage is dominant for most R_e-I_c combinations. When the R_e is chosen correctly, cancellation occurs. In these cancellation points, the C_{bc} distortion of the CB-stage limits the OIP3. The cancellation point for the exponential distortion occurs for a lower R_e value than in the Gummel-Poon model. This is due to the emitter resistance that is already present in the transistor itself. Just as for the differential CE-stage, the differential cascode amplifier has a linearity problem due to the

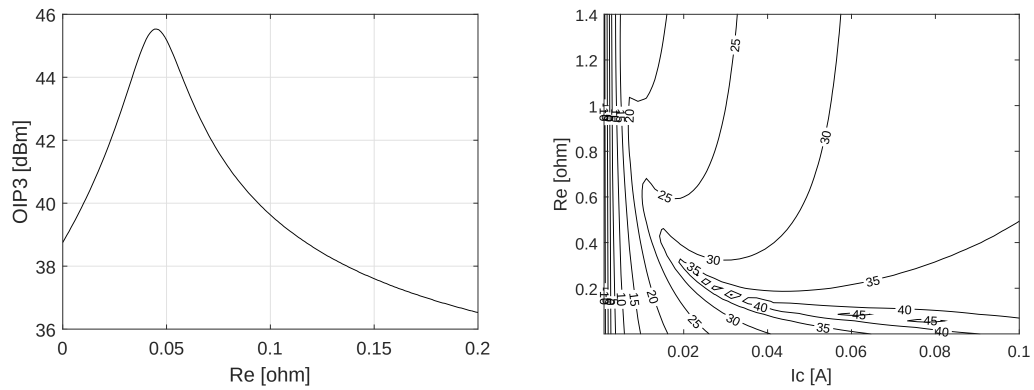

(a) R_e sweep, I_c=80mA

(b) R_e and I_c sweep

Figure 4.12: OIP3 versus R_e and OIP3 contours in the I_c-R_e plane for emitter tuning

C_{bc} distortion. However, in the cascode amplifier, the C_{bc} generating the most distortion is not a feedback element, while it is a feedback element in the CE-stage. Therefore, the nonlinearity is not amplified, giving the cascode amplifier a higher OIP3.

4.3. CHARACTERISTICS OF THE C_{bc} IN THE CASCODE AMPLIFIER

In Section 4.1 it has been demonstrated that the OIP3 of the CB-stage is limited by the C_{bc} capacitance, if the CB-stage is current driven. In Section 4.2 it has been demonstrated that the OIP3 of the cascode amplifier is limited by the C_{bc} of the CB-stage, when the exponential distortion is canceled. Therefore, this section will discuss a method that can be used to analyze the nonlinear behavior of the C_{bc} capacitance in the CB-stage.

The simplified large signal model of the CB-stage can be found in Figure 4.13. In the CB-stage the

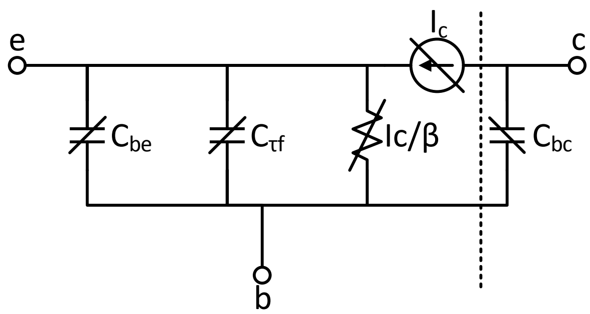

Figure 4.13: The simplified large signal model of the CB-stage

base is normally AC-grounded, which means that the C_{bc} is in parallel with the output of the CB-stage. The exponential distortion of the CB-stage can be ignored, if the CB-stage is current driven. This means that if the CB-stage is current driven by a linear device, the only nonlinearity would be the C_{bc} capacitance. Therefore, the amplifier can be modeled as a current source with a parallel C_{bc} capacitance for simple Volterra analyses.

In Figure 4.14 the simple model for the Volterra analysis is given. The complete Volterra analysis can be found in Appendix A.1.

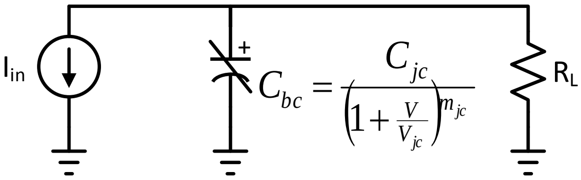

Figure 4.14: The simple large signal model for Volterra analysis of the C_{bc} capacitance

The Volterra analysis for this simple model gives the following equations for OIP3:

$$OIP3_{low} \approx 2\sqrt{\left|\frac{1}{(2s_1 - s_2)R_L^3\left[3K_{3C_{bc}} - 2K_{2C_{bc}}^2 \cdot R_L \cdot (3s_1 - s_2)\right]}\right|}[A] \tag{4.7}$$

$$OIP3_{high} \approx 2\sqrt{\left|\frac{1}{(2s_2 - s_1)R_L^3\left[3K_{3C_{bc}} - 2K_{2C_{bc}}^2 \cdot R_L \cdot (3s_2 - s_1))\right]}\right|}[A] \tag{4.8}$$

where $s_1 = j2\pi f_1$ and $s_2 = j2\pi f_2$, with $f_1 < f_2$ being the fundamental frequencies, $K_{3C_{bc}}$ is the third order Taylor coefficient of C_{bc} and $K_{2C_{bc}}$ is the second order Taylor coefficient of C_{bc}. The second order and third order Taylor coefficients are described by the following equations [12]:

$$K_{2C_{bc}} = -\frac{1}{2} \cdot \frac{m}{V_{jc} + V} \cdot C_{bc}[F/V] \tag{4.9}$$

$$K_{3C_{bc}} = \frac{1}{6} \cdot \frac{(m+1)m}{(V_{jc} + V)^2} \cdot C_{bc}[F/V^2] \tag{4.10}$$

where m is the grading coefficient of the base-collector junction, V_{jc} is the built-in voltage of the base-collector junction, V is the DC-voltage on the base-collector junction and C_{bc} is the DC value of the base-collector capacitance. In Figure 4.15, $K_{2C_{bc}}$ and $K_{3C_{bc}}$ have been given for the QUBiC4Xi BNA HV 0.5μm x 20.7μm x 1 device, modeled with the Gummel-Poon model and with the Mextram model.

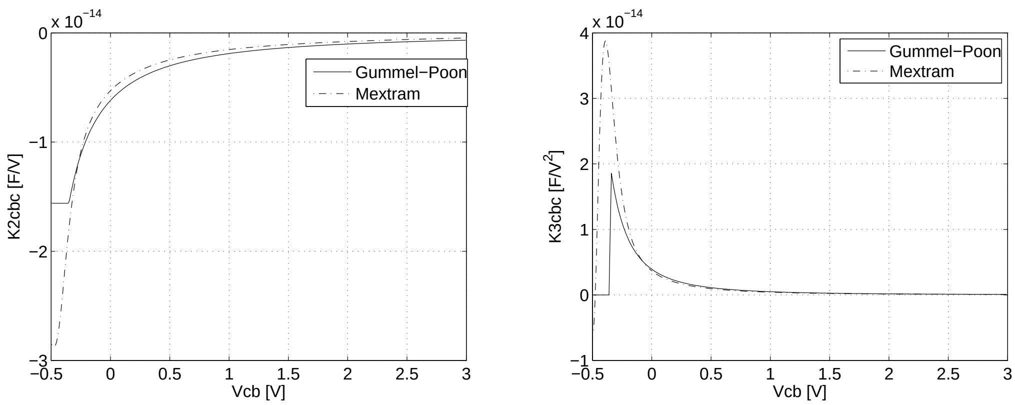

(a) $K_{2C_{bc}}$ (b) $K_{3C_{bc}}$

Figure 4.15: $K_{2C_{bc}}$ and $K_{3C_{bc}}$ for the QUBiC4Xi BNA HV 0.5μm x 20.7μm x 1

When we short the even harmonics and intermodulation products, Equation (4.7) and (4.8) simplify to:

$$OIP3_{low} \approx 2\sqrt{\left|\frac{1}{3(2s_1 - s_2)R_L^3 K_{3C_{bc}}}\right|}[A] \tag{4.11}$$

$$OIP3_{high} \approx 2\sqrt{\left|\frac{1}{3(2s_2 - s_1)R_L^3 K_{3C_{bc}}}\right|}[A] \tag{4.12}$$

According to these equations, the OIP3 due to the C_{bc} should drop for higher frequencies. A higher biasing voltage or a lower load impedance would improve the OIP3. However, the biasing voltage and load impedance are set in the CB-stage by output power considerations, so a high P_{1dB} can be reached. Therefore, the C_{bc} capacitance can only be linearized using special compensation techniques, if optimization between P_{1dB} and $OIP3$ needs to be avoided.

4.3.1. ANTI-PARALLEL C_{bc} COMPENSATION

The concept of anti-parallel C_{bc} compensation is shown in Figure 4.16.

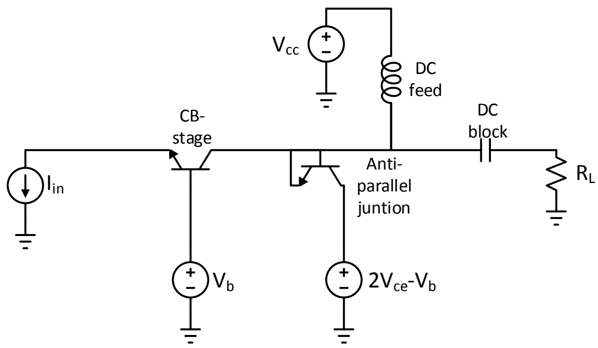

Figure 4.16: Anti-parallel C_{bc} compensation

The principle of anti-parallel compensation is easy to explain: the anti-parallel junction is connected with the base to the collector of the CB-stage. The collector of the anti-parallel junction is biased such that the voltage on the C_{bc} of the anti-parallel junction is exactly the same as on the C_{bc} of the CB-stage. Anti-parallel C_{bc} compensation has been first described for variable-capacitance diodes (varactors) in [21]. The Taylor formula's for the capacitances can be described by the following equations [21]:

$$C_1(v) = K_0 + K_1 v + K_2 v^2 + ...[F] \tag{4.13}$$

$$C_2(v) = L_0 - L_1 v + L_2 v^2 + ...[F] \tag{4.14}$$

where C_1 is the C_{bc} capacitance, K_0 is the first order Taylor coefficient of the C_{bc} capacitance, K_1 is the second order Taylor coefficient of the C_{bc} capacitance, K_2 is the third order Taylor coefficient of the C_{bc} capacitance, C_2 is the anti-parallel C_{bc} capacitance, L_0 is the first order Taylor coefficient of the anti-parallel C_{bc} capacitance, L_1 is the second order Taylor coefficient of the anti-parallel C_{bc} capacitance, L_2 is the third order Taylor coefficient of the anti-parallel C_{bc} capacitance and v is the voltage on the output node of the CB-stage.

The total capacitance can then be calculated as [21]:

$$C_T = (K_0 + L_0) + (K_1 - L_1)v + (K_2 + L_2)v^2 + ...[F] \tag{4.15}$$

As can be seen, the second Taylor coefficient cancels if the capacitances are identical, but the third does not. Therefore, second order harmonics and intermodulation products cancel, but the third order harmonics and intermodulation products don't. This can be advantageous in a single ended system, if the even order out-of-band components need to be canceled. However, in a differential circuit, the balun already cancels the even order out-of-band components. Also the IM3 increases when the second order harmonics and intermodulation products are canceled as can be seen in Equation (4.7), (4.8) and [21].

Although the anti-parallel junction lowers IM3, it can be used when the second order harmonics and intermodulation products need to be canceled. In Chapter 5 and Chapter 6 structures for future investigation are proposed making use of the anti-parallel configuration. Please notice that this analysis is only valid as long as the Gummel-Poon estimation of the C_{bc} capacitance is used. When Mextram is used, the current dependency is included [20], which could influence the conclusions of this analysis.

4.4. CONCLUSIONS

In this chapter, the influence of the CB-stage on the nonlinearity performance of the bipolar amplifier has been studied. In Section 4.1 the CB-stage has been studied. It has been concluded that for the current driven CB-stage, the exponential distortion has been canceled up to the f_t of the device. For the voltage driven CB-stage, the exponential distortion is dominant for almost the whole frequency range. The current driven CB-stage is dominated by C_{bc} distortion even for lower RF-frequencies. The voltage-driven CB-stage is only dominated by C_{bc} distortion for higher frequencies, above the f_t of the device.

In Section 4.2 the differential cascode has been studied. Using the Gummel-Poon model, it can be concluded that the C_{bc} of the CB-stage is dominant for OIP3 if the exponential distortion of the CE-stage has been canceled. When the C_{bc} of the CB-stage is not included in the Gummel-Poon model, the diffusion and depletion capacitances of the CE-stage seem to limit the OIP3. The C_{bc} capacitance of the CE-stage is neutralized by the CB-stage, resulting in a high OIP3. It has also been demonstrated that the cascode amplifier has a larger P_{1dB} point than the CE-stage amplifier, when the supply voltage is increased, due to the decreased quasi-saturation.

In Section 4.3, a simple model for the C_{bc} of the CB-stage has been proposed to simplify Volterra analysis. From Volterra analysis it could be concluded that the frequency, biasing voltage and load resistance could be changed to increase the OIP3. However, these variables are already used for other considerations in the design, like the output power in terms of P_{1dB}. To get a more orthogonal design, circuit solutions have to be made to counteract the C_{bc} distortion. These can be found in Chapter 5, Chapter 6 and Chapter 7. Also anti-parallel C_{bc} compensation has been studied. It has been argued that the anti-parallel configuration would not increase the OIP3 of the cascode amplifier. It would cancel the second order harmonics and intermodulation products, making it an interesting option for use in combination with other C_{bc} compensation circuits.

5

OUT-OF-BAND MATCHING FOR C_{bc} DISTORTION

In Chapter 4, it has been demonstrated that the C_{bc} distortion of the CB-stage is dominant for OIP3 performance in a cascode amplifier, if the exponential distortion of the CE-stage has been canceled. Therefore, to improve the OIP3 of the cascode amplifier, the impact of the nonlinear C_{bc} capacitance needs to be compensated. As Chapter 4 shows, the C_{bc} capacitance of the CB-stage is dominant for its linearity. To cancel the IM3 components of this C_{bc} capacitance, out-of-band matching has been evaluated. As described in [6], out-of-band matching has significant advantages over in-band compensation techniques. It does not compromise on gain and power consumption [6]. Therefore it is an important candidate for cancellation of the C_{bc} nonlinearities. With out-of-band matching, the impedances at the baseband and second harmonic frequencies have been designed independently from the impedance at the fundamental frequencies. Since nonlinear components create nonlinear currents at the baseband and second harmonic frequency, changing these impedances influences the voltage at the baseband and second harmonic frequency. This change in voltage is crucial. Since the baseband and second harmonic voltage mix with the voltages on the fundamental frequency and create an IM3 current that is superimposed on the IM3 components resulting from the direct third order mixing. When the impedances at the baseband and second harmonic frequency are chosen properly, the indirect mixing will counteract the IM3 current created through direct mixing resulting in a highly linear operation. The basic principle of this phenomena is illustrated in Figure 5.1 [19].

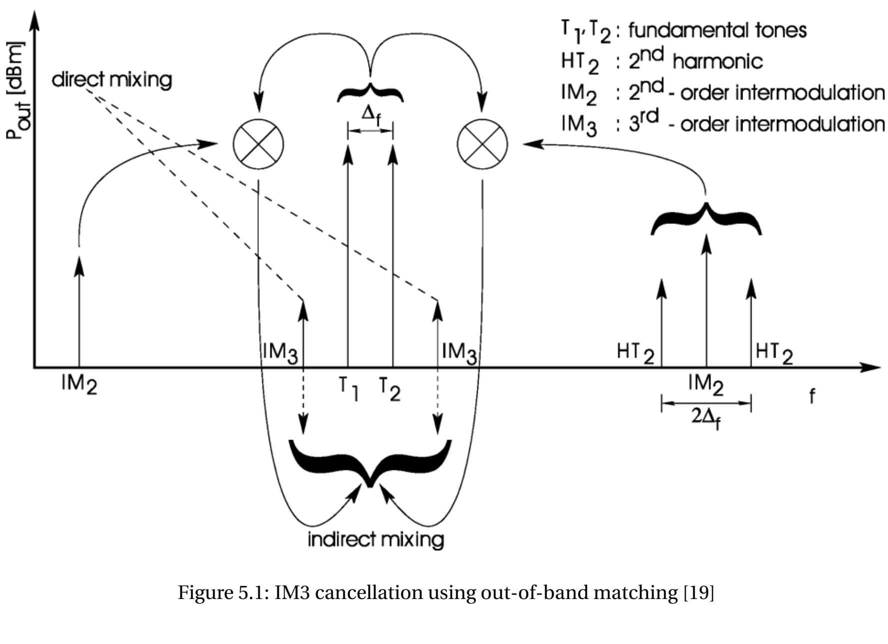

Figure 5.1: IM3 cancellation using out-of-band matching [19]

This chapter will discuss the possibilities of out-of-band matching for C_{bc} cancellation. In Section 5.1 the option for out-of-band cancellation will be discussed when only the CB-stage is considered. It will show that there is indeed an option for out-of-band matching. However, in Section 5.2, it will be demonstrated that the CE-stage has influence on this out-of-band C_{bc} cancellation in a cascode configuration. This influence is problematic for the out-of-band C_{bc} cancellation, as will be shown in Section 5.2. In Section 5.3 the underlying problem will be addressed. The chapter will finish with conclusions in Section 5.4. Since out-of-band matching for C_{bc} distortion could not be fully finished within the scope of this project, Section 5.4 will also give suggestions which path to take in further research on out-of-band matching for C_{bc} cancellation.

5.1. OUT-OF-BAND MATCHING FOR C_{bc} COMPENSATION

To see whether out-of-band matching is a viable option for the C_{bc} capacitance, Volterra analysis and simulations have been used. Since Volterra analyses can lead to extensive expressions, the circuit used for Volterra analysis has been kept simple. Since the C_{bc} of the CB-stage is the nonlinearity of interest, a current driven, single ended CB-stage has been used for the Volterra analysis. Since the CB-stage has been current driven, the exponential distortion can be neglected, as discussed in Chapter 4. The transit time τ_f and depletion capacitance C_{je} have been ignored. Therefore, the CB-stage can be modeled as a current source in parallel with the C_{bc} capacitance, as has been demonstrated in Section 4.3. In Section 5.2, out-of-band C_{bc} cancellation in the differential cascode will be discussed.

5.1.1. VOLTERRA ANALYSIS OF OUT-OF-BAND MATCHING FOR THE C_{bc} CAPACITANCE

The model used for Volterra analysis is given in Figure 5.2.

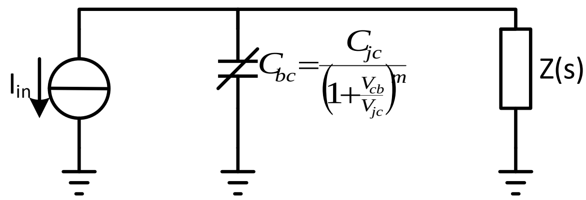

Figure 5.2: The circuit used for Volterra analysis of out-of-band matching of the C_{bc} capacitance

The complete Volterra analysis can be found in Appendix A.2. In this section, the main conclusions will be discussed. For the Volterra-analysis, the Gummel-Poon approximation of the C_{bc} has been used. Therefore, the current dependency has not been included, meaning that this compensation might not yield the expected results when the Mextram model will be used. There are two IM3 currents created by the C_{bc}, which are $IM3_{low}$ at $2 \cdot f_1 - f_2$ and $IM3_{high}$ at $2 \cdot f_2 - f_1$. Equation (5.1) and (5.2) describe the $IM3_{low}$ and $IM3_{high}$ currents created by the C_{bc} capacitance:

$$i_{IM3L,C_{bc}} = (2 \cdot s_1 - s_2) \cdot H_1(s_1)^2 H_1(-s_2) \left[K_{3C} + \frac{2}{3} K_{2C}^2 (2 \cdot (s_1 - s_2) H_2(s_1 - s_2) + 2 s_1 H_2(2 s_1)) \right] [1/A^2] \quad (5.1)$$

$$i_{IM3H,C_{bc}} = (2 \cdot s_2 - s_1) \cdot H_1(s_2)^2 H_1(-s_1) \left[K_{3C} + \frac{2}{3} K_{2C}^2 (2 \cdot (s_2 - s_1) H_2(s_2 - s_1) + 2 s_2 H_2(2 s_2)) \right] [1/A^2] \quad (5.2)$$

where $s_1 = j \cdot 2\pi f_1$, $s_2 = j \cdot 2\pi f_2$, H_1 is the linear transfer between the input current and the voltage, K_{3C} is the third Taylor coefficient of the C_{bc}, K_{2C} is the second Taylor coefficient of the C_{bc} and H_2 is the linear transfer between the nonlinear current source and the voltage. The Taylor coefficients of the C_{bc} are given by the following equations [12]:

$$K_{2C_{bc}} = -\frac{1}{2} \cdot \frac{m}{V_{jc} + V_{bias}} \cdot C_{bc,bias} [F/V] \quad (5.3)$$

$$K_{3C_{bc}} = \frac{1}{6} \cdot \frac{(m+1)m}{(V_{jc} + V_{bias})^2} \cdot C_{bc,bias} [F/V^2] \quad (5.4)$$

where $C_{bc,bias}$ is the value of the C_{bc} capacitance at the biasing point, m is the grading coefficient of the base-collector junction, V_{jc} is the built-in voltage of the collector-base junction and V_{bias} is the DC bias voltage on the collector-base junction. In this chapter, a narrowband situation has been assumed. Therefore $|s_1 - s_2| = \Delta s$ and $s_1 \approx s_2 = s$. To improve the OIP3, the expressions from Equation (5.1) and Equation (5.2) need to be 0. In a narrowband situation, this leads to Equation (5.5):

$$2sH(2s) + 2\Delta sH(\Delta s) = -\frac{3}{2}\frac{K_{3C}}{K_{2C}^2} \tag{5.5}$$

From Equation (A.14) H can be found. If this H_2 and the Taylor coefficients from Equation (5.3) and (5.4) are filled in Equation (5.5), the following equation is found:

$$2s\frac{Z(2s)}{2s \cdot C_{bc,bias} \cdot Z(2s) + 1} + 2\Delta s\frac{Z(\Delta s)}{\Delta s \cdot C_{bc,bias} \cdot Z(\Delta s) + 1} = \frac{m+1}{mC_{bc,bias}} \tag{5.6}$$

where $Z(2s)$ is the impedance of Z at the second harmonic and $Z(\Delta s)$ is the impedance of Z at the baseband frequency. When the tone spacing of the system changes, $Z(2s)$ is affected, but not as much as $Z(\Delta s)$. To keep the system as wideband as possible, the Δs term needs to be removed from the equation. There are two options to accomplish this:

1. Make $Z(\Delta s)$ very large, such that $\Delta s \cdot C_{bc,bias} \cdot Z(\Delta s) \gg 1$
2. Make $Z(\Delta s)$ zero, so that the term dependent on Δs becomes zero

Both options are tried in Appendix A.2. The following equations for $Z(2s)$ can be derived:

$$Z(2s) = j \cdot \frac{m-1}{2m-1}\frac{1}{2\pi \cdot (2f_1)C_{bc,bias}}[\Omega] \tag{5.7}$$

$$Z(2s) = j \cdot \frac{m+1}{2\pi \cdot (2f_1)C_{bc,bias}}[\Omega] \tag{5.8}$$

where Equation (5.7) refers to option 1 and Equation (5.8) refers to option 2. If in Equation (5.7) the grading coefficient m gets between $\frac{1}{2}$ and 1, the expression becomes negative. So in that case, a negative imaginary impedance (a capacitance) would give cancellation. However, in all other situations, a positive imaginary impedance, an inductor, gives cancellation. The QUBiC4Xi BNA HV transistor has a grading coefficient smaller than $\frac{1}{2}$, so an inductor should give cancellation of the IM3 components of the C_{bc}.

When an inductor is used, situation 2 becomes more likely, since an inductor can also deliver a short at baseband frequencies. Therefore, Equation (5.8) gives the best option for cancellation when the QUBiC4Xi technology is used.

Although the out-of-band impedance needs to be positive imaginary, so an inductor, it is inversely proportional to the frequency. This means that the required inductor value will vary as a function of frequency, making the solution narrowband. When the grading coefficient m gets between $\frac{1}{2}$ and 1, a capacitor can be used, which is inverse proportional to frequency, making this solution more wideband. However, most processes result in a grading coefficient below $\frac{1}{2}$.

5.1.2. SIMULATIONS OF OUT-OF-BAND MATCHING FOR THE C_{bc} CAPACITANCE

To verify the Volterra analysis, a simulation has been done with a single CB-stage that is current driven. Figure 5.3 gives the circuit used for this simulation.

The biasing current I_c has been chosen at 80mA, the biasing voltage V_{bias} at 1.6V and the supply voltage V_{cc} at 3.3V. The biasing is therefore the same as the biasing that has been used in Section 4.2. Therefore, to get the correct loadline and a high P_{1dB}, a load of 31Ω is needed. Therefore $Z(s)$ has been made 31Ω.

I_{in} provides the currents at the fundamental frequencies $f_1 = 1.795$GHz and $f_2 = 1.805$GHz. The currents at the fundamental frequency have an amplitude of 0.1 mA for each tone. With a two-tone test, the $OIP3_{low}$ and the $OIP3_{high}$ have been determined. Z_1 is a compensation inductor L_{com}. For the reference simulation,

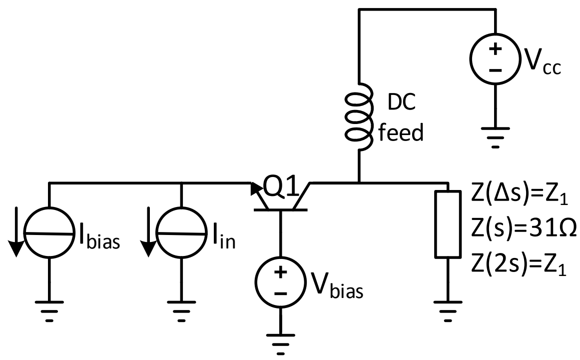

Figure 5.3: A current driven CB-stage with out-of-band matching for C_{bc} linearization

Table 5.1: Gummel-Poon parameters for studying out-of-band C_{bc} cancellation

Parameter	**Description**	**Value**
β	Forward current gain	2000
I_s	Saturation current	0.5fA
τ_f	Transit time	13ps
C_{je0}	Zero-bias base-emitter depletion capacitance	0.12 pF
C_{jc}	Zero-bias base-collector depletion capacitance	26fF
V_{je} & V_{jc}	Built-in voltage of the base-emitter and base-collector junction	0.7V
m_{je} & m_{jc}	Grading coefficient of the base-emitter and base-collector junction	1/3
A	Area transistor	25

Z_1 has been made 31Ω, which is the same impedance as the impedance on the fundamental frequency. In Table 5.1 the Gummel-Poon parameters used for the Q1 transistor have been given. In Figure 5.4a the OIP3 values as function of L_{com} are given.

As can be seen, the OIP3 has a minimum and a maximum. At the maximum value, the OIP3 reaches 50dBm, which is 18dB better than the reference OIP3. At the minimum value, L_{com} and the C_{bc} come into resonance at the second harmonic frequency, resulting in a high H_2. This results in a low OIP3, as can be concluded from Equation (5.1) and (5.2). Very close to this minimum OIP3 value is the optimum OIP3 value, making this cancellation very sensitive to process variations.

For the optimum inductor value, a sweep over tone spacing Δf has been done. The results can be

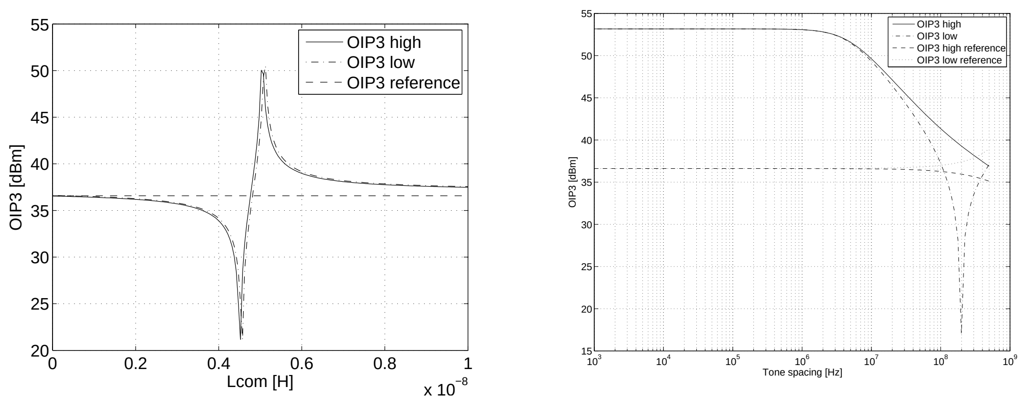

(a) $OIP3$ vs L_{com} (b) $OIP3$ vs tone spacing

Figure 5.4: The simulations results for out-of-band C_{bc} cancellation in a single ended CB-stage

seen in Figure 5.4b. The OIP3 values start to divert at 10MHz, confirming the expectation that perfect cancellation has a narrowband character. However, the OIP3 remains above the reference level up to 100MHz, making the compensation wideband.

5.2. INFLUENCE OF CE-STAGE ON OUT-OF-BAND MATCHING

In a real amplifier, the CB-stage is preceded by a CE-stage, to form a cascode amplifier. As discussed in Chapter 4, a cascode has the dominant C_{bc} nonlinearity in the CB-stage: the nonlinear C_{bc} capacitance in the CE-stage is not dominant. Therefore, out-of-band matching should also be possible in the cascode amplifier. To make out-of-band matching easier, a differential cascode has been used. The circuit used has been shown in Figure 5.5. In this amplifier, the R_e resistance is used to cancel the exponential distortion of

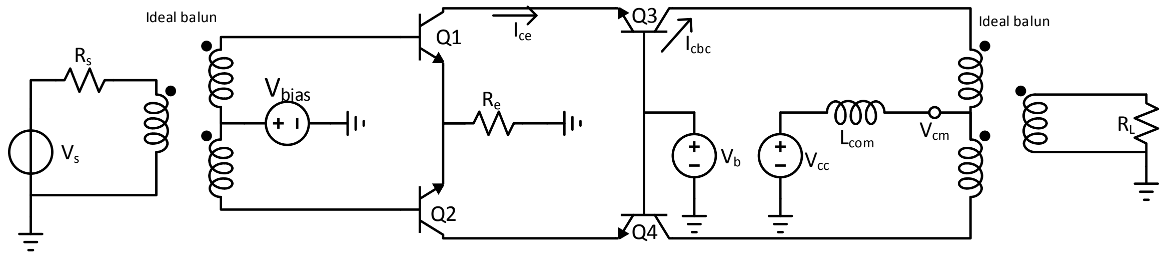

Figure 5.5: The differential cascode amplifier with out-of-band matching to C_{bc} linearization

the CE-stage, while the L_{com} is used to cancel the C_{bc} distortion of the CB-stage. The simulation values are given in Table 5.2. The Gummel-Poon model is given in Table 5.3. In this setup, the simulation values are

Table 5.2: Simulation conditions for studying out-of-band C_{bc} cancellation in the cascode amplifier

Parameter	Description	Value
I_c	DC collector current	80mA
R_e	Emitter resistance	80.4mΩ
V_b	Base voltage of the CB-stage	1.6V
V_{cc}	Supply voltage	3.3V
p_{rf}	Amplitude of the input power for each tone	-40dBm
f_c	Center frequency	1.8GHz
Δf	Tone spacing	10MHz
T_{in}	Turns ratio input balun	2:3
T_{out}	Turns ratio output balun	5:4

Table 5.3: Gummel-Poon parameters for studying out-of-band C_{bc} cancellation in the cascode amplifier

Parameter	Description	Value
β	Forward current gain	2000
I_s	Saturation current	0.5fA
τ_f	Transit time	13ps
C_{je0}	Zero-bias base-emitter depletion capacitance	0.12 pF
C_{jc}	Zero-bias base-collector depletion capacitance	26fF
V_{je} & V_{jc}	Built-in voltage of the base-emitter and base-collector junction	0.7V
m_{je} & m_{jc}	Grading coefficient of the base-emitter and base-collector junction	1/3
A	Area transistor	25

the same as in Section 4.2. Since the setup has only been tested with the Gummel-Poon model, no P_{1dB} has been done. However, since the compensation has been done out-of-band, it is expected that the influence on the P_{1dB} is low.

Just as with the single ended CB-stage, the L_{com} inductor is swept to see whether there is still an optimum. To obtain a reference OIP3, the L_{com} inductor has been shorted. Figure 5.6 shows the results of this simulation.

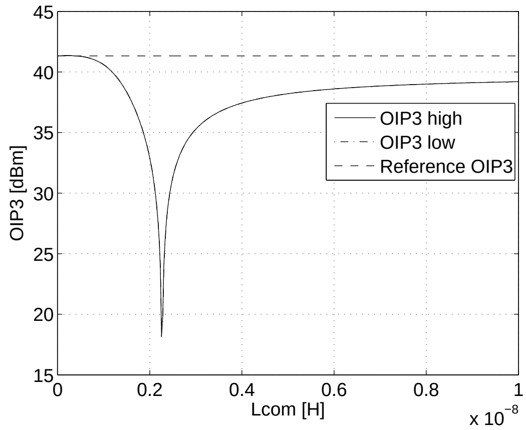

Figure 5.6: The OIP3 in a cascode amplifier with an out-of-band inductor to linearize the C_{bc} capacitance

As can be seen, the OIP3 doesn't improve anywhere, so the optimum found in Figure 5.4a is gone. As seen in Section 4.2, the C_{bc} of the CB-stage is dominant for the distortion, since the exponential distortion from the CE-stage has been canceled using the emitter tuning. Therefore, the OIP3 should improve due to the out-of-band matching. The OIP3 does not improve, suggesting that the IM2 and HD2 voltages are not the same as anticipated. The OIP3 does have a minimum, since the inductor L_{com} and C_{bc} can still resonate for the HD2 frequency, causing a high HD2 voltage. This results in extra high IM3 currents created by the C_{bc} as can be seen from Equation (5.1) and (5.2).

Out-of-band matching works by influencing the IM2 and HD2 voltages on the nonlinear components. The nonlinear components create IM2 and HD2 currents, and an out-of-band impedance translates this into a certain IM2 and HD2 voltage. Since in this case, neither the IM2 and HD2 currents of the C_{bc} capacitance have been changed, nor has the out-of-band impedance, other IM2 and HD2 currents have to be present to disrupt the cancellation mechanism. Since the CE-stage is the only new stage in this analysis, the IM2 and HD2 currents should come from the CE-stage.

The IM2 and HD2 currents produced by C_{bc} of the CB-stage should only be visible at the output of the CB-stage, since the CB-stage is unilateral in this case. Therefore, the currents I_{ce} and I_{cbc} from Figure 5.5 should add up. The IM2 and HD2 currents from the CE-stage have a different phase and amplitude than those of the CB-stage, influencing the cancellation. To provide evidence that the IM2 and HD2 currents of the CE-stage are problematic for the cancellation, a circuit has been made where the IM2 and HD2 currents of the CE-stage are shorted. This circuit is shown in Figure 5.7.

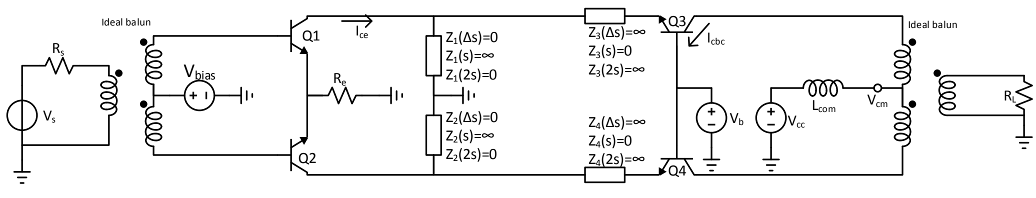

Figure 5.7: A cascode amplifier with shorted IM2 and HD2 currents from the CE-stage

To prevent voltage driven conditions on the IM2 and HD2 frequencies for the CB-stage, an open is added on these frequencies. Although Figure 5.7 doesn't show DC-feed and DC-block components, these have been added in the simulations to ensure correct biasing conditions for the CE-stage and CB-stage. The simulation values have been given in Table 5.2 and the Gummel-Poon model used has been given in Table 5.3. For the reference OIP3, the L_{com} inductor has been shorted. The results of this simulation is given in Figure 5.8.

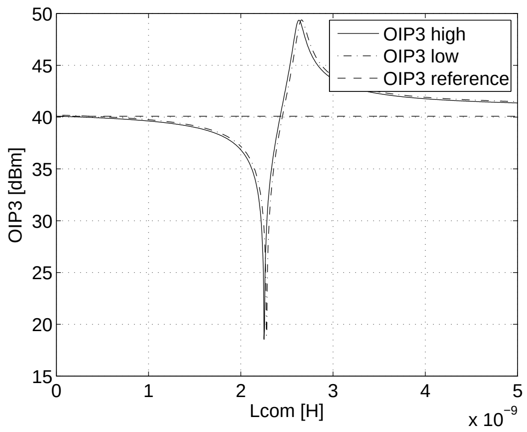

Figure 5.8: The OIP3 in the differential cascode amplifier when the IM2 and HD2 currents of the CE-stage are blocked

As can be seen, there is a cancellation point again, with OIP3 figures around 49dBm, which is an 9dB improvement on OIP3. Since now only the IM2 and HD2 currents from the CB-stage are present at the output, this confirms that the IM2 and HD2 currents of the CE-stage interfere with the out-of-band matching for the C_{bc}.

For out-of-band matching, the IM2 and HD2 voltages are important. These voltages will create an IM3 current when they mix with the fundamental tone. Therefore the out-of-band impedance could be changed, so the changed IM2 and HD2 currents do not interfere with the C_{bc} cancellation anymore. For this purpose, the circuit shown in Figure 5.9 has been created.

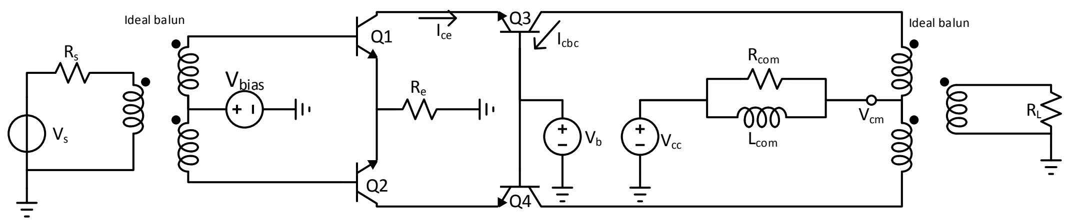

Figure 5.9: The cascode amplifier with adapted an out-of-band impedance for C_{bc} cancellation

When this circuit has been simulated, L_{com} and R_{com} have been swept. Using contour plots, the optimal L_{com}-R_{com} combination can be found. The simulation values have been given in Table 5.2 and the Gummel-Poon model used has been given in Table 5.3. In Figure 5.10 the simulation results have been given.

As can be seen, a cancellation point can be found. However, this cancellation point requires the use of a negative resistance at the common mode point. Negative resistances highly increase the risk on common-mode oscillations, making this option undesirable. Therefore, a method needs to be found in which the IM2 and HD2 currents of the CE-stage are canceled. The following section will examine some of these methods to cancel the IM2 and HD2 currents.

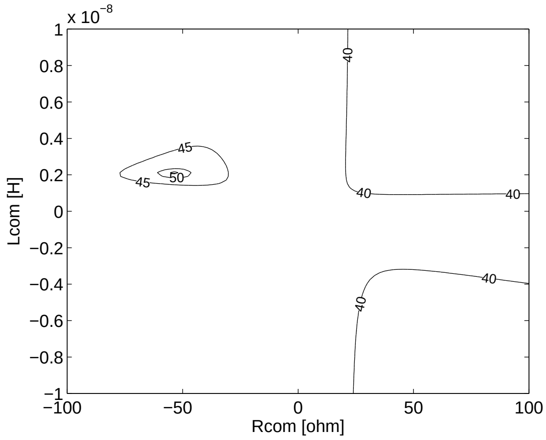

Figure 5.10: The OIP3 contours in the R_{com}-L_{com} plane for the differential cascode amplifier

5.3. IM2 AND HD2 CANCELLATION IN THE CE-STAGE

In Section 5.2 it has been shown that the IM2 and HD2 currents from the CE-stage interfere with the out-of-band C_{bc} cancellation. Therefore, these currents need to be canceled. In Figure 5.11 the circuit for out-of-band C_{bc} cancellation is shown. The IM2 and HD2 voltages that are important for out-of-band C_{bc} are created at the V_{cm} node, due to the L_{com} inductor. Therefore, the IM2 and HD2 currents from the CE-stage need to be canceled at that point.

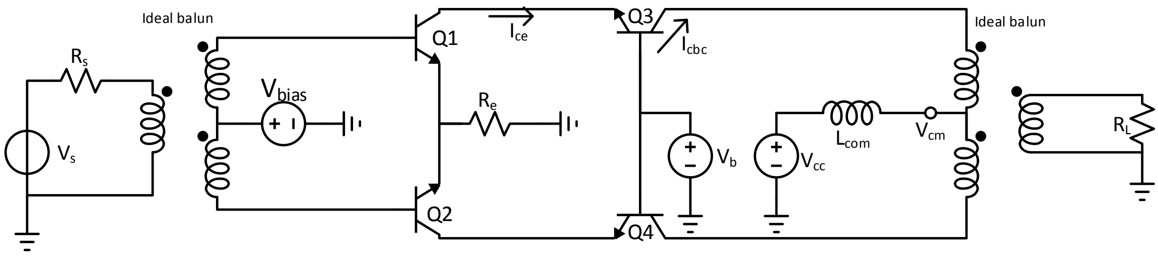

Figure 5.11: The differential cascode amplifier with out-of-band matching to C_{bc} linearization

Several options are available for IM2 and HD2 cancellation in the CE-stage. Before these options are discussed it is important to realize that the $IM2_{low}$ component is not important. As explained in Section 5.1, the $Z(\Delta s)$ is zero, which means that the $IM2_{low}$ is shorted and does not influence the cancellation. So for correct cancellation, the $IM2_{high}$, $HD2_{low}$ and $HD2_{high}$ of the CE-stage need to be considered. Three methods are studied for IM2 and HD2 cancellation:

- Feedforward IM2 and HD2 cancellation
- IM2 and HD2 cancellation with common-mode impedances
- Transformer-based IM2 and HD2 cancellation

Only the last option, transformer-based IM2 and HD2 cancellation has potential for successful IM2 and HD2 cancellation. The following sections will show why this is the case.

5.3.1. FEEDFORWARD IM2 AND HD2 CANCELLATION

In the CE-stage, the main source of nonlinearity is the exponential distortion. Therefore, to cancel the IM2 and HD2 currents, IM2 and HD2 distortion due to the exponential distortion needs to be canceled. For exponential distortion, the collector current leaving the transistor is related to the base current entering the transistor as described in Equation (5.9) [3]:

$$I_b = \frac{I_c}{\beta} = \frac{I_s\left(e^{V_{be}/V_t} - 1\right)}{\beta}[A] \tag{5.9}$$

where I_b is the base current, I_c is the collector current, β is the forward current gain and $V_t = \frac{k \cdot T}{q}$ is the thermal voltage with k being Boltzmann's constant $(1.38 \cdot 10^{-23} J/K)$, T being the temperature in kelvin and q being the elementary charge $(1.6 \cdot 10^{-19} C)$. Due to this relationship, the nonlinear IM2 and HD2 currents can be detected at the common-mode node of the input transformer. From that node, an amplification with β would create the original IM2 and HD2 currents in antiphase, which can be used to get cancellation. Figure 5.12 shows this principle.

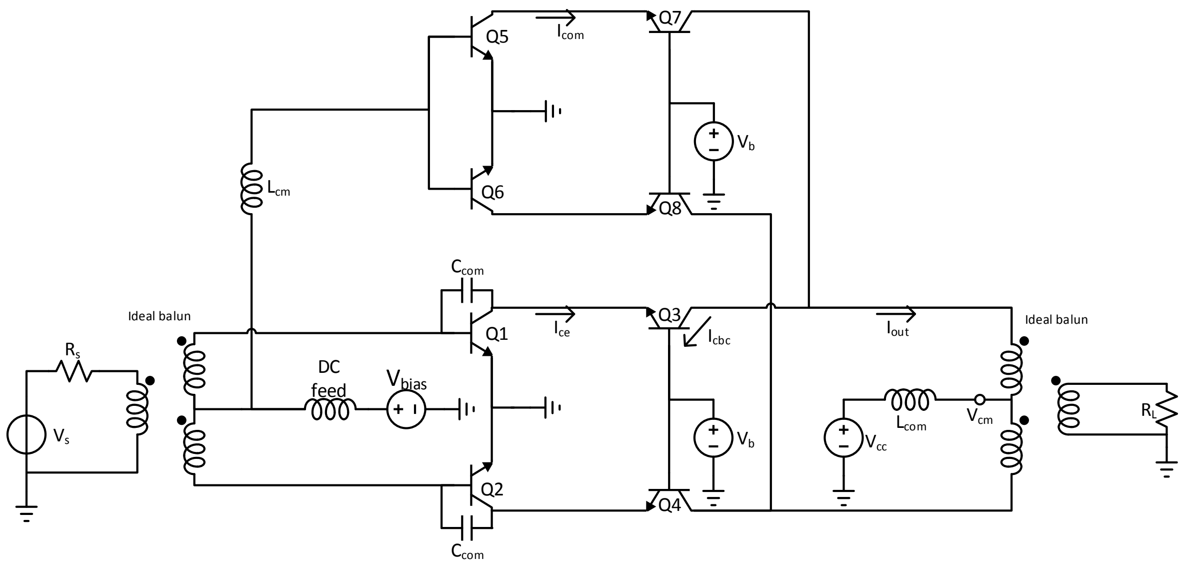

Figure 5.12: Schematic for feedforward cancellation of the IM2 and HD2 currents

In this schematic, L_{cm}=28pH and C_{com}=5pF have been added to compensate for the diffusion and depletion capacitances in the CE-stage. A polar plot has been made to compare the IM2 and HD2 components of I_{com} with I_{ce}. The sum of these currents is called I_{tot}, which is a measure of the IM2 and HD2 currents left after feedforward compensation. In Table 5.2 the simulation values have been given. In Table 5.3 the Gummel-Poon model used has been given. In Figure 5.13 the polar plot is shown. The currents cancel, so

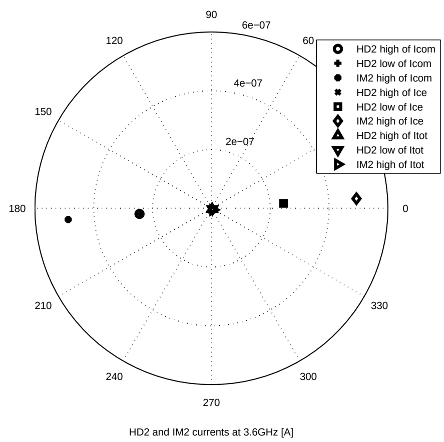

Figure 5.13: IM2 and HD2 currents in a feedforward topology

there is no IM2 and HD2 current left to interfere with the out-of-band C_{bc} cancellation.

Since the IM2 and the HD2 currents of the CE-stage have been canceled, the L_{com} inductor has been swept again, to see whether C_{bc} cancellation is possible. For the reference results, L_{com} has been shorted.

The simulation results can be found in Figure 5.14.

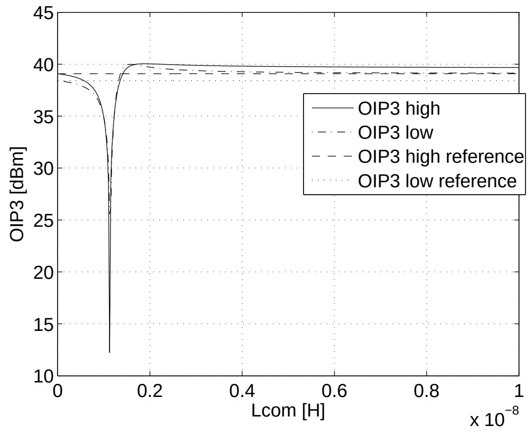

Figure 5.14: OIP3 versus L_{com} for the feedforward topology

As can be seen, no compensation points have been found. This is due to the exponential distortion of the CE-stage. To counteract the exponential distortion of the CE-stage, emitter tuning has been used. However, emitter tuning requires a short at the base of the CE-stage for baseband and second harmonic impedances. Since the feedforward cannot deliver these impedances, the exponential distortion of the CE-stage is dominant. The C_{bc} distortion is only dominant when the C_{bc} and L_{com} resonate at the second harmonic frequency, increasing the IM3. Therefore, no OIP3 improvement can be achieved with out-of-band C_{bc} cancellation when feedforward HD2 and IM2 cancellation is used.

5.3.2. IM2 AND HD2 CANCELLATION WITH COMMON-MODE IMPEDANCES

Another way of compensating the IM2 and HD2 currents is adapting the common-mode impedances at the base and emitter of the CE-stage. To find the correct cancellation conditions, a Volterra analysis in Maple has been done. The Maple script can be found in Appendix C. Figure 5.15 shows the circuit that has been used for Volterra analysis common-mode impedance matching for IM2 and HD2 cancellation.

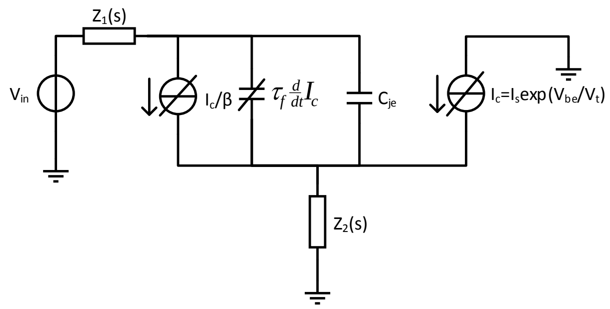

Figure 5.15: Circuit used for Volterra analysis of IM2 and HD2 cancellation with common-mode impedances

Using the Maple script, the following equation can be found for IM2 and HD2 cancellation:

$$g_m \cdot \frac{\beta \tau_f s_x (Z_1(s_x) + Z_2(s_x)) + (\beta+1) Z_2(s_x) + Z_1(s_x)}{s_x C_\pi \beta (Z_1(s_x) + Z_2(s_x)) + g_m \cdot (\beta+1) Z_2(s_x) + g_m Z_1(s_x) + \beta} = 1 \tag{5.10}$$

where s_x is $j \cdot 2\pi(f_1 + f_2)$, C_π is the combined depletion capacitance C_{je} and diffusion capacitance $\tau_f \frac{dI_c}{dV_{be}}$, and g_m is the linear transconductance of the transistor. When source impedance Z_1 and emitter impedance Z_2 are brought in resonance, so $Z_1(s_x) = -Z_2(s_x) = Z(s_x)$,Equation (5.10) simplifies to:

$$1 = \frac{Z(s_x)\left(-g_m(\beta+1) + g_m\right)}{Z(s_x)\left(-g_m(\beta+1) + g_m\right) + \beta} \approx \frac{-Z(s_x) g_m \beta}{-Z(s_x) g_m \beta + \beta} \tag{5.11}$$

When $Z(s_x) \gg 1$, this equation is true and IM2 and HD2 cancellation is accomplished. This can also be seen in simulation. In Figure 5.16 the circuit used for simulation is shown.

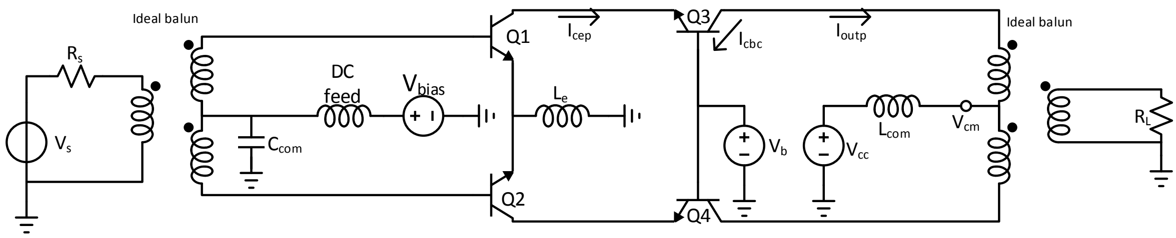

Figure 5.16: Circuit used for IM2 and HD2 cancellation with common-mode impedances

The currents at the collector from the CE-stage I_{cep} and the collector of the CB-stage I_{outp} are compared. If the IM2 and HD2 currents successfully have been canceled, the IM2 and HD2 currents at the collector from the CE-stage should be very small compared to those from the collector of the CB-stage. The simulation values can be found in Table 5.4. The Gummel-Poon model has been given in Table 5.3. In Figure 5.17 the simulation results have been shown.

Table 5.4: Simulation conditions for studying out-of-band C_{bc} cancellation with common mode impedances for IM2 and HD2 cancellation

Parameter	Description	Value
I_c	DC collector current	80mA
L_e	Emitter inductance	1nH
C_{com}	Compensation capacitor	1.954pF
V_b	Base voltage of the CB-stage	1.6V
V_{cc}	Supply voltage	3.3V
p_{rf}	Amplitude of the input power for each tone	-40dBm
f_c	Center frequency	1.8GHz
Δf	Tone spacing	10MHz
T_{in}	Turns ratio input balun	2:3
T_{out}	Turns ratio output balun	5:4

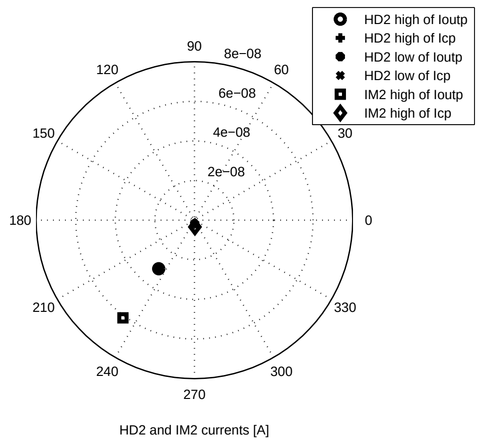

Figure 5.17: The polar plot of the collector currents when common-mode impedance IM2 and HD2 cancellation is used

As can be seen, the IM2 and HD2 currents coming from the CE-stage are significantly lower than the IM2 and HD2 currents from the CB-stage, so the IM2 and HD2 currents are dominated by the CB-stage. Since the exponential distortion of the CB-stage is not dominant, because it is current driven, the IM2 and

HD2 currents are created by the C_{bc} capacitance.

Since the IM2 and the HD2 currents of the CE-stage have been canceled, the L_{com} inductor has been swept again, to see whether C_{bc} cancellation is possible. For the reference results, L_{com} has been shorted. The simulation results can be found in Figure 5.18.

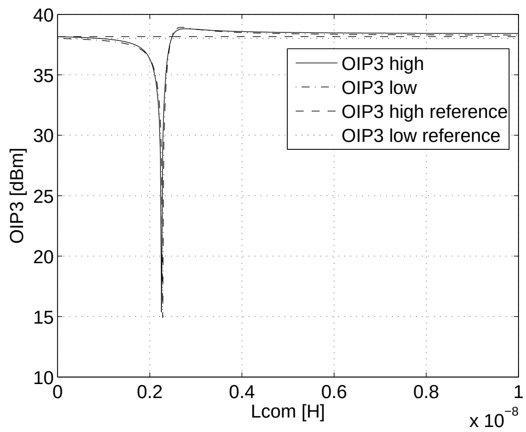

Figure 5.18: The IM3 currents in the cascode amplifier when common-mode impedances are used for IM2 and HD2 cancellation

As can be seen, no compensation points have been found. This is due to the exponential distortion of the CE-stage. To counteract the exponential distortion of the CE-stage, emitter tuning has been used. However, emitter tuning requires a short at the base of the CE-stage for baseband and second harmonic impedances. Since the common mode impedances do not deliver these impedances, the exponential distortion of the CE-stage is dominant. The C_{bc} distortion is only dominant when the C_{bc} and L_{com} resonate at the second harmonic frequency, increasing the IM3. Therefore, no OIP3 improvement has been achieved with out-of-band C_{bc} cancellation when common mode impedances for HD2 and IM2 cancellation have been used.

5.3.3. TRANSFORMER-BASED IM2 AND HD2 CANCELLATION

A good cancellation of the IM2 and HD2 currents of the CE-stage does not affect the IM3 cancellation of the exponential distortion. Since these IM2 and HD2 currents are common-mode signals and the fundamental signal is a differential signal, a transformer based solution can be found. In Figure 5.19 this concept is shown.

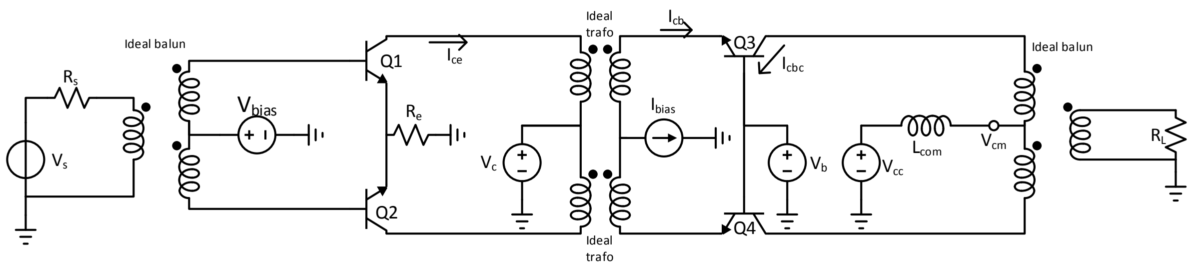

Figure 5.19: Transformer-based IM2 and HD2 cancellation

For the concept to work, the common-mode point of the transformer at the side of the CB-stage has to be an AC open. If this isn't the case, exponential IM2 and HD2 currents created by the CB-stage will not be linearized, since these are common-mode signals. When the common-mode point is an AC short, the CB-stage is voltage driven for the IM2 and HD2 frequencies. As explained in Chapter 4, this will introduce exponential distortion.

The simulation values for this setup are given in Table 5.5. The Gummel-Poon model has been given in Table 5.3. In Figure 5.20, the spectrum of the current entering the CB-stage is shown.

Table 5.5: Simulation conditions for studying out-of-band C_{bc} cancellation with transformer based IM2 and HD2 cancellation

Parameter	Description	Value
I_c	DC collector current	80mA
R_e	Emitter resistance	80.4mΩ
V_b	Base voltage of the CB-stage	1.6V
V_{cc}	Supply voltage	3.3V
p_{rf}	Amplitude of the input power for each tone	-40dBm
f_c	Center frequency	1.8GHz
Δf	Tone spacing	10MHz
T_{in}	Turns ratio input balun	2:3
$T_{intermediate}$	Turns ratio intermediate transformers	1:1
T_{out}	Turns ratio output balun	5:4

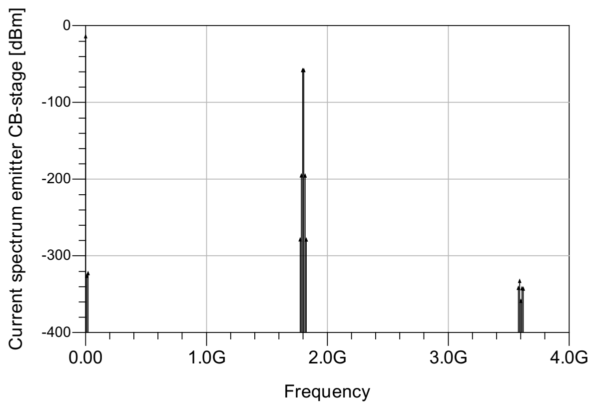

Figure 5.20: The current spectrum of the current entering the CB-stage

As can be seen, the IM2 and HD2 currents are below -300dBm, which is the numerical noise floor of the simulator. Therefore it can be concluded that the IM2 and HD2 currents of the CE-stage have been successfully canceled. Since the exponential distortion of the CE-stage is still canceled using emitter tuning, there should be an optimum again in which the IM3 of the C_{bc} is canceled. Using the simulation values from Table 5.5 and the Gummel-Poon model from Table 5.3, the OIP3 has been simulated versus L_{com}. For the reference OIP3, L_{com} has been shorted. In Figure 5.21 the simulations results have been given.

There is a clear optimum for OIP3, which is around 2.7 nH. In this optimum, the OIP3 has improved by 9dB compared to the reference OIP3. This demonstrates that a intermediate transformer is an effective way to cancel the IM2 and HD2 currents.

To see whether the addition of the transformer influenced the amplifier in any significant way, the effect of the transformer on the -1dB compression point P_{1dB} has been studied. In Section 4.2 a P_{1dB} of 24dBm could be reached in the Mextram model. Since the simpler Gummel-Poon model has been used for this simulation, the P_{1dB} should be at least 24dBm. In Figure 5.22 the OIP3 and gain have been plotted versus output power.

P_{1dB} occurs at 25dBm output power, while the OIP3 stays constant up to 10dBm. Above 10dBm, the OIP3 starts to drop due to the the higher order intermodulation products present at the IM3 frequency. Since the OIP3 has improved with 9dB and the P_{1dB} has not been compromised, out-of-band C_{bc} cancellation with transformer based IM2 and HD2 compensation can be considered a viable option for C_{bc} compensation.

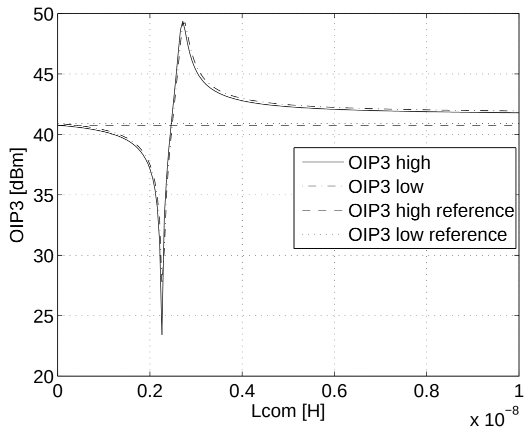

Figure 5.21: The OIP3 as function of L_{com} in a transformer-based IM2 and HD2 cancellation cascode

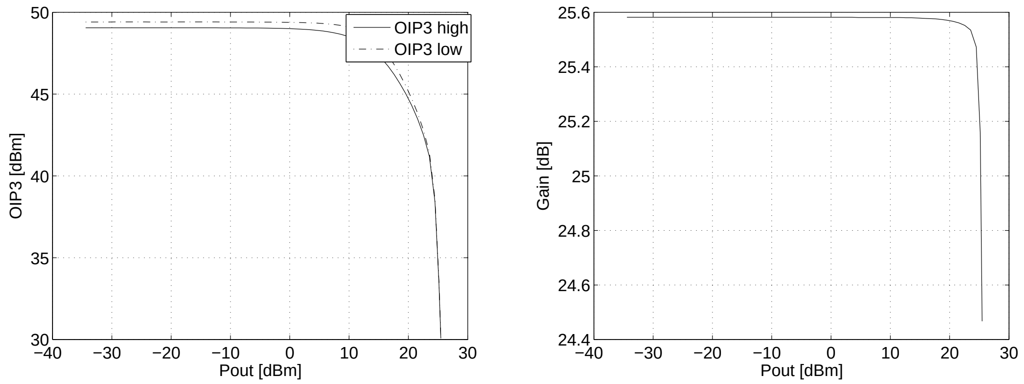

(a) OIP3

(b) Gain

Figure 5.22: The OIP3 and gain as a function of output power

5.4. CONCLUSION

In this chapter, the option of out-of-band matching has been discussed. Out-of-band matching can give C_{bc} linearization, without compromising on gain and power consumption [6]. Therefore, more design orthogonality is gained with out-of-band matching.

In Section 5.1 it has been shown that out-of-band C_{bc} cancellation is possible using an inductor which provides a short at baseband frequencies and an impedance as shown in Equation (5.8) for the second harmonic frequencies. This has also been shown in simulation, where a peak OIP3 of 50dBm has been reached. This OIP3 stays constant up to Δf=10MHz. Above Δf=10MHz, the $OIP3_{low}$ and $OIP3_{high}$ start to divert. However, the OIP3 has still been improved up to 100MHz. To get a more wideband cancellation, a capacitive compensation could be used, but this requires a device with a grading coefficient of the base-collector junction between 0.5 and 1. Even if these devices could be fabricated, this solution would make biasing conditions very difficult, since it requires an open at baseband frequencies.

Section 5.2 has demonstrated that when using out-of-band C_{bc} cancellation, the IM2 and HD2 currents of the CE-stage need to be taken in consideration. When these IM2 and HD2 currents are not taken in consideration, no OIP3 improvement could be obtained using out-of-band C_{bc} cancellation.

Since IM2 and HD2 currents from the CE-stage interfere with the out-of-band matching, several methods have been tried in Section 5.3 for cancellation of these currents. Feedforward and common-mode impedance both cancel the IM2 and HD2 currents but reintroduce the IM3 of the exponential distortion in the CE-stage, which becomes the dominant contributor to OIP3. Therefore, an intermediate transformer has been used to cancel the IM2 and HD2 currents from the CE-stage. With this intermediate transformer, OIP3 figures of 50dBm could once again be reached. With a P_{1dB} compression point around 25dBm and a constant OIP3 of 50 dBm up to 10dBm in output power, this option is considered to be the most promising for out-of-band C_{bc} cancellation. Further proposals have been done for the future. For the transformer-based solution, more complex modeling is considered to be the next step to see whether this solution is viable.

5.4.1. FUTURE POSSIBILITIES WITH OUT-OF-BAND MATCHING

Due to the time limitation on this project, there is still a lot to investigate on out-of-band matching. There are multiple challenges, like keeping the out-of-band impedance shorted at baseband frequencies, implementing the transformers and replacing the Gummel-Poon model used for out-of-band matching with the full Mextram model of the QUBiC4Xi BNA HV device. A few suggestions can be done concerning the next steps in the investigation of out-of-band matching for the C_{bc} capacitance.

TRANSFORMER-BASED IM2 AND HD2 CANCELLATION

For transformer based IM2 and HD2 cancellation, probably the next important step to take is to replace the Gummel-Poon model by the Mextram model of the QUBiC4Xi BNA HV device. Using this model, it can be investigated whether the amplifier is fully stable and whether the cancellation still works. Since the Mextram model also incorporates current dependency in the C_{bc} model, it is not sure whether the out-of-band C_{bc} cancellation still works in this case. Also the addition of stabilization circuits might negatively influence the out-of-band C_{bc} cancellation. Finally it should be noted, that although out-of-band C_{bc} cancellation with transformer-based IM2 and HD2 cancellation works well in simulations, the implementation requires a lot of coils to make up the inductors and transformers. Therefore, this solution uses a lot of on-chip area.

ANTI-PARALLEL AIDED OUT-OF-BAND MATCHING

To get linearization of the C_{bc} capacitance, an inductor has to be used when $m < 0.5$. Also 3 transformers are in use: an input-balun, an intermediate transformer and an output-balun. With all these coils, the chip area significantly increases and also the chance on magnetic coupling increases. This could make the out-of-band matching not usable as a practical solution. However, at the moment, the IM2 and HD2 currents of the C_{bc} are used for out-of-band matching. One could also use the IM2 and HD2 currents of the exponential distortion of the CE-stage. By using anti-parallel C_{bc} capacitances, as described in Section 4.3, the IM2 and HD2 currents of the C_{bc} capacitance can be canceled, leaving only the IM2 and HD2 currents of the exponential distortion. However, it is not known how the anti-parallel configuration will react to IM2 and HD2 voltages. Still, it is an interesting idea, since it might reduce the amount of coils in the design significantly.

COMMON-MODE FEEDBACK/FEEDFORWARD OUT-OF-BAND COMPENSATION

By using common-mode feedback or common-mode feedforward, the IM2 and HD2 currents can be adapted in phase and amplitude, without changing the fundamental signals. By choosing the right common-mode feedback or common-mode feedforward topology, the total IM2 and HD2 currents might be adapted in such a way that new IM3 sweet spots can be found using out-of-band matching. Currently, the only sweet spot found for the cascode amplifier required a negative resistance, but common-mode feedback or feedforward might turn this in a positive resistance, which is easier to make and gives a lower chance on common-mode oscillations.

6

PASSIVE IN-BAND C_{bc} COMPENSATION

In Chapter 5 the out-of-band solution has been discussed. Out-of-band matching works with indirect mixing to manipulate the IM3 products. The other option is in-band compensation, affecting the direct mixing. This option does not have the advantages out-of-band matching has, like orthogonality for gain and power consumption. On the other hand the IM2 and HD2 currents of the CE-stage cannot interfere with in-band cancellation methods, since these currents can be shorted out-of-band.

The idea for passive in-band C_{bc} compensation is based on a distortion-free varactor stack [22]. This stack uses an anti-series diode configuration for IM3 cancellation. However, by adapting the principles of the distortion-free varactor stack, IM3 currents can be injected in the circuit, counteracting the IM3 contribution of the C_{bc} in the CB-stage.

In this chapter passive in-band C_{bc} compensation will be discussed. In Section 6.1 the concept of passive in-band C_{bc} compensation will be analyzed. The used circuit will be studied and a Volterra analysis will be performed. The concept of passive in-band C_{bc} compensation has been realized on chip. In Section 6.2 the schematics and layout of the test chip are presented. In Section 6.3 the measurement results of the test chip are given. In Section 6.4 conclusions will be drawn with respect to passive in-band C_{bc} compensation and recommendations for the future will be given.

6.1. CONCEPTUAL ANALYSIS OF PASSIVE IN-BAND C_{bc} COMPENSATION

As discussed in Chapter 4, the main contribution to IM3 distortion in a cascode amplifier is the C_{bc} capacitance of the CB-stage, assuming that the exponential distortion of the CE-stage is canceled. This C_{bc} capacitance is in parallel with the output and injects nonlinear currents in the base of the CB-stage and in the collector of the CB-stage. Since the base of the CB-stage is typically AC grounded the only relevant currents are those of the collector of the CB-stage. With a passive in-band C_{bc} compensation circuit the same IM3 current could be created with an opposite phase to the C_{bc} current, as shown in Figure 6.1.

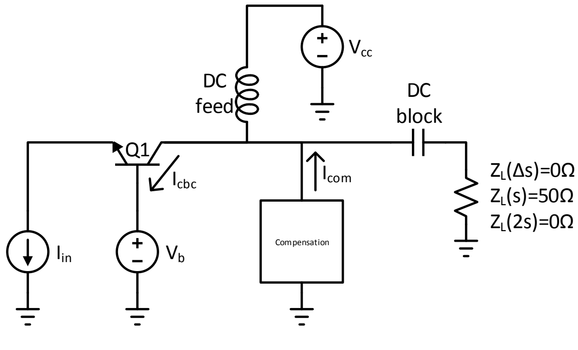

Figure 6.1: The concept of passive in-band C_{bc} compensation

In this circuit, the compensation current I_{com} is opposite to I_{cbc}. Therefore no nonlinear current will run through the load impedance. Since the load impedance is shorted for baseband and second harmonic frequencies, no residual IM2 and HD2 currents from the CE-stage can interfere with the cancellation mechanism. Since there is no relevant IM2, HD2 and IM3 distortion from the CE-stage, the CE-stage can be modeled as a current source for IM3 analysis.

To increase the correlation between the passive in-band C_{bc} compensation signal and the C_{bc} signal, a depletion capacitance can be used that is similar to the C_{bc} capacitance. A transistor with only the base and collector connected will already accomplish this assuming that the C_{bc} has no dependency on the collector current, which is the case for the Gummel-Poon model. For the Mextram model, this assumption is not valid: therefore, it is not sure whether this solution will also work with the Mextram model. Figure 6.2 shows the concept of passive in-band C_{bc} compensation. The Z_{com} impedance should provide for a 180 degrees phase shift for the IM3 currents created by Q2.

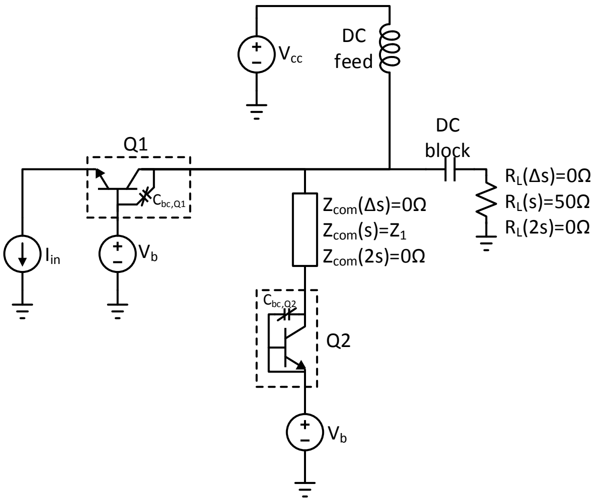

Figure 6.2: Passive in-band C_{bc} compensation using depletion capacitances

For IM2 and HD2 frequencies, Z_{com} should be shorted, so the correlation between $C_{bc,Q1}$ and $C_{bc,Q2}$ is still present. For biasing it is also important for Z_{com} to be DC-shorted. If these conditions are met, the passive in-band C_{bc} compensation method is a purely in-band cancellation method, while the DC-operating point for Q1 and Q2 is similar.

6.1.1. VOLTERRA ANALYSIS OF PASSIVE IN-BAND C_{bc} COMPENSATION

To find the correct implementation of Z_{com}, Volterra analysis has been used. In Figure 6.3 the circuit for Volterra analysis is given.

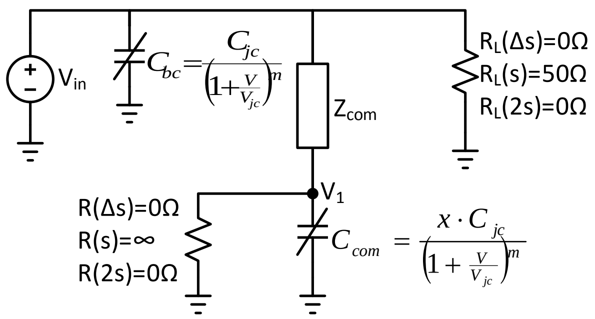

Figure 6.3: The circuit used for Volterra analysis of passive in-band C_{bc} compensation

By driving the circuit with a voltage source V_{in} the linear transfer between fundamental current and fundamental voltage has been ignored. If a current source would have been used, a V_{in} voltage would have been established as the result of the linear relationship with I_{com}. The only difference is that all the distortion is forced into the current-domain: in the voltage-domain, no IM3 signals can be found at the output.

In Appendix A.3 the total analysis can be found. Only the important results have been shown here. The IM3 current produced by the C_{bc} has been described by the following equation:

$$I_{IM3_{low}} = -(2s_1 - s_2) \cdot K_{3C}[A/V^3] \tag{6.1}$$

$$I_{IM3_{high}} = -(2s_2 - s_1) \cdot K_{3C}[A/V^3] \tag{6.2}$$

where $s_2 > s_1$, $s_1 = 2\pi f_1$ with f_1 being the lower fundamental frequency, $s_2 = 2\pi f_2$ with f_2 being the higher fundamental frequency and K_{3C} is the third Taylor coefficient of the C_{bc} capacitance.

The IM3 currents created by the compensation circuit are described by the following equations:

$$I_{com,IM3_{low}} = x \cdot (2s_1 - s_2) \cdot \frac{B(2s_1 - s_2)}{Z_{com}(2s_1 - s_2)} \cdot h_1(s_1)^2 \cdot h_1(-s_2) \cdot K_{3C}[A/V^3] \tag{6.3}$$

$$I_{com,IM3_{high}} = x \cdot (2s_2 - s_1) \cdot \frac{B(2s_2 - s_1)}{Z_{com}(2s_2 - s_1)} \cdot h_1(s_2)^2 \cdot h_1(-s_1) \cdot K_{3C}[A/V^3] \tag{6.4}$$

where x is the ratio between the C_{bc} capacitance and the C_{com} capacitance, $s_2 > s_1$, $s_1 = 2\pi f_1$ with f_1 being the lower fundamental frequency, $s_2 = 2\pi f_2$ with f_2 being the higher fundamental frequency, $B(s)$ is the linear transfer from the nonlinear current of the C_{com} capacitance to the current injected into the output node and $h_1(s)$ is the linear transfer between the input voltage and the voltage on the C_{com} capacitance.

In a narrowband situation $2s_1 - s_2 \approx s_1 \approx s_2 \approx 2s_2 - s_1 = s$. Then Equation (6.1) and (6.2) will simplify to the following general equation:

$$I_{IM3} = -s \cdot K_{3C}[A/V^3] \tag{6.5}$$

Equation (6.3) and (6.4) will simplify to the following general equation:

$$I_{com,IM3} = x \cdot s \cdot \frac{B(s)}{Z_{com}(s)} \cdot h_1(s)^2 \cdot h_1(-s) \cdot K_{3C}[A/V^3] \tag{6.6}$$

For cancellation, the following condition has to hold:

$$I_{com,IM3} + I_{IM3} = 0 \tag{6.7}$$

Using Equation (6.5) and (6.6) and $h_1(s)$ and $B(s)$ as given in Appendix A.3, the following equation for cancellation can be found:

$$x \cdot \left(\frac{1}{1 + Z_{com}(j\omega) \cdot j\omega \cdot x \cdot C_{bc}} \right)^3 \cdot \frac{1}{-1 + Z_{com}(-j\omega) \cdot j\omega \cdot x \cdot C_{bc}} = 1 \tag{6.8}$$

where C_{bc} is the nominal value of the base collector capacitance and $\omega = 2\pi f$ with f being the fundamental frequency. To get this equation satisfied, the complex parts have to disappear from the denominators. To do this, the 1 and -1 terms in the denominator have to be removed. This can be done by using an inductor that is in resonance with the $x \cdot C_{bc}$ capacitance:

$$L = \frac{1}{\omega^2 \cdot xC_{bc}}[H] \tag{6.9}$$

A series resistance has been added to make sure that the denominators won't equal to 0. Therefore, $Z_{com} = R + sL$. When this has been used in Equation (6.8), the following equation has been obtained:

$$x \cdot \frac{1}{\left(j\omega \cdot R \cdot xC_{bc}\right)^4} = 1 \tag{6.10}$$

As a result, there is a series combination with an inductor and a resistor. The inductor is in resonance with the compensation capacitance. The following equation holds for IM3 cancellation in this circuit:

$$R = \frac{\sqrt[4]{x}}{\omega \cdot x C_{bc}} [\Omega] \tag{6.11}$$

It is important to notice that, according to Equation (6.8), the dependency on Z(s) is present to the power 4. Therefore parasitics are very dominant in this cancellation mechanism. This will be important for the layout of the test chip, which will be discussed in the following section.

6.1.2. SIMULATION RESULTS FOR PASSIVE IN-BAND C_{bc} COMPENSATION

To demonstrate that passive in-band C_{bc} compensation gives a better OIP3, the circuit in Figure 6.4 has been made. With the circuit shown in Figure 6.4 a harmanic balance simulation has been done to determine the

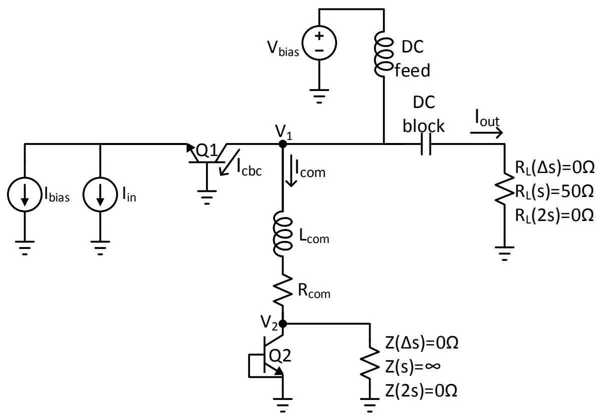

Figure 6.4: The simulation circuit used to demonstrate passive in-band C_{bc} compensation cancellation

OIP3. In this simulation a two-tone signal is applied with the I_{in} source. The Q2 transistor has been made twice as large as the Q1 transistor. The magnitude of the injected IM3 current has been controlled with R_{com}. In Table 6.1 the simulation values have been given. In Table 6.2 the Gummel-Poon model has been given.

Table 6.1: Simulation values used for studying passive in-band C_{bc} compensation

Parameter	Description	Value
I_{bias}	DC biasing current	80mA
V_{bias}	DC biasing voltage	700mV
I_{in}	Amplitude per tone of the input signal	0.1mA
f_c	Center frequency	1.8GHz
Δf	Tone spacing	1MHz
L_{com}	Value of the compensation inductor	7.58nH
R_{com}	Value of the compensation resistor	101.9Ω

Table 6.2: Gummel-Poon parameters used for studying passive in-band C_{bc} compensation

Parameter	Description	Value
β	Forward current gain	2000
I_s	Saturation current	0.5fA
C_{jc}	Zero-bias base-collector depletion capacitance	26fF
V_{jc}	Built-in voltage of the base-collector junction	0.7V
m_{jc}	Grading coefficient of the base-collector junction	1/3
A_{Q1}	Area of the Q1 transistor	25
A_{Q2}	Area of the Q2 transistor	50

As can be seen, the biasing voltage is rather low. Due to this low voltage, the P_{1dB} will be low. However, as can be seen in Section 4.3, the distortion due to C_{bc} increases when the biasing is decreased, since $K_{3C_{bc}}$ increases. Therefore, this increases the nonlinearity of the C_{bc}, making it easier to study the effect of the compensation. In Figure 6.5 the polar plot of the resulting IM3 currents and the net-current has been given.

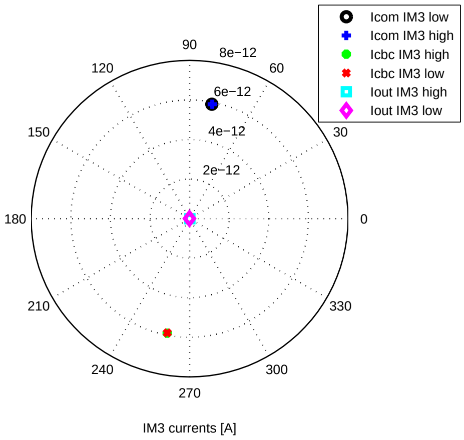

Figure 6.5: Simulation results of the conceptual passive in-band C_{bc} compensation simulation

As can be seen, the IM3 currents cancel. Due to this cancellation, the OIP3 increases. Without the compensation the OIP3 has a level of 31dBm. With the compensation, the OIP3 is 57.1dBm. To see whether this cancellation is a viable solution, the tone spacing Δf has been swept from 1kHz up to 5MHz. The results can be seen in Figure 6.6.

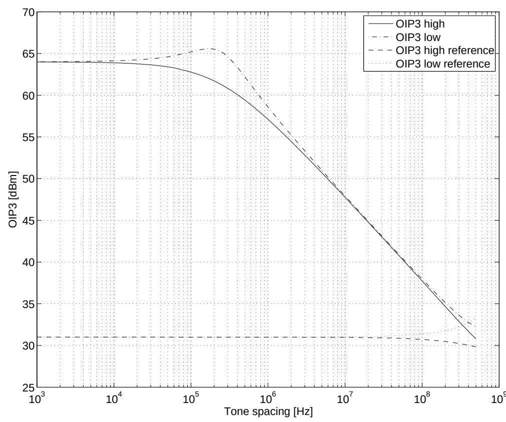

Figure 6.6: OIP3 versus Δf for passive in-band C_{bc} compensation

Although the compensation does not give perfect cancellation for high tone spacings, the OIP3 stays improved up to Δf =300MHz. The compensation gives perfect compensation up to Δf = 10kHz, above this frequency, the $OIP3_{high}$ and $OIP3_{low}$ start to divert. As a last test, the input tone has been varied from 10μA up to 30mA, to see how the compensation reacts to higher output powers. The OIP3 and the gain have been given in Figure 6.7. The P_{1dB} of the circuit is 14dBm. For the reference circuit, the OIP3 is constant up to the P_{1dB} point. For the compensated circuit, the OIP3 starts to drop at lower powers. This is due to higher order intermodulation products, becoming dominant at the IM3 frequencies. As can be seen, the OIP3 is higher in the compensated case up to the P_{1dB} point. The gain is lower in the compensated circuit. This is due to the in-band character of the compensation. The compensation makes an in-band damped resonator, causing a lower gain.

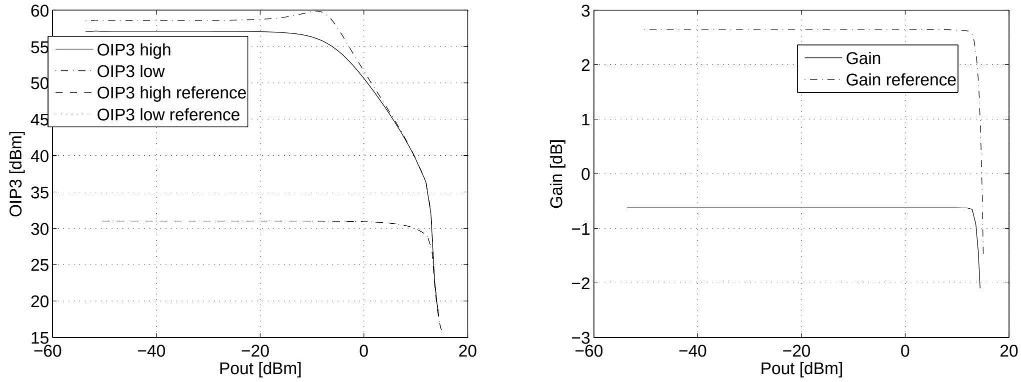

(a) OIP3 (b) Gain

Figure 6.7: The OIP3 and gain as a function of output power

The OIP3 stays high up to the P_{1db} point, and the OIP3 improves up to 300MHz tone spacing. Therefore, passive in-band C_{bc} compensation is a viable solution for C_{bc} distortion.

6.2. DESIGN OF A TEST CHIP FOR PASSIVE IN-BAND C_{bc} COMPENSATION

To demonstrate the feasibility of passive in-band C_{bc} compensation, a test chip has been made. The implementation of the test chip is discussed in this section. Since only the CB-stage is concerned in the concept of passive in-band C_{bc} compensation, the CE-stage has not been implemented. Only a CB-stage has been implemented with a compensation network, so the working principle of the compensation network could be studied without any influence from other stages.

6.2.1. SCHEMATICS FOR PASSIVE IN-BAND C_{bc} COMPENSATION

There are two ways to test whether the concept of passive in-band C_{bc} compensation works:

1. Use a C_{bc} capacitance with compensation, the shunt-configuration
2. Use a CB-stage with compensation, the CB-configuration

The first configuration has a lower risk of additional distortion mechanisms. However, the nonlinear behavior of the C_{bc} is not purely voltage dependent as the Gummel-Poon model suggests. There is also a current dependency, as described by the Mextram model [23]. When the shunt-configuration is used, this current dependency is ignored. The second configuration does take into account for this current dependency. However, when the second configuration is used, additional distortion mechanisms can occur, such as exponential distortion or avalanche.

SCHEMATICS FOR THE SHUNT-CONFIGURATION

The schematics of the reference and C_{bc} compensated shunt-configuration have been shown in Figure 6.8.

Since in a CB-stage, resistive base degeneration with the use of a resistor is commonly used for mitigating stability issues [24], two implementations have been made: one with a base resistance R_{base} and one without a base-resistance. All the shunt variants made are given in Table 6.3.

Table 6.3: Shunt configuration variants on the testchip

Circuit name	**Type**	R_{base}	L_{com}	R_{com}
JMM03	Compensated	0Ω	14.33nH	256.9Ω
JMM04	Compensated	15Ω	14.61nH	259.8Ω
JMM09	Reference	0Ω	-	-
JMM10	Reference	15Ω	-	-

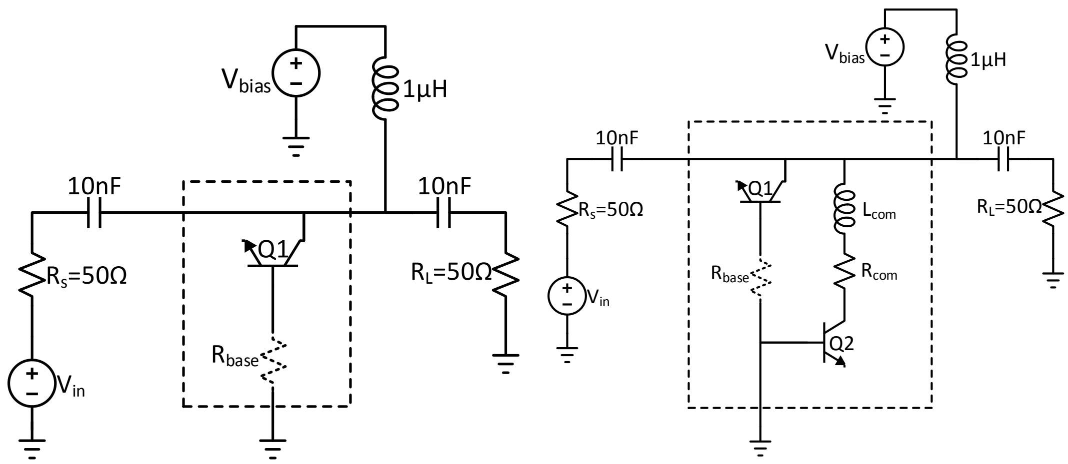

(a) Reference circuit (b) Compensated circuit

Figure 6.8: The schematic of the shunt-configuration of the test chip

The transistor Q1 has been implemented using a QUBiC4Xi BNA HV 0.5μm x 10.3μm x 24 transistor. The transistor Q2 has been implemented using a QUBiC4Xi BNA HV 0.5μm x 10.3μm x 36 transistor, which is 1.5 times larger than the Q1 transistor.

In this report, only the variants without base-resistance will be presented. These are the JMM03 and the JMM09 variants. To get a high OIP3, Equation (6.9) and (6.11) have been used as a starting point to obtain the values for L_{com} and R_{com}. No second order shorts have been added in the circuit, to increase flexibility during measurement and to simplify the design of the testchip. As a consequence, Equation (6.9) and (6.11) do not give the correct combination of L_{com} and R_{com} and can only be used as a starting point for the design.

The combination of L_{com} and R_{com} have been found using the simulation values given in Table 6.4. The DC biasing voltage on the collector-base junction has been kept low, since this increases the C_{bc} distortion as has been shown in Section 4.3. This increased C_{bc} distortion helps to demonstrate that passive in-band C_{bc} compensation improves the OIP3. In Table 6.5 the simulations results have been given.

Table 6.4: Simulation values for the shunt configurations

Parameter	**Description**	**Value**
V_{bias}	DC biasing voltage collector-base junction	0.7V
P_{in}	Input power for each tone	-25dBm
f_c	Center frequency	1.8GHz
Δf	Tone spacing	1MHz

Table 6.5: Simulation results for the shunt-configuration for the test-chip for passive in-band C_{bc} compensation

	OIP3 low [dBm]	**OIP3 high [dBm]**
Reference circuit	37.5	37.5
Compensated circuit	53.7	55.1

To see how wideband the solution is, a sweep has been done over tone spacing Δf. Also a sweep has been done over input power to see for which input powers this solution works. In Figure 6.9 the OIP3 over tone spacing is shown.

As can be seen, the OIP3 stays rather constant up to 1MHz tone spacing. Above 1MHz it starts to fall.

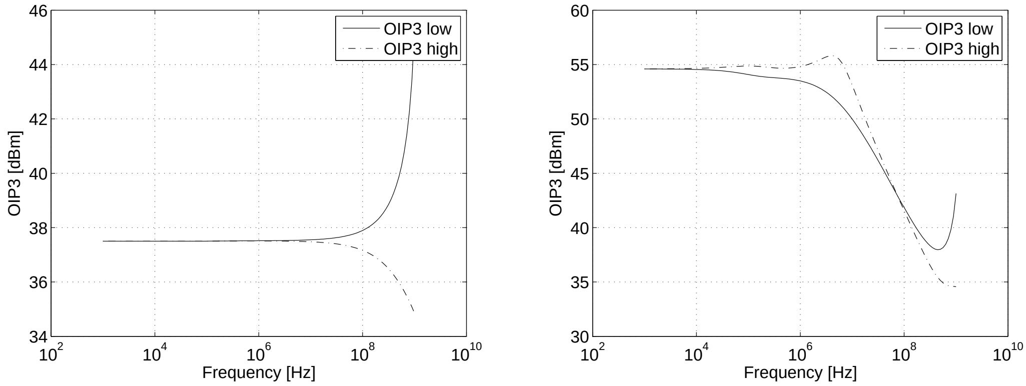

(a) Reference circuit (b) Compensated circuit

Figure 6.9: OIP3 versus tone spacing for the reference circuit and compensated circuit in the shunt-configuration for P_{in}=-25dBm

However, the compensation circuit will improve the OIP3 up to 100MHz in tone spacing.

To see how the compensation performs over power, the input power has been swept from -40dBm up to 10dBm. In Figure 6.10 the OIP3 over input power is shown. The OIP3 stays rather constant up to 0dBm

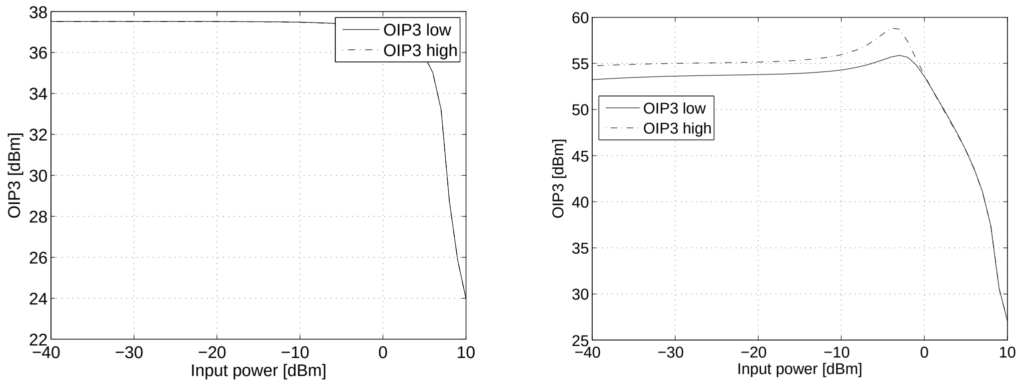

(a) Reference circuit (b) Compensated circuit

Figure 6.10: OIP3 versus input power for the reference circuit and compensated circuit in the shunt-configuration for Δf=1MHz

input power. Above this input power, the OIP3 starts to decline. The OIP3 shows an improvement up to at least 5 dBm input power. Above this input power, higher order intermodulation products on the IM3 frequency start to influence the OIP3.

SCHEMATICS FOR THE CB-CONFIGURATION

The schematics of the reference and C_{bc} compensated CB-configuration have been shown in Figure 6.11.

Again, since in a CB-stage, base degeneration with the use of a resistor is commonly used for mitigating stability issues [24], two implementations have been made: one with a base resistance R_{base} and one without a base-resistance. All the CB-variants made have been given in Table 6.6.

JMM13 up to JMM15 are circuits in which the R_{com} has been adapted to account for process variations. Transistor Q1 has been implemented using a QUBiC4Xi BNA HV 0.5μm x 10.3μm x 24 transistor. Q2 has been implemented using a QUBiC4Xi BNA HV 0.5μm x 10.3μm x 36 transistor, which is 1.5 times larger than the Q1 transistor.

Again the focus will be on the one without base-resistance. These are the JMM01 and JMM05. To get

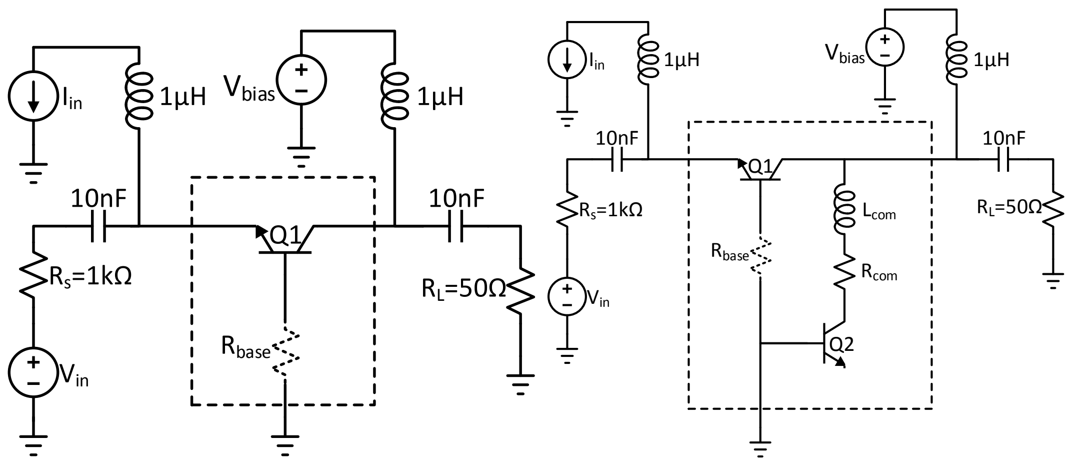

(a) Reference circuit (b) Compensated circuit

Figure 6.11: The schematic of the CB-configuration of the test chip

Table 6.6: CB-configuration variants on the testchip

Circuit name	**Type**	R_{base}	L_{com}	R_{com}
JMM01	Reference	0Ω	-	-
JMM02	Reference	15Ω	-	-
JMM05	Compensated	0Ω	13.9nH	165.4Ω
JMM06	Compensated	15Ω	14.1nH	165Ω
JMM13	+5% Compensated	15Ω	14.1nH	173Ω
JMM14	+10% Compensated	15Ω	14.1nH	181.4Ω
JMM15	-5% Compensated	15Ω	14.1nH	156.7Ω
JMM16	-10% Compensated	15Ω	14.1nH	148.5Ω

a high OIP3, Equation (6.9) and (6.11) have been used as a starting point to obtain the values for L_{com} and R_{com}. Again, no second order shorts have been added to increase the flexibility during measurement and to simplify the design of the testchip. As a consequence, Equation (6.9) and (6.11) do not give the correct combination for L_{com} and R_{com}, but can be used as a starting point for the design.

The combination of L_{com} and R_{com} have been found using the simulation values given in Table 6.7. The DC biasing voltage on the collector-base junction has been kept low, since this increases the C_{bc} distortion as has been shown in Section 4.3. This increased C_{bc} distortion helps to demonstrate that passive in-band C_{bc} compensation improves the OIP3. In Table 6.8 the simulation results have been given.

Table 6.7: Simulation values for the CB configurations

Parameter	**Description**	**Value**
V_{bias}	DC biasing voltage collector-base junction	0.7V
I_{in}	DC biasing current	40mA
P_{in}	Input power for each tone	-25dBm
f_c	Center frequency	1.8GHz
Δf	Tone spacing	1MHz

Compared to the shunt-configuration, the CB-configuration yields a much lower OIP3. There are two main reasons for this. The first is due to the current driven condition in the CB-stage. As discussed in

Table 6.8: Simulation results for the CB-configuration for the test-chip for passive in-band C_{bc} compensation

	OIP3 low [dBm]	OIP3 high [dBm]
Reference circuit	29.1	29.1
Compensated circuit	48.2	48.5

Section 4.1, the OIP3 due to the exponential distortion can be described by the following equation:

$$OIP3_{CB,cd} \approx 2I_c \sqrt{\frac{R_s}{r_e}\left|\frac{1+sr_eC_\pi}{1+sR_sC_{je}}\right|}[A] \tag{6.12}$$

where I_c is the collector current, $s = j2\pi f$, where f is the center frequency, R_s is the source impedance, $C_\pi = C_{\tau_f} + C_{je}$, C_{τ_f} is the base-emitter diffusion capacitance, C_{je} is the base-emitter depletion capacitance and $r_e = 1/g_m$ with g_m being the linear transconductance of the transistor. In the chosen configuration, the current is 40mA, much lower than the configuration studied in Section 4.1. However, the source impedance is higher. Lower current generally also tends to give lower current gain factors [20], decreasing the influence of the high input impedance. Therefore, the OIP3 ceiling is probably caused by an increased effect of exponential distortion.

There is also a second reason for the low OIP3. In the shunt configuration, the input and output are in parallel with each other. This means that for the IM3 frequencies, there is a parallel combination of 50Ω resistances. This gives a total load of 25Ω. For the CB-configuration, only the load of 50Ω is present. Therefore the IM3 voltage is much lower in the shunt configuration compared to the CB configuration if the same IM3 currents are generated.

To see how wideband the solution is, a sweep has been done over tone spacing Δf. Also a sweep has been done over input power to see for which input powers this solution works. In Figure 6.12 the OIP3 over tone spacing is shown. As can be seen, the OIP3 stays rather constant up to 100kHz tone spacing. Above 100kHz it rises shortly to peak at Δf=1MHz, above which it starts to fall.The rise in OIP3 is probably be a result of the current dependency of the C_{bc}, since the circuit has been optimized for a Δf of 1MHz. Since the current is frequency dependent, this can give a slight change in OIP3. However, this has not been confirmed using simulation and is therefore still open for investigation. The compensation circuit will improve the OIP3 up to 100MHz in tone spacing.

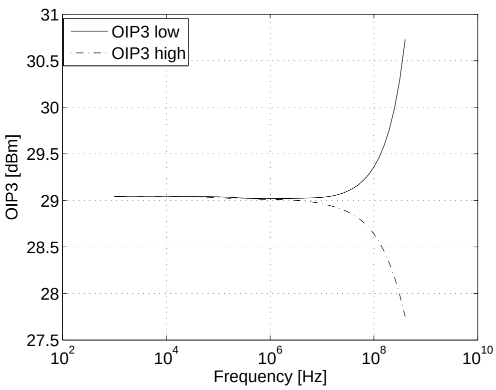

(a) Reference circuit

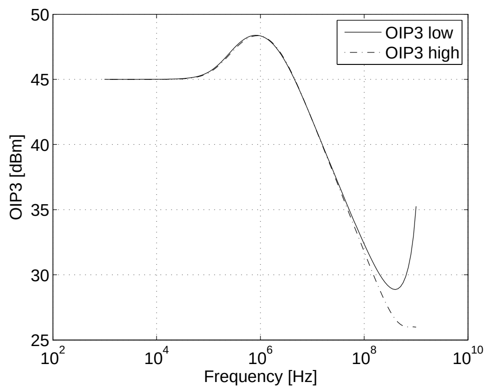

(b) Compensated circuit

Figure 6.12: OIP3 versus tone spacing for the reference circuit and compensated circuit in the CB-configuration for P_{in}=-25dBm

In Figure 6.13 the OIP3 over input power is shown.

As can be seen, the OIP3 varies a lot over input power for the compensated circuit. Further research is needed to explain why the OIP3 varies this much over input power. The OIP3 has been improved up to

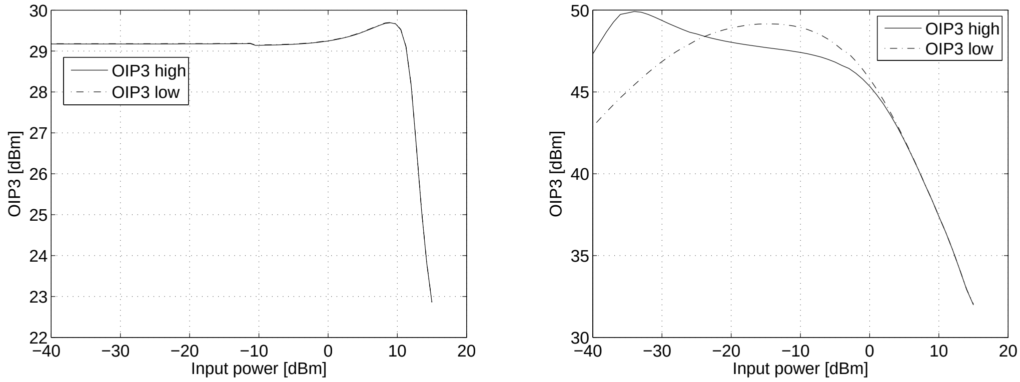

(a) Reference circuit (b) Compensated circuit

Figure 6.13: OIP3 versus input power for the reference circuit and compensated circuit in the CB-configuration for Δf=1MHz

15dBm. At higher powers, higher order intermodulation products start to play a role, which is why the OIP3 drops.

6.2.2. LAYOUT FOR PASSIVE IN-BAND C_{bc} COMPENSATION

The layout for the reference circuits is given in Figure 6.14. There are multiple variants on this, depending on whether a shunt- or CB-configuration has been used, and whether the base-resistance is present.

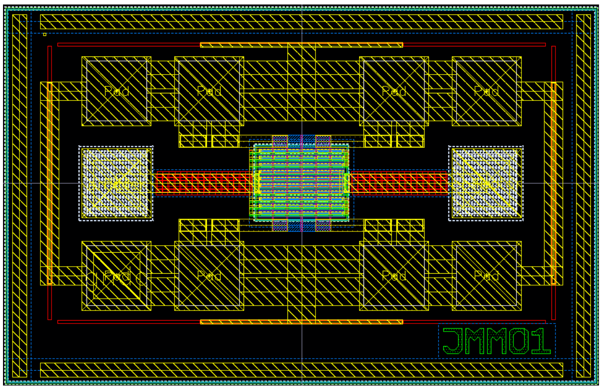

Figure 6.14: Layout of the reference circuit for the test chip for passive in-band C_{bc} compensation

The layout for the compensated circuits is given in Figure 6.15. Again there are multiple variants on this layout, depending on whether a shunt-or CB-configuration is used, and whether the base-resistance is present.

As can be seen from the Volterra analysis in Section 6.1, the main cancellation is dependent on the value of the inductor and the resistor. From the Volterra analysis it is also clear that a dependency to the power 4 on the impedance Z(s) is present. In other words: variations in the inductor and resistor value and parasitic components will influence the cancellation mechanism strongly. Therefore, in the layout the parasitics need to be optimized for a low contribution.

First of all, the signal paths are kept separated as much as possible to prevent capacitive coupling between the signal tracks. The places where the signal tracks cross, the tracks are separated as much as possible, by placing one track on metal 6, the highest metal, and one track on metal 1, the lowest metal in QUBiC4Xi. This can also be seen in Figure 6.16.

Secondly, the coupling to the substrate should be kept to a minimum. Therefore, the substrate below

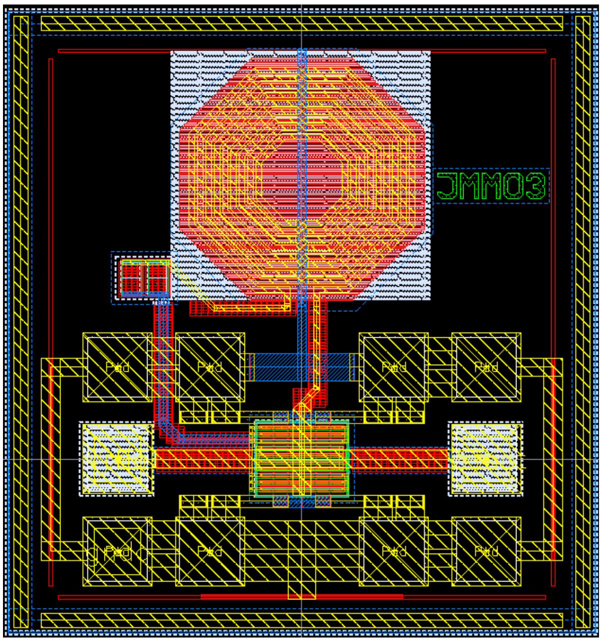

Figure 6.15: Layout of the compensated circuit for the test chip for passive in-band C_{bc} compensation

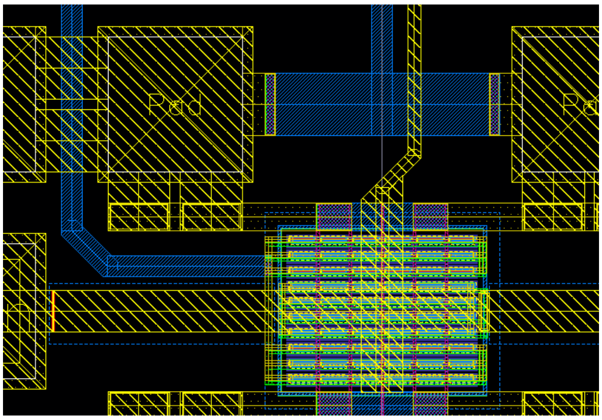

Figure 6.16: Seperation of tracks by moving them to the lowest and highest metal layer possible

and around the signal tracks is covered with Deep Trench Isolation (DTI). This makes the substrate very high-ohmic, decreasing the influence of capacitive coupling with the substrate [25]. Also the substrate below the resistor has been covered with DTI and an additional DTI ring around the transistor helps to further decrease the influence of capacitive parasitics. In Figure 6.17 the DTI structure can be seen. For the inductor, shielding has been used to reduce coupling with the substrate, lowering the influence of the substrate on the parasitics in the inductor [26]. Since the parasitics originating from the substrate are difficult to model, the shielding provides a higher predictability for the parasitic components. Due to the high value inductors needed, parasitics in the inductor are very easy to get, making it harder to get perfect cancellation.

RC EXTRACTION OF THE LAYOUT FOR THE SHUNT CONFIGURATIONS

To verify whether the parasitic components have a large influence on the OIP3 of the reference and compensation circuit, a RC extraction has been done on the different layouts. Two extractions have been done. In the first extraction, only the resistive parasitics have been extracted. In the second extraction, the capacitive and resistive parasitics have been extracted. Using the simulation values as mentioned in Table 6.4, sweeps over input power P_{in} have been done. In Figure 6.18 and Figure 6.19 the results can be seen for the JMM03 and JMM09, which are respectively the compensated circuit and the reference circuit without base resistance.

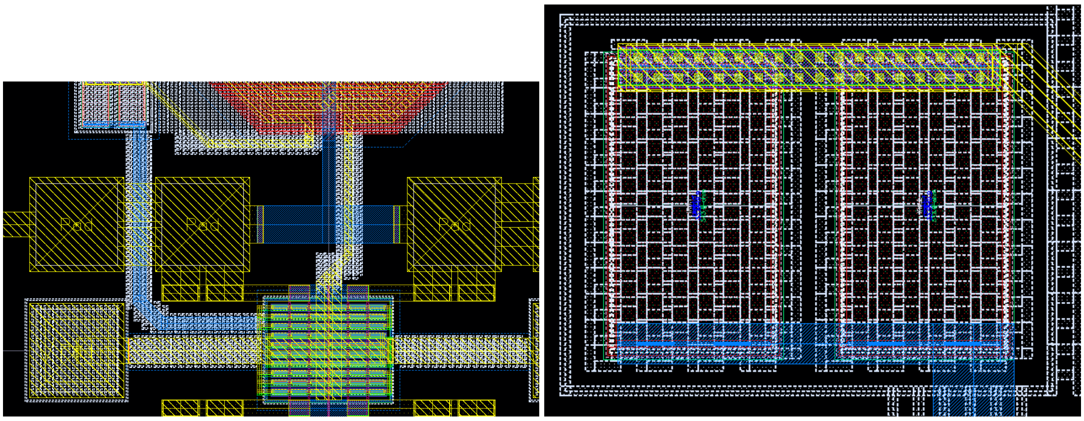

(a) Signal paths (b) Resistor

Figure 6.17: DTI below the signal paths and the resistor to decrease parasitics resulting from these components

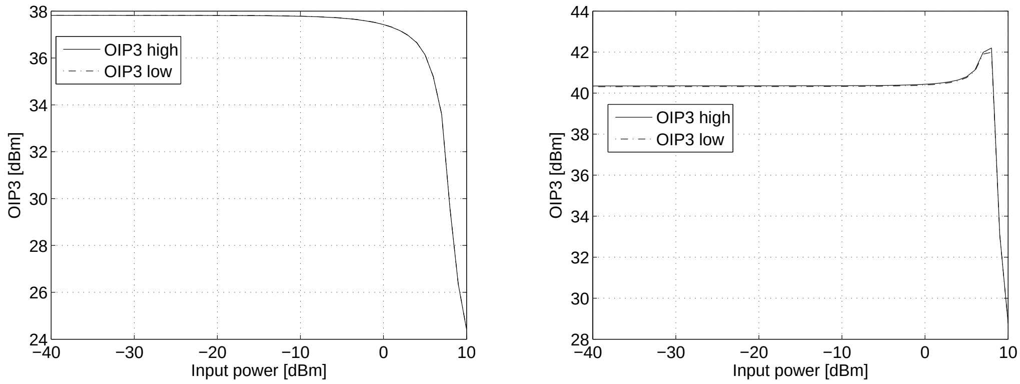

(a) Reference circuit (b) Compensated circuit

Figure 6.18: OIP3 versus input power for the R-only extracted reference circuit and compensated circuit in the shunt configuration for Δf=1MHz

As can be seen, when only the resistive parasitics have been extracted, an OIP3 improvement of 2.5dB could be obtained. However, when the resistive and capacitive parasitics have been extracted, only 1dB of improvement could be obtained. One should note that RC-extraction does not account for DTI. Therefore, the influence of the capacitive parasitics is expected to decrease. Like expected, the parasitics have a big influence on the compensation.

RC EXTRACTION OF THE LAYOUT FOR THE CB CONFIGURATIONS

To verify whether the parasitic components have a large influence on the OIP3 of the reference and compensation circuit, a RC extraction has been done on the different layouts. Two extractions have been done. In the first extraction, only the resistive parasitics have been extracted. In the second extraction, the capacitive and resistive parasitics have been extracted. Using the simulation values as mentioned in Table 6.7, sweeps over input power P_{in} have been done. In Figure 6.20 and Figure 6.21 the results can be seen for the JMM01 and JMM05, which are respectively the compensated circuit and the reference circuit without base resistance.

As can be seen, when only the resistive parasitics have been extracted, an OIP3 improvement of 5dB could be obtained. However, when the resistive and capacitive parasitics have been extracted, no significant OIP3 improvement could be obtained. One should note that RC-extraction does not account for DTI. Therefore, the influence of the capacitive parasitics is expected to decrease. Like expected, the parasitics have a big influence on the compensation.

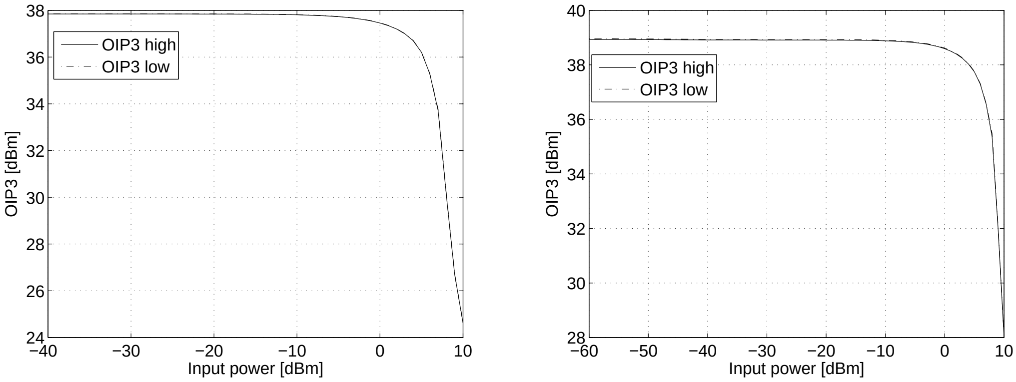

(a) Reference circuit (b) Compensated circuit

Figure 6.19: OIP3 versus input power for the RC-extracted reference circuit and compensated circuit in the shunt configuration for Δf=1MHz

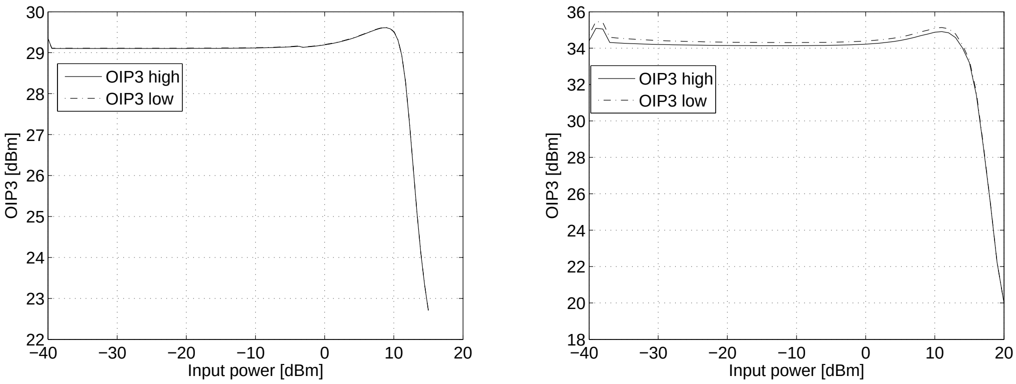

(a) R-extracted reference circuit (b) R-extracted compensated circuit

Figure 6.20: OIP3 versus input power for the R-only extracted reference circuit and compensated circuit in the CB configuration for Δf=1MHz

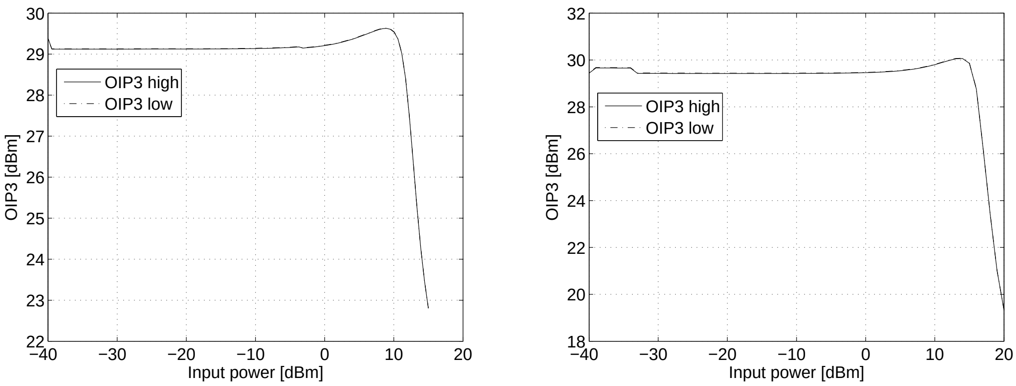

(a) RC-extracted reference circuit (b) RC-extracted compensated circuit

Figure 6.21: OIP3 versus input power for the RC-extracted reference circuit and compensated circuit in the CB configuration for Δf=1MHz

6.3. MEASUREMENT RESULTS FOR PASSIVE IN-BAND C_{bc} COMPENSATION

To test the test chip for passive in-band C_{bc} compensation from Section 6.2, the system shown in Figure 6.22 has been used.

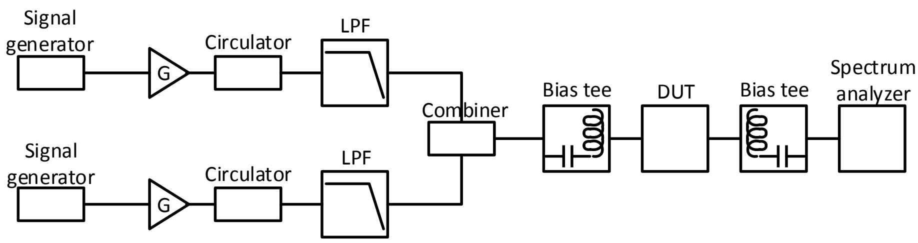

Figure 6.22: Measurement setup used to test passive in-band C_{bc} compensation

The two signal generators create tones at 1.8001GHz and 1.8008GHz, so with a tone spacing of 700kHz. By using very linear variable gain amplifiers, the linearity on the signal generators can be relaxed. The circulators and low pass filters help to isolate the amplifiers. In the combiner, the two signals are combined to 1 signal. Using bias tees, the device under test (DUT) has been connected to the combiner and the spectrum analyzer.

Due to timing constraints, only the shunt configurations without base degeneration have been tested (JMM03 and JMM09). Since the reference already has an OIP3 of 38dBm in the simulation, the linearity and noise floor of the measurement system becomes important. Since the IM3 signals of the system are very low and the P_{1dB} compression point is also low, the range in which measurements are possible is limited. Therefore an optimization has been done for each measurement point. For each measurement point, the system has been connected to a thru, to optimize the measurement system for noise floor and linearity. This has been done by adapting the gain of the amplifiers and the attenuation of the spectrum analyzer. After this optimization, the devices have been tested.

The measured values can be found in Figure 6.23 and Figure 6.24.

For lower power levels, the noise floor and the IM3 of the measurement system is very close to the IM3 measured for the reference circuit and the compensated circuit. Therefore, an important part of the IM3 signal at lower powers is determined by the measurement system. Since no phase information is available, no correction could be done on these IM3 figures. Only above -6dBm output power, the IM3 of the measurement system is 10dB lower than the IM3 of the device under test. Therefore, the only measurements considered useful are the ones above -6dBm output power.

The resulting OIP3 figures can be found in Figure 6.25.

As can be seen, for lower power levels, the OIP3 of the thru is rather low, indicating that the measurement setup creates distortion that could influence the OIP3. However, for higher power levels, the OIP3 is determined by the device under test. It can be concluded that the OIP3$_{low}$ of the compensation circuit is 0.5dB better than the OIP3$_{low}$ of the reference circuit. The OIP3$_{high}$ of the compensation circuit is 1dB better than the OIP3$_{high}$ of the reference level.

The OIP3 difference between measurement and setup can be explained by the additional parasitics that could not be obtained using RC-extraction of the layout, like inductive parasitics. It is also known within NXP that the C_{bc} modeling in the Mextram model equations is not fully correct, creating a difference between measurement and simulation [27]. However, the measurements do confirm the improvement that can be obtained using passive in-band C_{bc} compensation, although this improvement is minor. The parasitic components are too influential to consider this compensation technique as a viable option.

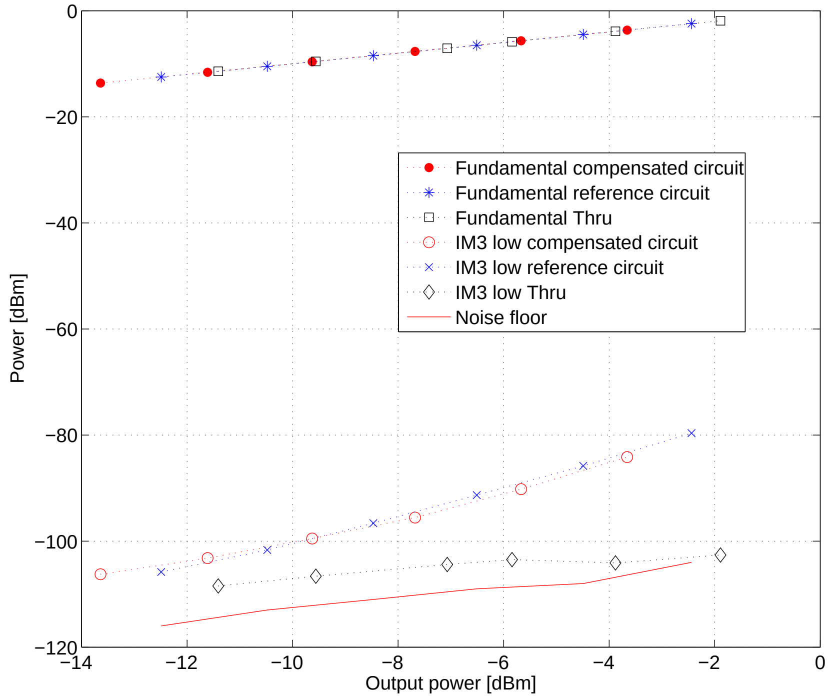

Figure 6.23: Measured fundamental and IM3 low power reference for the reference circuit, compensated circuit and the thru

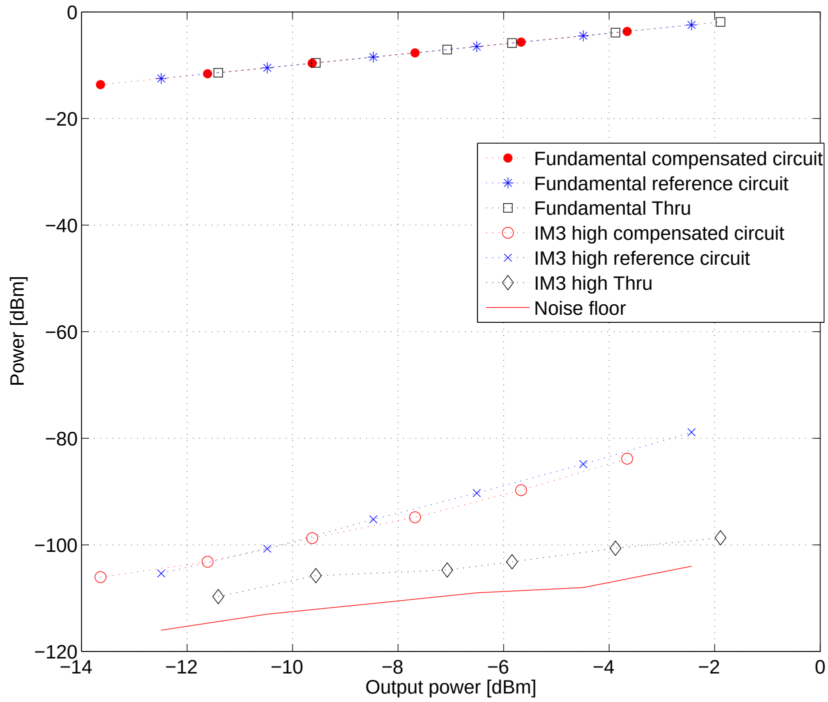

Figure 6.24: Measured fundamental and IM3 power levels for the reference circuit, compensated circuit and the thru

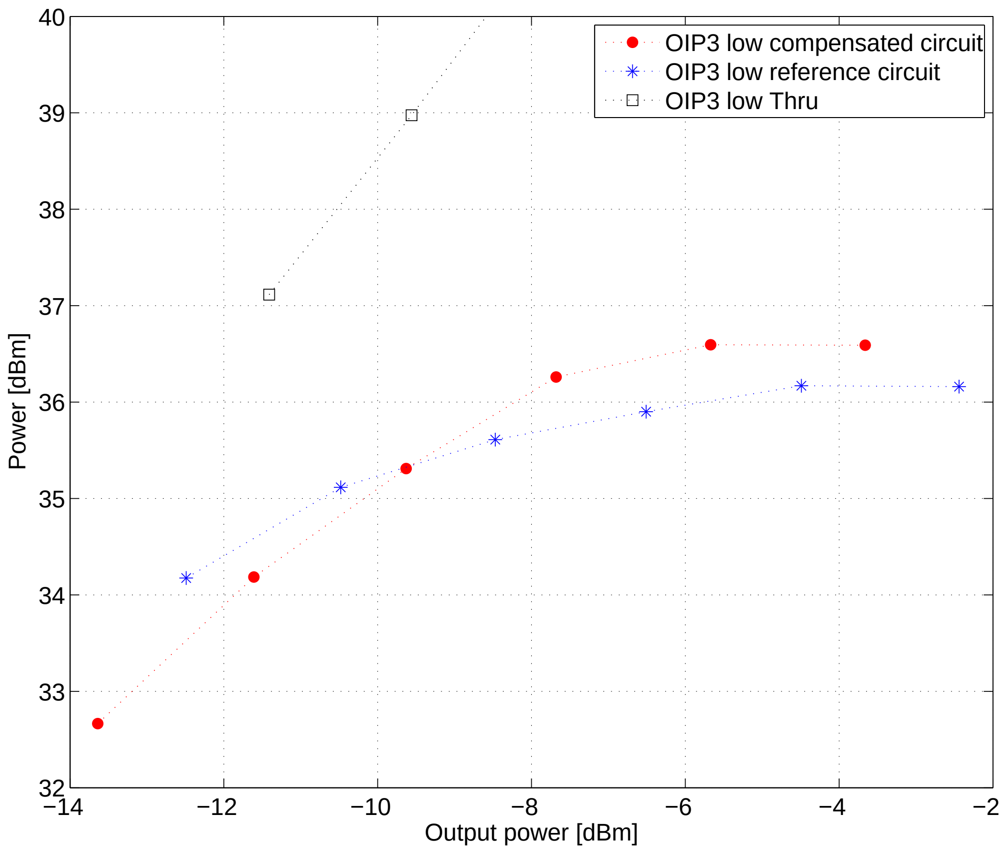

(a) OIP3 low

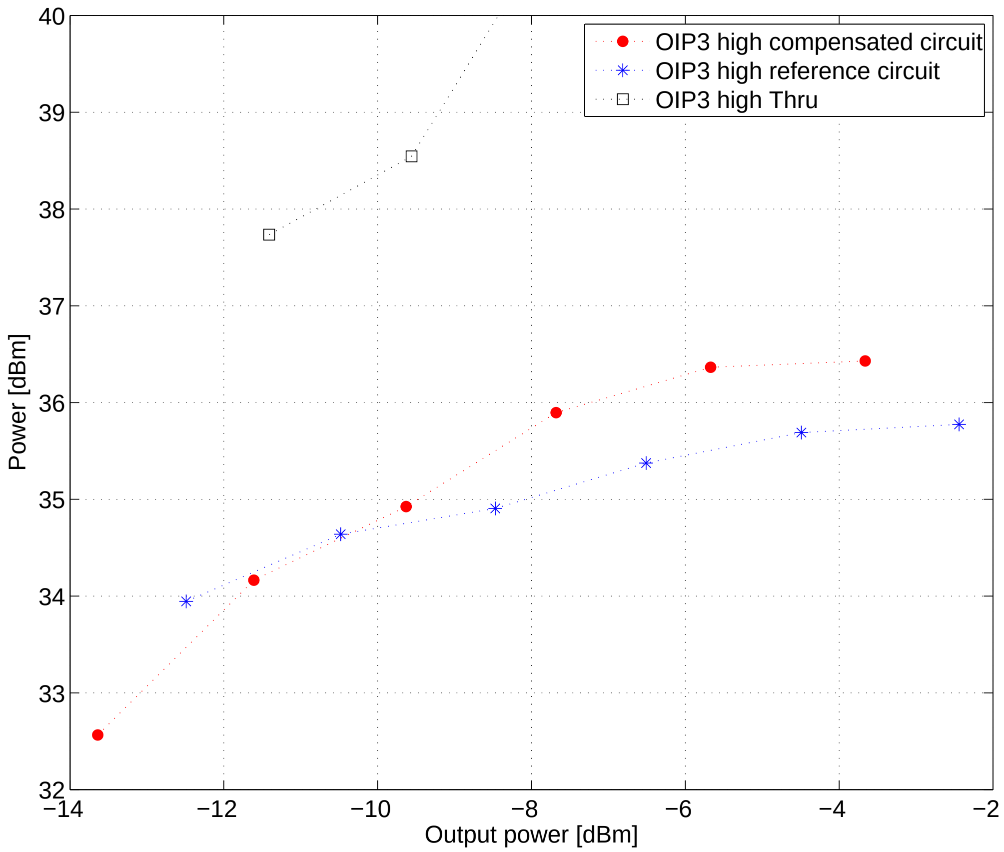

(b) OIP3 high

Figure 6.25: OIP3 figures for the measured reference shunt circuit, compensated shunt circuit and the thru

6.4. CONCLUSIONS AND FUTURE POSSIBILITIES

In this chapter, passive in-band C_{bc} compensation has been discussed as a way to cancel the IM3 distortion of the C_{bc} capacitance. A series combination of a depletion capacitance C_{com} with a compensation network Z(s) has been used to make IM3 currents with opposite phase compared to the C_{bc} capacitance. For this purpose in Section 6.1, a series combination of an inductor, resistor and depletion capacitance have been proposed as a viable solution for IM3 cancellation. With simulation it has been shown that this can give perfect cancellation. Using Volterra analysis, the correct combination of inductor value L_{com}, resistor value R_{com} and depletion capacitance C_{com} has been found.

In Section 6.2 the schematics and layout of the test chip have been presented. On schematic level, the OIP3 results have been presented, including sweeps over tone spacing Δf and input power P_{in}. On layout level, the choices concerning the layout have been explained. Since parasitics have an influence to the power 4 on the cancellation, the layout tries to minimize these parasitics. It has been shown with extracted views of the layout that an OIP3 improvement from 0 up to 2dB could be obtained.

In Section 6.3 the measurement results have been presented. It has been shown that an OIP3 improvement around 0.5dB could be obtained. However, not many measurement points have been taken, due to the limited power range in which measurements could be done.

FUTURE POSSIBILITIES

For the design of the test chip, the second order harmonics have not been shorted. This gives more flexibility for measurements. However, for the Volterra analysis, second order shorts have been assumed. For both depletion capacitances, the base collector capacitance C_{bc} and the compensation capacitance C_{com}, second harmonics shorts are assumed. The realization of second harmonic shorts can be done by going differential, as described in Section 2.5. However, this is not possible for the C_{com} capacitance. To provide the same effect as a second order short, the IM2 and HD2 currents of the C_{com} capacitance have to be canceled. This can be done by using an anti-parallel configuration as described in Section 4.3. This can also be seen in Figure 6.26.

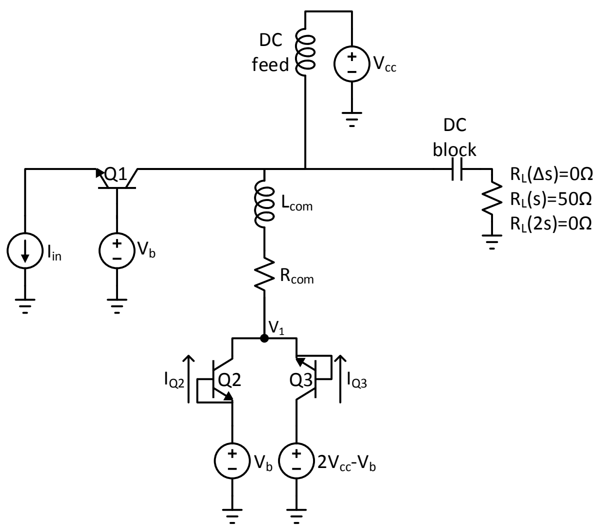

Figure 6.26: Second harmonic cancellation in the compensation capacitance using an anti-parallel configuration

For the chip design, an additional measure has to be taken for second order shorts. As described in Section 6.2, a base resistor is commonly added to the CB-stage for stability issues. This base resistor removes the second order short at the base of the CB-stage. Again, an antiparallel configuration might help in this situation. In Figure 6.27 this situation is depicted.

Although the current at node V_1 is not compensated, the purpose of the anti-parallel configuration in this part is that the IM3 currents caused by the second harmonic base voltages in I_{cbc} are compensated by the IM3 currents caused by the second harmonic voltages in I_{ap}. So the indirect mixing components should

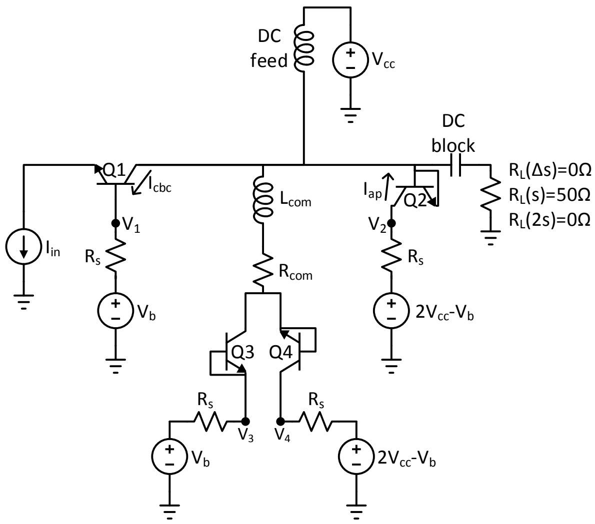

Figure 6.27: Compensation of the indirect mixing of the C_{bc} using an anti-parallel configuration

cancel each other. This idea has not been tested, but it is worthwhile to investigate, since it makes the results of the Volterra analysis much more relevant if it works. After all, when indirect mixing is present, the Volterra analysis from Section 6.1 doesn't apply anymore.

For measurement purposes, the P_{1dB} point should be optimized in future research. The P_{1dB} point has not been optimized in this configuration, causing the limited measurement range. By optimizing for the P_{1dB} point, one could easily expand the power range in which measurements are possible.

Since the measurements show that passive in-band C_{bc} compensation has a large dependency on device parasitics, digitally assisted optimization might help to counteract these effects. In order for this to work, a small adaptation in the bias voltage and a variable resistance value would enlarge the possible OIP3 improvement. A small adaptation in the bias voltage changes the value of the depletion capacitance, which might tune out parasitics, while a variable resistance is needed to comply with the equations derived from Volterra analysis.

7

ACTIVE C_{bc} COMPENSATION

In Chapter 5 and Chapter 6 the options of out-of-band matching and passive in-band C_{bc} compensation have been discussed. These methods are all passive methods for OIP3 improvement. Although passive in-band C_{bc} compensation uses transistors, these are connected in such a way that they behave as nonlinear passive devices. Using transistors, active compensation can be used to achieve higher OIP3 numbers.

The main disadvantage of active compensation is the extra power consumption needed to drive the compensation. Passive compensation does not add to the power consumption. On the other hand, all the passive compensation methods are narrowband in their behavior. Active compensation, if applied correctly, has the potential to be much more wideband than the passive compensation methods. This is because the active compensation does not have to depend on the tone spacing Δf. On the other hand, passive components have the potential to work on higher frequencies, since active components lose their gain at higher frequencies.

The basic principle of active compensation is shown in Figure 7.1. The IM3 currents produced by the C_{bc} capacitance are injected back in the circuit, making the net IM3 current zero.

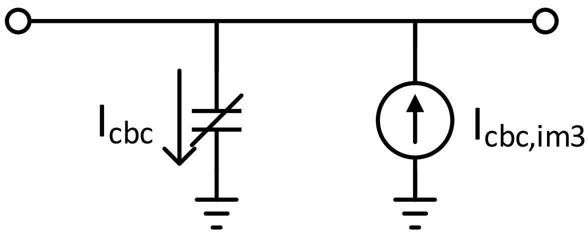

Figure 7.1: The basic principle of active compensation

This chapter will discuss the research done on active compensation so far. In Section 7.1 the basic concept of active compensation for C_{bc} distortion is shown. It will demonstrate that in a differential configuration active compensation can be used as an option for C_{bc} compensation, when current controlled current sources are used. In Section 7.2 active compensation will be studied using the Gummel-Poon model. First the Gummel-Poon model of the CB-stage will be expanded, after which the Gummel-Poon model of the CE-stage will be expanded. In Section 7.3 the same will be done, with one crucial difference: the second harmonics and intermodulation products will be canceled. In Section 7.4 the Gummel-Poon model will be replaced by the Mextram model, starting with the CB-stage. Since active compensation uses a current controlled current source, Section 7.5 will discuss several options to implement this current controlled current source. The chapter will end with the conclusions in Section 7.6. Due to timing constraints, the investigation of active compensation could not be finished in this thesis project. This is why this chapter will not present the wideband behavior of active compensation. However, as will become clear from the basic principle described in Section 7.1, active compensation has the potential to be very wideband. Due to time constraints, this has not be proven in this report. Further investigation has to prove this claim.

7.1. BASIC CONCEPT OF ACTIVE COMPENSATION

For active compensation, the current running through the C_{bc} capacitance has to be fed back with a 180 degrees phase in the circuit. Therefore, a current controlled current source (CCCS) can be used, as shown in Figure 7.2.

Due to the differential behavior of the amplifier, generating the current produced by the C_{bc} capacitances is

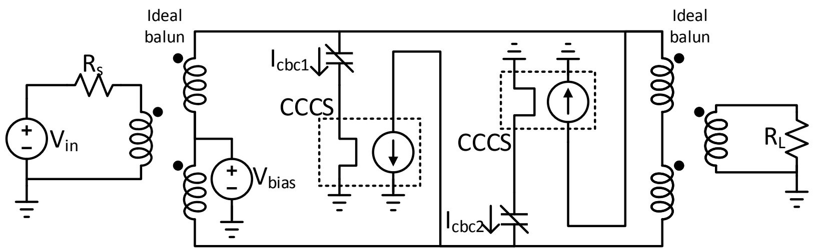

Figure 7.2: The basic configuration for active C_{bc} compensation

much easier. With a 0 or 180 degree phase in the CCCS the current can be injected in the circuit by connecting the CCCS properly. In this configuration, only the differential currents are canceled, since the solution uses the differential circuit structure to inject a signal with 180 degrees phase shift. This means that all even order harmonics and intermodulation products are not canceled internally, since these are common mode signals. The even harmonics and intermodulation products are canceled at the output due to the output balun.

As long as the CCCS functions properly, there is no problem in the frequency behavior. The CCCS just senses the currents running through the C_{bc}, making it insensitive to the tone spacing. Further investigation has to prove this claim and whether it holds for more complicated models, but for now it is assumed that this solution is the most wideband of all solutions discussed so far.

In Figure 7.3 the current amplification of the CCCS is swept. As can be seen, when the CCCS gives an amplification of 1, the current is exactly copied and a peak in OIP3 occurs. For the reference OIP3, a current amplification of 0 has been used.

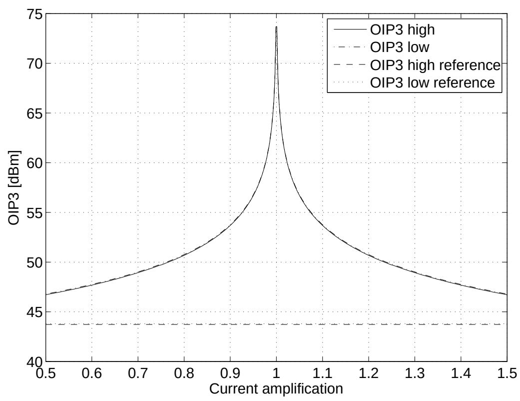

Figure 7.3: The OIP3 versus the amplification of the CCCS for the basic active compensation configuration

7.2. ACTIVE COMPENSATION IN THE GUMMEL-POON MODEL

With C_{bc} capacitances only, active compensation works as is demonstrated in Section 7.1. However, in a transistor this doesn't have to be the case. After all, in a transistor, other nonlinearities are also of importance. Therefore a Gummel-Poon analysis has been done to study the effect of the different nonlinearities in the amplifier on active compensation.

The circuit used in this analysis is shown in Figure 7.4. In this circuit, R_e is used for cancellation of

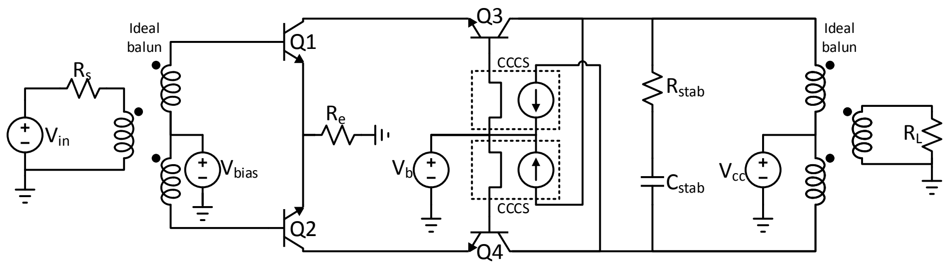

Figure 7.4: The circuit used for Gummel-Poon analysis of active compensation

the exponential distortion of the CE-stage. R_{stab} and C_{stab} are added for stability reasons. When using the Gummel-Poon model, these stabilization components aren't necessary. However, when using the Mextram model, stability is an issue, as will be discussed in Section 7.4. To get a fair comparison, the stabilization components are also added when using the Gummel-Poon model. The values of R_{stab} and C_{stab} are 100Ω and 2pF respectively.

The compensation network is put in the base of the CB-stage. As discussed in Chapter 4, the nonlinearities in the base-emitter junction of the CB-stage have been linearized, since the CB-stage is current driven. Since the AC currents in the emitter are significantly larger than those in the base, the base AC currents are dominated by the AC current coming from the base-collector junction. Therefore, the IM3 current coming from the base of the CB-stage mainly reflects the IM3 current produced by the C_{bc} capacitance.

In the course of this section, the CE-stage and CB-stage will be expanded with the τ_f, C_{je} and C_{jc} components of the Gummel-Poon model. While these Gummel-Poon models will be expanded, the other simulation values stay the same. The simulation values can be found in Table 7.1.

Table 7.1: Simulation values for studying active compensation

Parameter	Description	Value
I_c	Collector current	80mA
T_{in}	Turns ratio input balun	2:3
T_{out}	Turns ratio output balun	5:4
V_{cc}	Supply voltage	3.3V
R_s	Source impedance	50Ω
R_L	Load impedance	50Ω
P_{in}	Input power for each tone	-45dBm
f_c	The center frequency	1.8GHz
Δf	Tone spacing	10MHz

In the first simulation, the Gummel-Poon model starts with the basic model needed for simulation: exponential distortion in the CE-stage and CB-stage and the C_{jc} in the CB-stage. The model of the CB-stage used for this simulation is given in Table 7.2. A high value for β has been used, which is typical for the QUBiC4Xi process, as shown in Section 3.1.

Using this model, the circuit has been simulated. Again, the current amplification of the CCCS is swept. For the reference OIP3, a current amplification of 0 has been used. The OIP3 results are displayed

Table 7.2: Gummel-Poon parameters of the CB-stage for the basic model for active C_{bc} compensation

Parameter	Description	Value
β	Forward current gain	2000
I_s	Saturation current	0.5 fA
C_{je0}	Zero-bias base-emitter depletion capacitance	0 F
C_{jc}	Zero-bias base-collector depletion capacitance	26 fF
m_{je} & m_{jc}	Grading coefficient of the base-emitter and base-collector junction	1/3
V_{je} & V_{jc}	Built-in voltage of the base-emitter and base-collector junction	0.7 V
τ_f	Transit time	0 s
A	Area of the transistors	25

in Figure 7.5. Again for a current amplification of 1, the OIP3 peaks. The peak reaches 70dBm, indicating

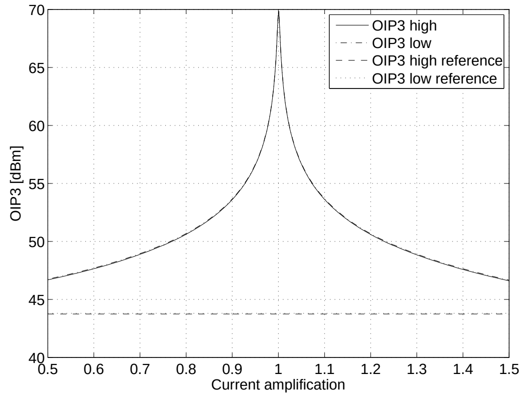

Figure 7.5: The OIP3 versus the current amplification of the CCCS for the basic Gummel-Poon model for active C_{bc} compensation

perfect cancellation.

An important assumption for this compensation is that the currents in the base of the CB-stage are dominated by the collector-base currents. Therefore, this assumption is tested first by expanding the Gummel-Poon model of the CB-stage. After this, the CE-stage will be expanded to see whether the nonlinear components of the CE-stage significantly degrade the active C_{bc} compensation.

7.2.1. EXPANDING THE GUMMEL-POON MODEL OF THE CB-STAGE

One of the assumptions for active compensation is that the AC currents in the base of the CB-stage are dominated by the AC currents of the collector-base junction. Therefore, when the forward transit time τ_f and the depletion capacitance C_{je} are added, no change should occur in the active C_{bc} compensation. In Table 7.3 the model of the CB-stage is given. The CE-stage has no τ_f, C_{je} or C_{jc} and therefore only has exponential distortion, canceled by R_e.

Table 7.3: Gummel-Poon parameters for the CB-stage with active C_{bc} compensation

Parameter	Description	Value
β	Forward current gain	2000
I_s	Saturation current	0.5 fA
C_{je}	Zero-bias base-emitter depletion capacitance	0.12 pF
C_{jc}	Zero-bias base-collector depletion capacitance	26 fF
m_{je} & m_{jc}	Grading coefficient of the base-emitter and base-collector junction	1/3
V_{je} & V_{jc}	Built-in voltage of the base-emitter and base-collector junction	0.7 V
τ_f	Transit time	13 ps
A	Area of the transistors	25

Using this model for the CB-stage, the current amplification of the CCCS has been swept. For the reference OIP3, a current amplification of 0 has been used. In Figure 7.6 the OIP3 results are given. Again, the

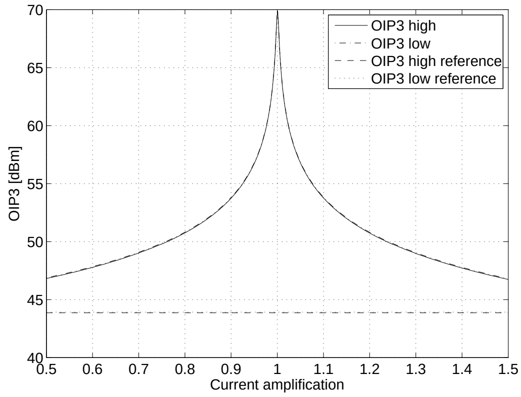

Figure 7.6: The OIP3 versus the current amplification of the CCCS for the expanded Gummel-Poon model for the CB-stage with active C_{bc} compensation

optimum is at a current amplification of 1. The OIP3 reached is again 70 dBm, proving that the (nonlinear) currents from the base-emitter junction play no significant role in the base of the CB-stage.

7.2.2. EXPANDING THE GUMMEL-POON MODEL OF THE CE-STAGE

In the previous sections, the CE-stage has been assumed to be only dominated by the exponential distortion. Other contributions to IM3 have been ignored. Since the IM3 components of the exponential distortion in the CE-stage have been canceled using R_e, the CE-stage can be viewed as completely linear in previous sections. As shown in Chapter 3, exponential distortion is not the only distortion present in the CE-stage. The transit time τ_f, and depletion capacitances C_{je} and C_{jc} also influence its linearity. In this section the influence of these different factors will be examined. The section will start with τ_f, next C_{je} will be discussed and at last C_{jc} will be discussed. For every step, the influence of the component concerned will be examined separately and in combination with previously added nonlinearities. The model of the CB-stage has not changed, so in the CB-stage τ_f, C_{je} and C_{jc} are already included.

TRANSIT TIME τ_f

As discussed in Chapter 3, the transit time τ_f adds extra distortion, directly correlated with the exponential distortion. Since high collector currents are used, I_c=80mA, the exponential distortion shouldn't influence the active compensation a lot. Also, since emitter degeneration is used, the cancellation of the exponential distortion should have a wideband characteristic [6]. Table 7.4 gives the Gummel-Poon model used for the CE-stage, when τ_f is added.

Table 7.4: Gummel-Poon parameters for the CE-stage with τ_f added for active C_{bc} compensation

Parameter	**Description**	**Value**
β	Forward current gain	2000
I_s	Saturation current	0.5 fA
C_{je}	Zero-bias base-emitter depletion capacitance	0 F
C_{jc}	Zero-bias base-collector depletion capacitance	0 F
m_{je} & m_{jc}	Grading coefficient of the base-emitter and base-collector junction	1/3
V_{je} & V_{jc}	Built-in voltage of the base-emitter and base-collector junction	0.7 V
τ_f	Transit time	13 ps
A	Area of the transistors	25

The current amplification of the CCCS has been swept to see whether cancellation is still possible. For

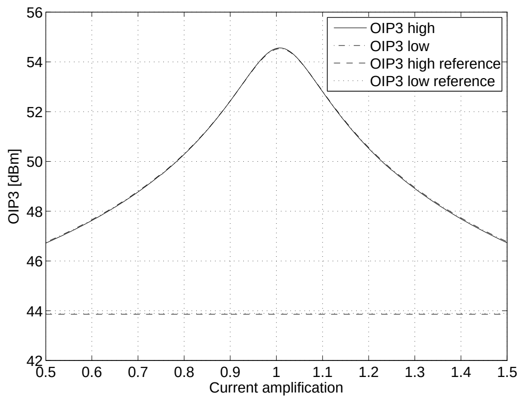

Figure 7.7: The OIP3 versus the current amplification of the CCCS for the CE-stage with τ_f with active C_{bc} compensation

the reference OIP3, a current amplification of 0 has been used. In Figure 7.7 the OIP3 results are given. As can be seen, the OIP3 still has an optimum for a current amplification of 1. However, the maximum reachable OIP3 has decreased to 54.6dBm. This is expected, since τ_f distortion has not been canceled in the CE-stage.

DEPLETION CAPACITANCE C_{je}

The depletion capacitance C_{je} also plays an important role for linearity. When the voltage swing at the input is high, the depletion capacitance produces IM3 currents that can be significant for the cancellation. However, the C_{je} can also help with linearizing the τ_f component, as described in [6].

Two situations are studied in this case. In the first situation, only the C_{je} has been added to the basic exponential Gummel-Poon model of the CE-stage. In the second situation the C_{je} and the τ_f have been added to the model. The complete models for the CE-stage are given in Table 7.5.

Table 7.5: Gummel-Poon parameters for the CE-stage with C_{je} and τ_f added for active C_{bc} compensation

Parameter	**Description**	**Situation 1**	**Situation 2**
β	Forward current gain	2000	2000
I_s	Saturation current	0.5 fA	0.5 fA
C_{je}	Zero-bias base-emitter depletion capacitance	0.12 pF	0.12 pF
C_{jc}	Zero-bias base-collector depletion capacitance	0 F	0 F
m_{je} & m_{je}	Grading coefficient of the base-emitter and base-collector junction	1/3	1/3
V_{je} & V_{jc}	Built-in voltage of the base-emitter and base-collector junction	0.7 V	0.7 V
τ_f	Transit time	0 s	13 ps
A	Area of the transistors	25	25

Using these models for the CE-stage, the current amplification of the CCCS has been swept. For the reference OIP3, a current amplification of 0 has been used. The results of the simulations are shown in Figure 7.8.

As can be seen, the C_{je} capacitance influences the OIP3 a lot when τ_f isn't present. Since the input impedance of the CE-stage is very high due to the high β value, a large voltage swing is present at the input. High voltage swings on depletion capacitances give more IM3 currents. It seems that a part of this IM3 current can be compensated by the active compensation, explaining the peak of 47.5dBm around the current amplification of 0.5. The reference OIP3 also has been increased. This can be attributed to the IM3 currents created by the C_{je} capacitance. These currents have an amplitude and phase such that the IM3 currents created by the C_{bc} capacitance of the CB-stage are partly compensated.

When using the transit time τ_f the diffusion capacitance significantly lowers the voltage swing at the input. At the same time, the C_{je} capacitance helps to linearize the diffusion capacitance. However, there

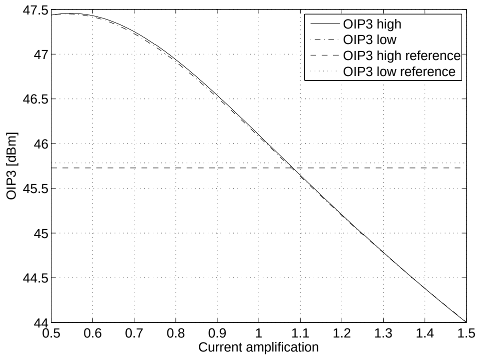

(a) With C_{je}

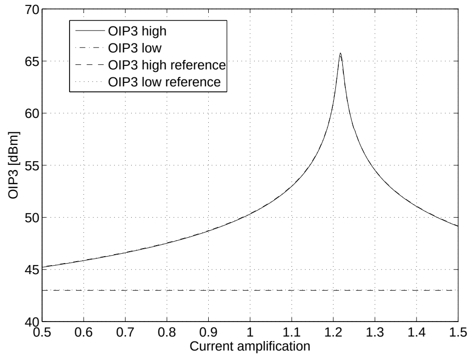

(b) With C_{je} and τ_f

Figure 7.8: The influence of the C_{je} of the CE-stage on the OIP3 versus the current amplification of the CCCS

are still IM3 currents created by the CE-stage. These IM3 currents are significantly lower and have a different phase and amplitude, which is why they do not compensate the C_{bc} capacitance of the CB-stage anymore. The IM3 currents created by the C_{je} and τ_f of the CE-stage are partly compensated by the active compensation, when the current amplification is around 1.2. The OIP3 peaks up to 66dBm.

DEPLETION CAPACITANCE C_{jc}

When cascoding the CE-stage, the C_{bc} of the CE-stage becomes less dominant for OIP3, like discussed in Chapter 4. However due to the stabilization network, the output impedance for the CB-stage is decreased, making the C_{bc} of the CB-stage also less dominant. This is why it is important to also consider the effect of the CE-stage, to see whether it is still not dominant in the transfer.

Two situations have been studied. In the first situation only the C_{jc} has been added to the exponential Gummel-Poon model of the CE-stage. In that situation, a large voltage swing is expected at the input of the amplifier, making the C_{bc} of the CE-stage more dominant. In the second situation also the C_{je} and τ_f have been added. This lowers the voltage swing, which should make the C_{bc} of the CE-stage less dominant. The models used are given in Table 7.6.

Table 7.6: Gummel-Poon parameters for the CE-stage with C_{jc} added for active C_{bc} compensation

Parameter	Description	Situation 1	Situation 2
β	Forward current gain	2000	2000
I_s	Saturation current	0.5 fA	0.5 fA
C_{je}	Zero-bias base-emitter depletion capacitance	0 F	0.12 pF
C_{jc}	Zero-bias base-collector depletion capacitance	26 fF	26 fF
m_{je} & m_{jc}	Grading coefficient of the base-emitter and base-collector junction	1/3	1/3
V_{jc} & V_{je}	Built-in voltage of the base-emitter and base-collector junction	0.7 V	0.7 V
τ_f	Transit time	0 s	13 ps
A	Area of the transistors	25	25

Using these models for the CE-stage, the current amplification of the CCCS has been swept. For the reference OIP3, a current amplification of 0 has been used. The results of the simulations are given in Figure 7.9. As can be seen, the maximum OIP3 decreases when only the C_{bc} has been added. Also the point where the current amplification gives the best OIP3 has changed to a value lower than 0.5. This indicates that the C_{bc} of the CE-stage adds extra IM3 currents, counteracting the C_{bc} of the CB-stage, which is why the reference level does increase. However, no perfect cancellation is present.

When C_{je} and τ_f are added, the OIP3 goes to 58 dBm for a current amplification of approximately 1.25. This indicates that the voltage swing over the C_{bc} has decreased. Figure 7.8b and Figure 7.9b are

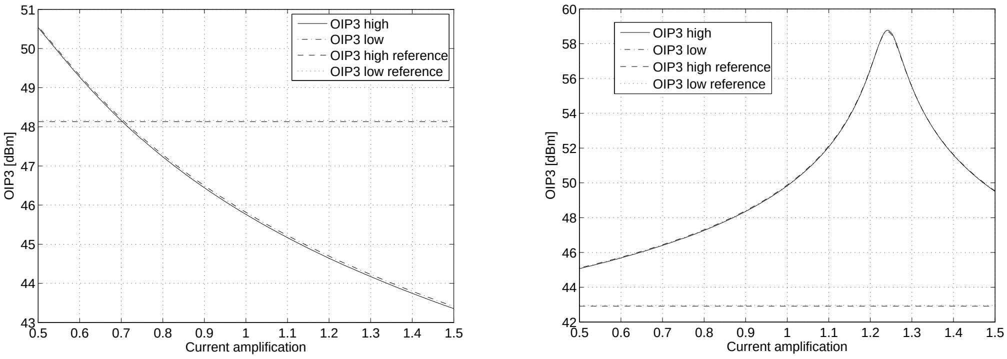

(a) With C_{jc} (b) With C_{jc}, C_{je} and τ_f

Figure 7.9: The influence of the C_{jc} of the CE-stage on the OIP3 versus the current amplification of the CCCS

very similar, indicating that the C_{je} and τ_f distortion is dominant in the compensation point. In the compensation point around 1.25 the IM3 currents of the C_{je} and τ_f distortion are partially compensated, and an upper limit of 58 dBm is reached due to the C_{jc} of the CE-stage.

7.2.3. CROSS-COUPLING THE CE-STAGE

As discussed in Chapter 3, cross-coupling the CE-stage can help to reduce the feedback effect of the C_{bc} of the CE-stage. Since the CB-stage already reduces the influence of the C_{bc} of the CE-stage, the cross-coupling does not provide a big benefit for unilaterization. However, the feedback of the C_{bc} of the CE-stage is reduced, which might positively influence the IM3 contribution of the C_{bc} of the CE-stage. Therefore, the circuit given in Figure 7.10 has been made.

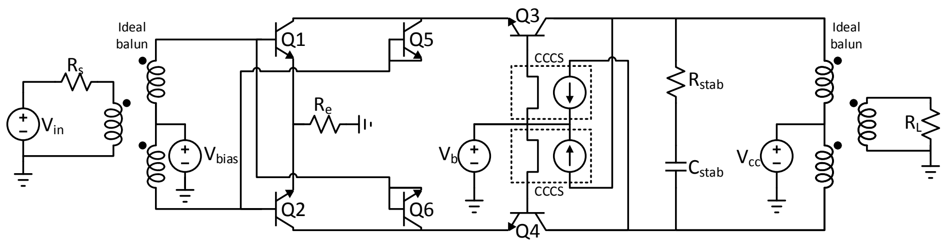

Figure 7.10: The cross-coupled cascode amplifier with active compensation

Again a Gummel-Poon model has been used for the transistors. In this case, all the transistors have a C_{jc}, C_{je} and τ_f parameter. The model for the transistors is given in Table 7.7. Using this model for the

Table 7.7: Gummel-Poon parameters for the cross-coupled cascode amplifier with active C_{bc} compensation

Parameter	**Description**	**Values**
β	Forward current gain	2000
I_s	Ideal reverse-biased saturation current	0.5 fA
C_{je}	Zero-bias base-emitter depletion capacitance	0.12 pF
C_{jc}	Zero-bias base-collector depletion capacitance	26 fF
m_{je} & m_{jc}	Grading coefficient of the base-emitter and base-collector junction	1/3
V_{je} & V_{jc}	Built-in voltage of the base-emitter and base-collector junction	0.7 V
τ_f	Transit time	13 ps
A	Area of the transistors	25

cascode amplifier, the current amplification of the CCCS has been swept. For the reference OIP3, a current amplification of 0 has been used. The results of the simulation are given in Figure 7.11. Again, the OIP3

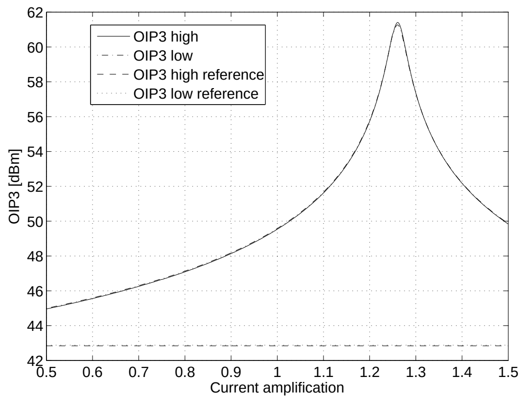

Figure 7.11: The influence of cross-coupling on the active C_{bc} compensation

peaks at a current amplification of 1.25. The effect of the C_{bc} has decreased a bit due to the reduced feedback effect. Therefore, the OIP3 gets 3dB higher than without cross-coupling, resulting in an OIP3 of 61dBm.

7.2.4. SUMMARY

In this section, active C_{bc} compensation has been studied using the Gummel-Poon model. The main results are displayed in Table 7.8.

Table 7.8: Summary of simulation results for active C_{bc} compensation using the Gummel-Poon model

CE-stage				CB-stage			$\Delta OIP3_{peak}$ [2]	$G_{\Delta OIP3_{peak}}$ [3]	$\Delta OIP3_{G=1}$ [4]
τ_f	C_{je}	C_{jc}	CC [1]	τ_f	C_{je}	C_{jc}			
0s	0F	0F	n	0s	0F	26fF	26dB	1	26dB
0s	0F	0F	n	13ps	0.12pF	26fF	26dB	1	26dB
13ps	0F	0F	n	13ps	0.12pF	26fF	11dB	1	11dB
0s	0.12pF	0F	n	13ps	0.12pF	26fF	1.8dB	0.5	0.3dB
13ps	0.12pF	0F	n	13ps	0.12pF	26fF	22dB	1.2	8dB
0s	0F	26fF	n	13ps	0.12pF	26fF	2.5dB	0.5	-2.5dB
13ps	0.12pF	26fF	n	13ps	0.12pF	26fF	16dB	1.25	7dB
13ps	0.12pF	26fF	y	13ps	0.12pF	26fF	18dB	1.25	6dB

[1] Cross-coupled
[2] The highest achievable OIP3 improvement compared to the reference OIP3
[3] The current amplification needed for the highest achievable OIP3 improvement
[4] The OIP3 improvement compared to the reference OIP3 for a current amplification of 1

As can be seen, the τ_f and C_{je} distortion in the CB-stage do not influence the OIP3. When the τ_f distortion from the CE-stage has been added, the OIP3 lowers, but the compensation has not been influenced: the peak in OIP3 improvement still occurs for a current amplification of 1. The C_{je} distortion from the CE-stage does influence the active compensation. Without the diffusion capacitance in the CE-stage, the OIP3 improvement is very low and the needed current amplification lowers significantly. The diffusion capacitance lowers the voltage swing and changes the phase of the C_{je} distortion. Therefore, when the τ_f component is added in the CE-stage, the OIP3 improvement increases. The current amplification needed for the highest OIP3 improvement does shift to 1.2, since the C_{je} distortion from the CE-stage is still present. When the C_{jc} of the CE-stage has been added, the OIP3 improvement lowers. With the τ_f and C_{je} parameters in the CE-stage, the needed current amplification for the highest OIP3 improvement barely changes, indicating that the IM3 current from the C_{je} capacitance are much more dominant than the IM3 currents of the C_{jc} in the CE-stage. Using cross-coupling reduces the feedback effect for the C_{jc} in the CE-stage, which has a positive influence on the highest OIP3 improvement that can be achieved.

7.3. ACTIVE COMPENSATION WITH SECOND ORDER SHORTS IN THE GUMMEL-POON MODEL

For linearity, second harmonics and intermodulation products play an important role. This is the reason why the exponential distortion can be canceled with R_e, or why an inductor can be used to counteract the C_{bc} of the CB-stage as described in Chapter 5. The analysis done in Section 7.2 ignores the effect of the IM2 and HD2 voltages between the CE-stage and the CB-stage. Therefore, the same analysis has been done with second harmonic shorts between the CE-stage and the CB-stage. To ensure current-driven conditions for the CB-stage, a second order open has been provided at the input of the CB-stage. The resulting circuit is given in Figure 7.12.

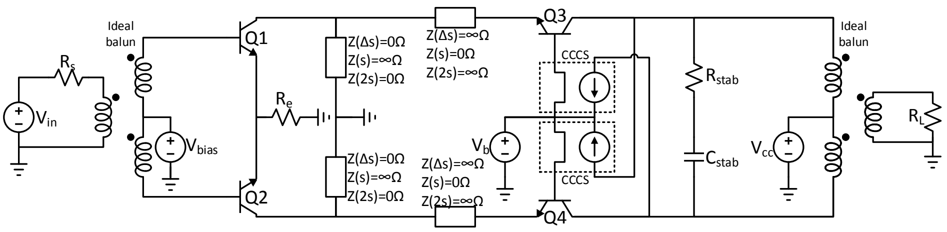

Figure 7.12: The circuit used for Gummel-Poon analysis of active compensation with second order shorts and opens

Throughout this section, the Gummel-Poon models of the CE-stage and CB-stage will be expanded. During this study, the other simulation values remain the same. The simulation values can be found in Table 7.1. Again, the first simulation is with only exponential distortion in the CE-stage and exponential and C_{bc} distortion in the CB-stage. For the reference OIP3, a current amplification of 0 has been used. The results are given in Figure 7.13. As can be seen, perfect cancellation occurs when the current amplification is 1. The

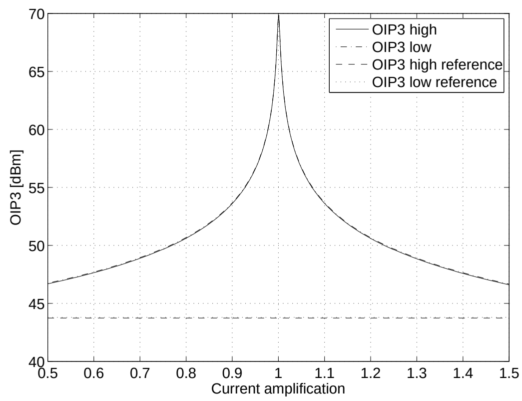

Figure 7.13: The OIP3 versus the current amplification of the CCCS for the basic Gummel-Poon model for active C_{bc} compensation

OIP3 reaches a level of 70 dBm. Again, first the model of the CB-stage will be expanded, since it is expected that this has the least influence on the compensation. Secondly, the CE-stage will be expanded.

7.3.1. EXPANDING THE GUMMEL-POON MODEL OF THE CB-STAGE

Just as in Section 7.2, the parameters τ_f and C_{je} have been added. Since the CB-stage is still current driven, it is expected that the current in the base of the CB-stage is mainly dominated by the current from the C_{bc} capacitance. The model of the CB-stage is given in Table 7.3. For the reference OIP3, a current amplification of 0 has been used. The results are given in Figure 7.14.

Just as without the second harmonic shorts and opens, the OIP3 goes to 70 dBm for a current amplification of 1. So again, the τ_f and C_{je} of the CB-stage do not influence the active C_{bc} compensation.

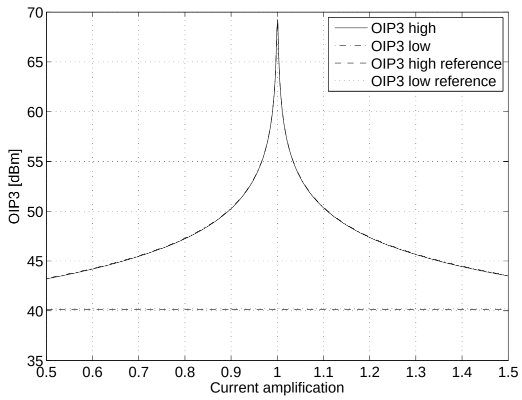

Figure 7.14: The OIP3 versus the current amplification of the CCCS for the expanded Gummel-Poon model for the CB-stage with active C_{bc} compensation

7.3.2. EXPANDING THE GUMMEL-POON MODEL OF THE CE-STAGE

Again the influence of the CE-stage is studied. The same steps as in Section 7.2 are taken. So first the influence of τ_f is investigated. Secondly, the influence of C_{je} is investigated, after which it is combined with the τ_f. Lastly the C_{jc} is investigated, its own influence and the combined influence of C_{jc}, C_{je} and τ_f on the active compensation.

TRANSIT TIME τ_f

When the τ_f is added, the cancellation of the exponential distortion of the CE-stage should not be perfect anymore. Just as in Section 7.2 this should result in a lower OIP3 in the optimum. The model used for the CE-stage is given in Table 7.4. For the reference OIP3, a current amplification of 0 has been used. The simulation results are given in Figure 7.15. As can be seen, the OIP3 has decreased to 55 dBm. However, the

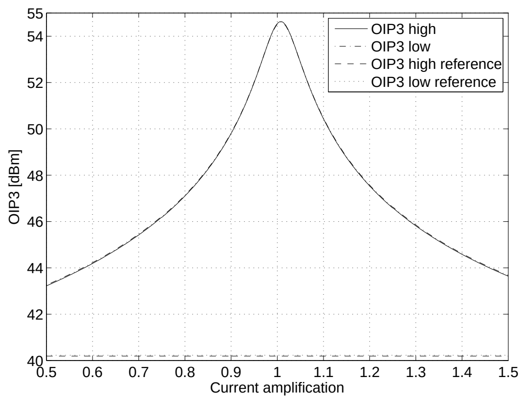

Figure 7.15: The OIP3 versus the current amplification of the CCCS for the CE-stage with τ_f with active C_{bc} compensation

optimal OIP3 is still achieved for a current amplification of 1.

DEPLETION CAPACITANCE C_{je}

The depletion capacitance C_{je} is expected to give extra IM3 currents. On the other hand, it should also decrease the IM3 component created by the diffusion capacitance created by transit time τ_f. Two situations have been studied. In the first situation only C_{je} is added to the Gummel-Poon model. In the second situation, C_{je} and τ_f are added to see the combined effect of these nonlinear components. In Table 7.5 the Gummel-Poon models for situation 1 and 2 are given. Using these models, the current amplification has been swept. For the reference OIP3, a current amplification of 0 has been used. In Figure 7.16 the simulations results are given.

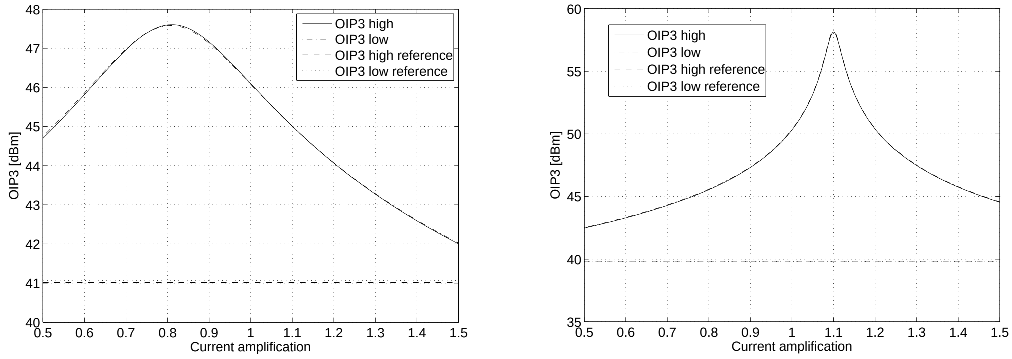

(a) With C_{je}

(b) With C_{je} and τ_f

Figure 7.16: The influence of the C_{je} of the CE-stage on the OIP3 versus the current amplification of the CCCS

As can be seen, again the optimum OIP3 changes when C_{je} is added. When only the C_{je} is added, the OIP3 has a peak of 47.5dBm at a current amplification of 0.8. With τ_f, the OIP3 peaks around a current amplification of 1.1, with an OIP3 of 58dBm. Again, this is larger than the OIP3 with only the τ_f added, due to the cancellation effect of C_{je} as described in Chapter 3.

Although the trends are the same in this simulation as in Section 7.2, there are some differences. Without second order shorts, the OIP3 peaks occur at different current amplifications. This suggests that the IM2 voltage at the intermediate nodes between the CE- and CB-stage plays a role for the IM3 contributions. The only nonlinear components at those nodes are the C_{je} and τ_f of the CB-stage. This implies that although these components do not seem to produce a significant IM3 contribution on their own, they do produce IM3 components under influence of IM2 voltages created by the CE-stage.

DEPLETION CAPACITANCE C_{jc}

Due to the C_{jc} the OIP3 decreased a lot in Section 7.2. However, once the τ_f and C_{je} have been added, the OIP3 went up, due to the reduced voltage swing at the input. With second order shorts between the CE- and CB-stage, the C_{jc} of the CE-stage should be directly affected, since it is connected to this node. Two situations are used for the simulation. In the first situation, only the C_{jc} is added to the Gummel-Poon model. In the second situation, also C_{je} and τ_f have been added. In Table 7.6 the models used for the simulations are given. Using these models, the current amplification has been swept. For the reference OIP3, a current amplification of 0 has been used. In Figure 7.17 the simulations results are given.

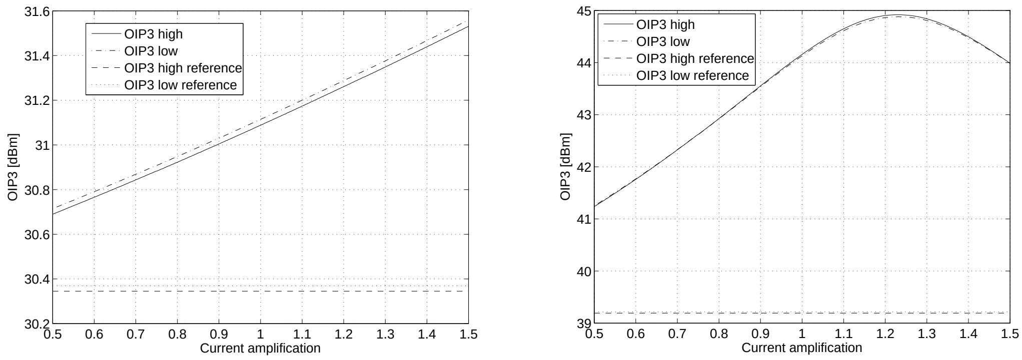

(a) With C_{jc}

(b) With C_{jc}, C_{je} and τ_f

Figure 7.17: The influence of the C_{jc} of the CE-stage on the OIP3 versus the current amplification of the CCCS

The influence of the C_{jc} is much stronger in this configuration. Section 7.2 demonstrated that the C_{jc}

gives a lower OIP3, but when C_{je} and τ_f are added, an OIP3 of 58dBm can still be reached. With second order shorts, an OIP3 of 45dBm seems to be the highest OIP3 figure achievable. Like said before, the active compensation probably also cancels some of the distortion created by the CE-stage, explaining the deviation from the ideal current amplification of 1. With second order shorts, the compensation current and the IM3 current from the CE-stage might not have a good phase-alignment. This explains the relatively low OIP3 figure. Also, second order shorts increase the IM3 created by depletion capacitances like the C_{jc}, as can be seen from Equation (A.8) and (A.9) and [21].

7.3.3. CROSS-COUPLING THE CE-STAGE

The feedback effect of the C_{jc} distortion in the CE-stage can be counteracted by cross-coupling the CE-stage. Section 7.2 demonstrated that this leads to a slightly higher OIP3. Therefore this is tested again. The full model, including C_{jc}, C_{je} and τ_f is used. This model is given in Table 7.7. The simulation results are shown in Figure 7.18.

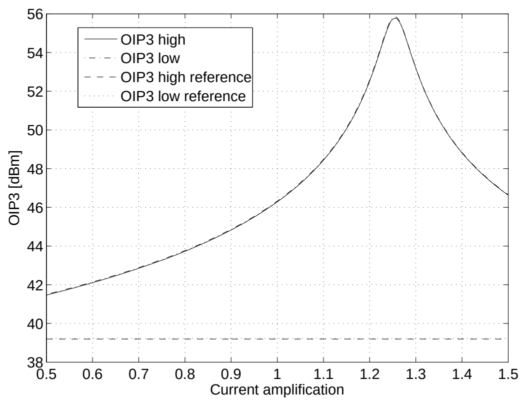

Figure 7.18: The influence of cross-coupling on the active C_{bc} compensation

As can be seen, the OIP3 is a lot larger for this simulation. This indicates that the feedback effect of the C_{jc} is much stronger in the CE-stage when the second order harmonics and intermodulation products are canceled at the collector. In fact, it almost seems like the C_{jc} gets fully compensated by the cross-coupled design, since the results are very similar to the case shown in Figure 7.16b. However, the current amplification has shifted, indicating that the active C_{bc} also plays a role in the cancellation of the C_{jc} of the CE-stage. Another explanation for the highly improved compensation is a change in phase of the IM3 currents produced by the CE-stage. If these are more in line with the IM3 currents produced by the C_{bc} of the CB-stage, the active compensation will be able to compensate them.

7.3.4. SUMMARY

In this section, active C_{bc} compensation has been studied using the Gummel-Poon model, with IM2 and HD2 short between the CE- and CB-stage. The main results are displayed in Table 7.9.

Table 7.9: Summary of simulation results for active C_{bc} compensation using the Gummel-Poon model with second order shorts

CE-stage				CB-stage			$\Delta OIP3_{peak}$ [2]	$G_{\Delta OIP3_{peak}}$ [3]	$\Delta OIP3_{G=1}$ [4]
τ_f	C_{je}	C_{jc}	CC [1]	τ_f	C_{je}	C_{jc}			
0s	0F	0F	n	0s	0F	26fF	26dB	1	26dB
0s	0F	0F	n	13ps	0.12pF	26fF	30dB	1	30dB
13ps	0F	0F	n	13ps	0.12pF	26fF	15dB	1	15dB
0s	0.12pF	0F	n	13ps	0.12pF	26fF	6.5dB	0.8	5dB
13ps	0.12pF	0F	n	13ps	0.12pF	26fF	18dB	1.1	10dB
0s	0F	26fF	n	13ps	0.12pF	26fF	1.1dB	1.5	0.7dB
13ps	0.12pF	26fF	n	13ps	0.12pF	26fF	6dB	1.2	5.5dB
13ps	0.12pF	26fF	y	13ps	0.12pF	26fF	17dB	1.25	7dB

[1] Cross-coupled
[2] The highest achievable OIP3 improvement compared to the reference OIP3
[3] The current amplification needed for the highest achievable OIP3 improvement
[4] The OIP3 improvement compared to the reference OIP3 for a current amplification of 1

As can be seen, the τ_f and C_{je} distortion in the CB-stage do not influence the OIP3 a lot. When the τ_f distortion from the CE-stage has been added, the OIP3 lowers, but the compensation has not been influenced: the peak in OIP3 improvement still occurs for a current amplification of 1. The C_{je} distortion from the CE-stage does influence the active compensation. Without the diffusion capacitance in the CE-stage, the OIP3 improvement is low, but not as low as without second order short, suggesting that the τ_f and C_{je} distortion from the CB-stage does play a role in compensating the IM3 currents from the CE-stage. The needed current amplification for the highest OIP3 improvement lowers to 0.8. The diffusion capacitance lowers the voltage swing and changes the phase of the C_{je} distortion. Therefore, when the τ_f component is added in the CE-stage, the OIP3 improvement increases. The current amplification needed for the highest OIP3 improvement does shift to 1.1, since the C_{je} distortion from the CE-stage is still present. When the C_{jc} of the CE-stage has been added, the OIP3 improvement lowers. With C_{je} and τ_f in the CE-stage, the C_{jc} distortion of the CE-stage still influences the compensation a lot, suggesting that the phases of the distortion from the CE-stage and from the distortion of the CB-stage are not aligned properly. Using cross-coupling helps to align those phases, making it possible for the active compensation to improve the OIP3 by 17dB.

7.4. ACTIVE COMPENSATION WITH THE MEXTRAM MODEL

In Section 7.2 and Section 7.3 the effects of the Gummel-Poon variables C_{jc}, C_{je} and τ_f on the active C_{bc} have been discussed. It demonstrated that for the CB-stage, the effects were low. However, the CE-stage did influence the active C_{bc} cancellation significantly. Therefore, this section will start with changing the CB-stage to the Mextram model. When this is done, the CE-stage will be converted to the Mextram model. The effect of cross-coupling will also be examined. The simulation values used have been given in Table 7.1.

The circuit used will not contain second order shorts. Therefore, it is comparable to the circuit used for the Gummel-Poon model, as depicted in Figure 7.4.

7.4.1. CONVERTING THE CB-STAGE TO MEXTRAM

Since in Gummel-Poon the active C_{bc} compensation is not affected by the C_{je} and τ_f of the CB-stage, the CB-stage will be converted to Mextram first. The CE-stage will be modeled using a Gummel-Poon model including the C_{jc}, C_{je} and τ_f variables. The model of the CE-stage is given in Table 7.7. Using these models for the CE- and CB-stage, the current amplification has been swept. For the reference OIP3, the current amplification has been set to 0. To compare, the OIP3 figures for the Gummel-Poon situation have also been given. The simulation results are given in Figure 7.19.

Since no second order shorts have been applied, the OIP3 plots should be comparable. However,

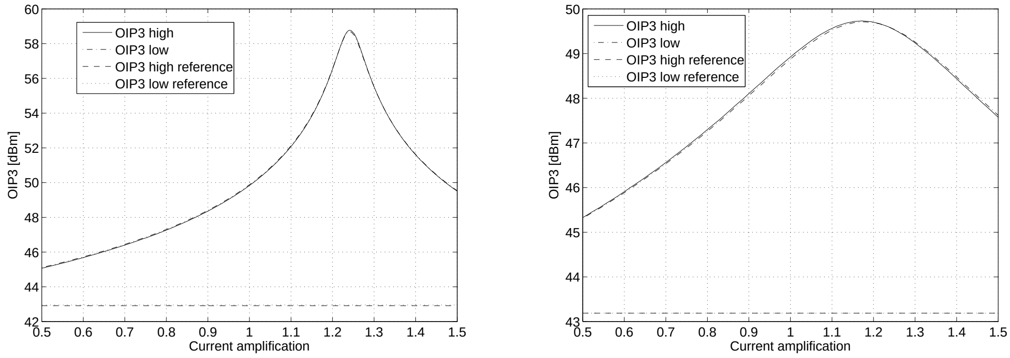

(a) Gummel-Poon modeled CB-stage

(b) Mextram modeled CB-stage

Figure 7.19: Active C_{bc} compensation with a Gummel-Poon modeled and a Mextram modeled CB-stage

when examining the results from Figure 7.19b, there is much more overlap with the results from Figure 7.17b, where second order shorts have been added. This can be explained by the changing phases of the IM3 currents in Mextram. In the original CB-stage, no base resistance has been added. In the Mextram model, this base resistance is present, changing the phase of the current from the CCCS and influencing the load of the CE-stage. Also the IM3 currents from the CE-stage experience a different phase shift in the CB-stage. As described in Section 7.2, the IM3 currents of the CE-stage are partially canceled by the active C_{bc} compensation. This cancellation is only possible if the phases of the compensation and of the IM3 current align well.

7.4.2. CONVERTING THE CE-STAGE TO MEXTRAM

The CE-stage has a significant influence on the OIP3 and the active C_{bc} compensation as shown in Section 7.2 and 7.3. Therefore, when changing the CE-stage to the Mextram model, significant changes are expected. Using the Mextram model for the CE- and CB-stage, the current amplification has been swept. For the reference OIP3, the current amplification has been set to 0. Figure 7.20 shows the simulation results when the total amplifier, including the CE-stage is converted to the Mextram model.

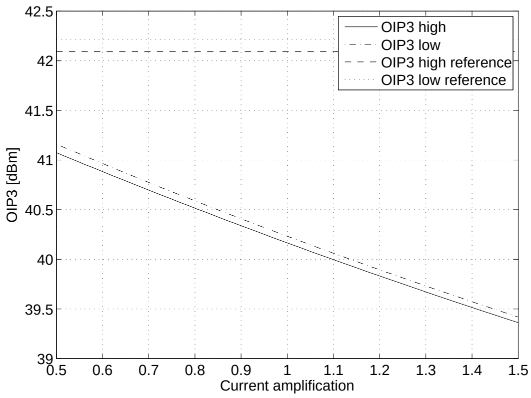

Figure 7.20: Active C_{bc} compensation in an amplifier using the Mextram model

The OIP3 plot shows no similarity whatsoever to the Gummel-Poon plots with C_{jc}, C_{je} and τ_f added. Instead, it has more similarity with Figure 7.8a and 7.9a, suggesting a much higher influence of the C_{je} and C_{jc} capacitance than anticipated. Due to the strong influence of the CE-stage, the active C_{bc} compensation does not give OIP3 improvement. In fact, the IM3 currents from the CE-stage seem to counteract the IM3 currents from the CB-stage, since the active C_{bc} compensation decreases the OIP3.

7.4.3. CROSS-COUPLING THE CE-STAGE

To counteract the influence of the C_{jc} capacitance of the CE-stage, the CE-stage has been cross-coupled. The current amplification has been swept again. For the reference OIP3, the current amplification has been set to 0. The results of this simulation can be seen in Figure 7.21.

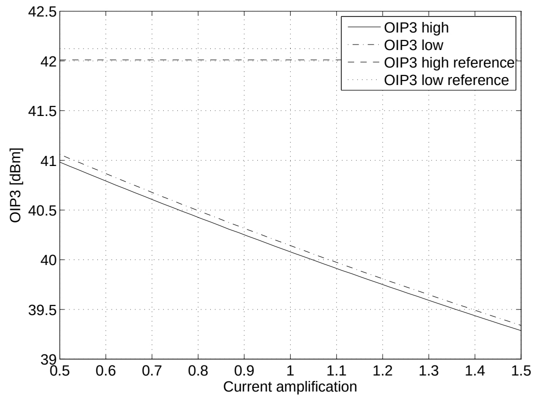

Figure 7.21: Active C_{bc} compensation in a cross-coupled amplifier using the Mextram model

As can be seen, the OIP3 did improve a little bit, but there isn't a big increase in OIP3. It seems that the CE-stage still introduces IM3 currents that interfere with the active C_{bc} compensation. In fact, it seems that the CE-stage introduces IM3 currents that compensate the IM3 currents of the CB-stage, which would explain why active C_{bc} compensation decreases the OIP3. At this moment, the exact cause of the decreasing OIP3 isn't known. There are several options:

- The C_{je} and C_{jc} have a too large voltage swing at their inputs, increasing their IM3 contribution
- The current dependency of the depletion capacitances becomes more significant in the CE-stage
- The τ_f introduces more IM3 than anticipated
- The phase of the CE- and CB-stage has changed in the Mextram model, and therefore the IM3 currents do not align anymore

These options are not confirmed yet and need to be investigated to be sure which (combinations of) options are the cause of the interfered active C_{bc} compensation.

7.4.4. STABILITY OF THE AMPLIFIER

The problems with the active C_{bc} compensation discussed so far have not been detected when the R_{stab} and C_{stab} stabilization components aren't present in the circuit. Due to these components, the IM3 current produced by the C_{bc} of the CB-stage decreases, since the voltage swing decreases. Therefore, the active C_{bc} compensation doesn't have as much of an effect. However, the stabilization components are necessary.

Without the stabilization components the stability factor k has been plotted, together with the S_{22} for the cross-coupled Mextram amplifier with active C_{bc} compensation. The current amplification of the CCCS has been set to 1. Figure 7.22 shows the k-factor and the S_{22} swept over frequency.

As can be seen, the k-factor is lower than 1 for very large frequency ranges, including the high-frequency region in which the amplifier operates. The k-factor even becomes negative for these high-frequency regions. As can be seen, the S_{22} is outside the Smith-chart for these regions. This suggest output instability. This instability occurs due to the high ohmic output of the CB-stage. Due to this high ohmic output, all the energy will be absorbed by the C_{bc} of the CB-stage. This energy will enter the active C_{bc} compensation, causing a positive feedback loop. By adding R_{stab} and C_{stab} this loop can be broken, as can be concluded from Figure 7.23.

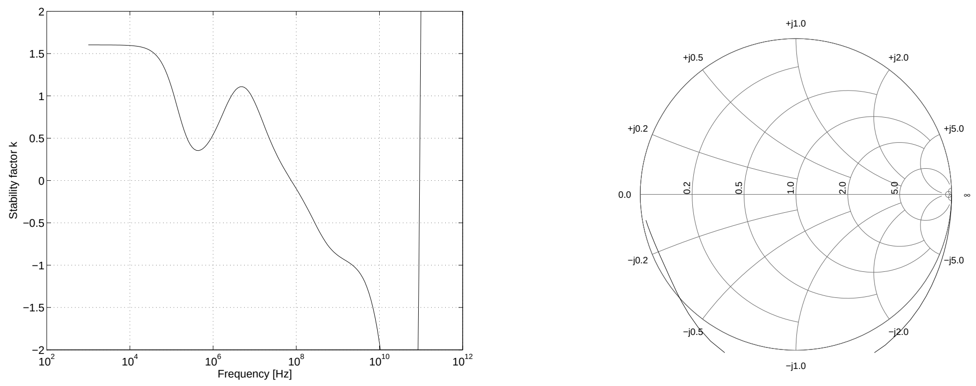

(a) k-factor (b) S_{22}

Figure 7.22: The k-factor and S_{22} of the cross-coupled Mextram amplifier without stabilization components

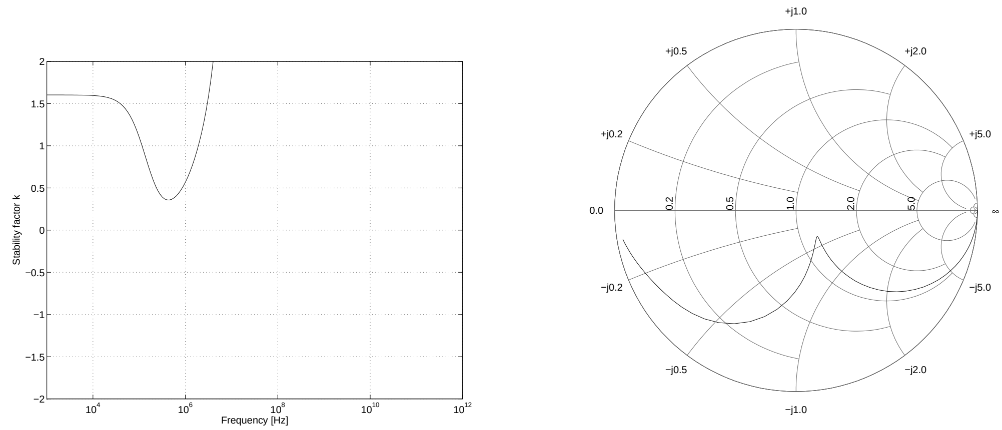

(a) k-factor (b) S_{22}

Figure 7.23: The k-factor and S_{22} of the cross-coupled Mextram amplifier with stabilization components

As can be seen, the stability factor k is above 1 for the high-frequency region. The S_{22} stays within the Smith-chart. At lower frequencies the k-factor is still below 1, but it stays positive all the time, and above 0.5 for most of the time. Therefore, it is much more likely that this amplifier can be made fully stable. Since this report is about linearity and not about stability, no further investigation has been done to the stability.

7.5. HIGH FREQUENCY CURRENT CONTROLLED CURRENT SOURCES

In active C_{bc} compensation, a current controlled current source (CCCS) is used to accomplish the compensation. There are several options for implementing this CCCS. In this section some of those options will be discussed.

There are a few requirements for the CCCS. First of all the input impedance of the CCCS should be very low, since the CCCS is located in the base of the CB-stage. If the input impedance is high, the input impedance of the total CB-stage increases, increasing the swing on the CE-stage. This leads to a lower OIP3 due to the C_{bc} of the CE-stage. Therefore a low input impedance is necessary. The input impedance can be measured using the Z_{11} parameter or the Y_{11} parameter. Since the output impedance is down converted to 30Ω by the balun at the output, the conditions for calculating the Y_{11} (a short at the output) are more in accordance with reality than the conditions for the Z_{11} (an open at the output). Since a low low input impedance is needed, the minimum requirement put on the Y_{11} is that it should not go below 1S up to the second order frequencies, which are around 3.6GHz in this report.

The second requirement is put on the output impedance of the CCCS. If this output impedance is low, gain of the amplifier is lost in the CCCS. Also the CCCS would leak current, meaning that the compensation won't work properly. Lastly, the output impedance influences the phase of the C_{bc}, making it harder to get correct compensation. The minimum impedance required is therefore chosen at 100Ω. There are two measures for output impedance: Z_{22} and Y_{22}. Since the input of the CCCS is neither shorted in any way, nor loaded with a low impedance, the Z_{22} is the most appropriate measure, since it assumes an open at the input. Y_{22} on the other hand assumes a short at the input, which is not realistic in this case.

The last requirement is on current amplification. In the ideal active C_{bc} compensation, a current amplification of 1 is needed. The phase of the current amplifier needs to be 0 or 180 degrees, depending on how the CCCS is connected. The measure used for the current amplification is D from the ABCD- or chain-matrix. The parameter D of the ABCD-matrix assumes a shorted output, just as is assumed for the input impedance. As requirement, the phase deviation should not exceed 5 degrees and the magnitude should not deviate 1% from 1.

7.5.1. CURRENT MIRROR

The current mirror is a circuit used in many analog circuitry for biasing reasons. The current mirror, as depicted in Figure 7.24, can also be used as a current controlled current source.

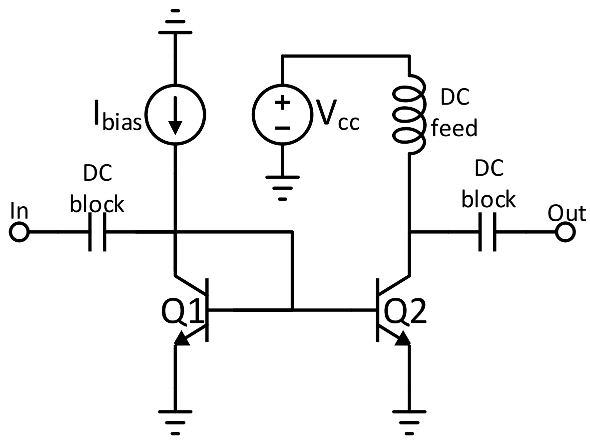

Figure 7.24: The current mirror

The current mirror has a low-ohmic input because Q1 is connected in diode configuration. By choosing I_{biac} correctly, the impedance of this diode can be set. The voltage on the base of Q1 is determined by the input current running through Q1, according to the diode equation:

$$V = V_t \cdot \ln\left(\frac{I}{I_s} + 1\right) [V] \tag{7.1}$$

where V_t is the thermal voltage, I_s is the saturation current and I is the current going through the transistor. Since Q2 has the same voltage-current relationship as Q1, the current entering Q1 is also generated by Q2. The current mirror has been simulated with the Mextram model. QUBiC4Xi HV BNA 0.5μm x 20.7μm x 10 transistors have been used. The biasing current is 35mA, chosen such that the input impedance is below 1Ω. The biasing voltage V_{cc} is set to 2.5V, and will be provided by a DC feed. In the final amplifier, the V_{cc} voltage will be provided by the output balun and the emitters of the transistors will be biased at a higher voltage to prevent avalanche. The simulation results are given in Figure 7.25.

The simulation results show that the Y_{11} is above 1S all the time. However, this is due to the high current consumption of 35mA. Since this current is mirrored, the high Y_{11} result takes up 70mA in current consumption for 1 CCCS. The Z_{22} is below 100Ω for a large range, including the fundamental frequency. However, the magnitude of D is not 1. The magnitude of D is influenced by the Early effect, which is why

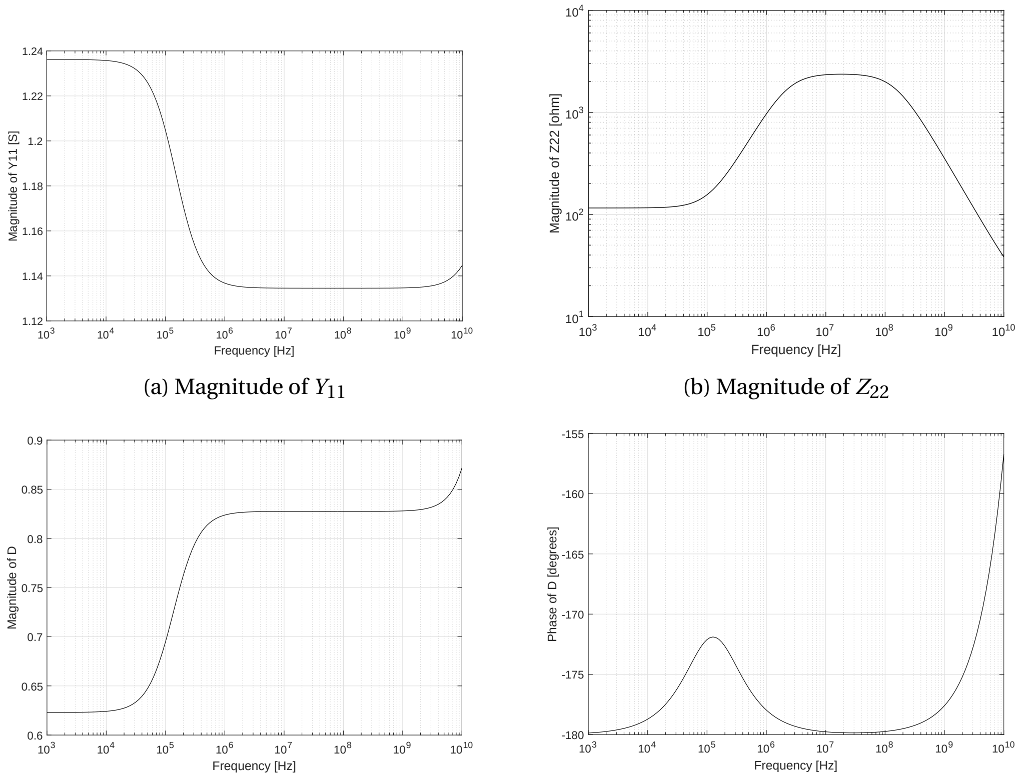

(a) Magnitude of Y_{11} (b) Magnitude of Z_{22}

(c) Magnitude of D (d) Phase of D

Figure 7.25: The simulation results of the current mirror implementation of the CCCS

it is not exactly 1. The phase deviation is approximately 5 degrees for the fundamental frequency. In the end, the magnitude of D is too low and the phase error just within specification. The current consumption is also rather high, in order to keep the input admittance high. Therefore, the current mirror isn't a good implementation of the CCCS.

7.5.2. FOUR-TRANSISTOR WILSON CURRENT MIRROR

The original Wilson current mirror has been invented in 1968 with the advantage of having a higher output impedance compared to the classical current mirror [28]. However, the original Wilson current mirror has a systematic gain error due to the Early effect. This gain error has been discovered by Barrie Gilbert and has later been rediscovered [29]. The solution to this problem is the addition of an extra diode-connected transistor in the current mirror [30]. When using this extra transistor, the circuit shown in Figure 7.26 is created.

Since the input impedance has to be low, a bias current of 80mA has to be used. The output of the CCCS has been biased using a DC feed, since in the amplifier the output balun can provide the biasing. V_{cc} has been set to 3.3V. With these simulation values, the simulations have been done. In Figure 7.27 the simulation results are given.

As can be seen from Figure 7.27a, the input admittance is above 1S up to very high frequencies. The output impedance is above 100 Ω up to a frequency of 5GHz. Figure 7.27c and 7.27d show the magnitude and phase behavior of D. Even for large frequencies, the magnitude of D stays within 1% range from the ideal value of 1. The phase stays within 5 degrees margin over the entire range. Therefore, the current amplification of this CCCS is very well suited. However, this implementation of the CCCS is not practical, due to the high currents needed (80mA for each branch, so 160mA for each CCCS). In the amplifier studied in this thesis report, this would amount to a tripling of the current consumption. Therefore an alternative needs to be found.

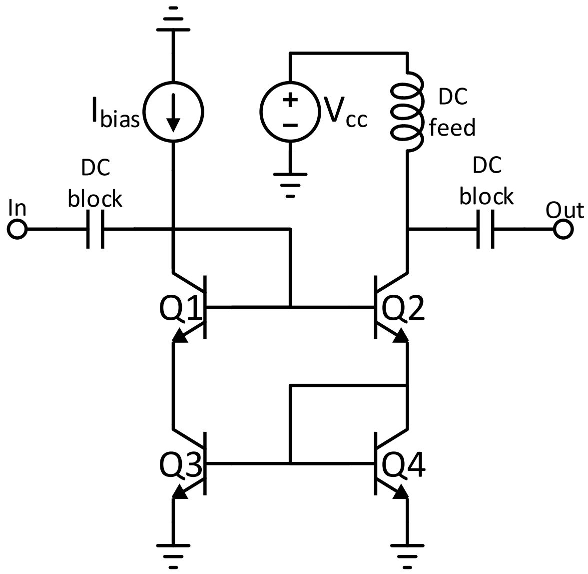

Figure 7.26: The four-transistor Wilson current mirror

7.5.3. CB-STAGE

The CB-stage is used in many amplifiers for cascoding purposes. As described in Chapter 4, the CB-stage does not deliver significant amplification in the current domain, but it does increase gain in amplifiers, due to the neutralization of the feedback capacitance C_{bc} in the CE-stage [8]. This is because the CB-stage acts as a current follower. In that sense, the CB-stage can be seen as a CCCS, with a low input impedance and a high output impedance. The CB-stage has a current amplification of approximately 1. In the current mirror, the current amplification can be adapted by correctly dimensioning the transistors. This is not an option for the CB-stage: the current amplification is approximately 1. In Figure 7.28, the test structure for the CB-stage is given.

The biasing voltage is set to 1.6V and the biasing current to 35mA, to keep the input impedance low. Q1 is implemented using a QUBiC4Xi HV BNA 0.5μm x 20.7μm x 10 device. The output biasing is done using a DC feed, representing the output balun used in the differential amplifier. V_{cc} is set at 3.3V. The simulation results are given in Figure 7.29.

As can be seen, the input admittance is above 1S for the whole frequency range. The output impedance is above 100Ω up to 10GHz. The magnitude of D stays within 1% error margin for the whole frequency range. The phase error does not exceed 5 degrees up to 3.6GHz. The main disadvantage of this CCCS is the high current consumption of this CCCS of 35mA. The high current is needed to achieve a large input admittance. Also the CB-stage introduces its own C_{bc} distortion. This C_{bc} distortion is lower than the original distortion, since the area is lower: the CB-stage of the amplifier has a multiplication factor of 25, while the CCCS has a multiplication factor of 10. Due to the high current consumption and the extra IM3 currents created, alternative options need to be found.

7.5.4. LOW-OHMIC CB-STAGE

There are several options to make the input impedance of the CCCS very low without having a high current consumption. However, one of the most common is a low-ohmic CB-stage. This structure can be found in several forms in earlier work. The low-ohmic CB-stage can be used as a stage in front of the current mirror, to make the input of the current mirror low ohmic [31]. It has also been used as a MOS-variant in amplifiers to boost the gain of the cascode amplifier [32]. The low-ohmic CB-stage structure tested in this case is given in Figure 7.30.

In this circuitry, Q1 is the CB-stage. Q3 amplifies incoming currents and creates a voltage on Q2. Q2 is a voltage follower, so the voltage created by Q3 is transfered to the input of Q1. The voltage on Q1 makes

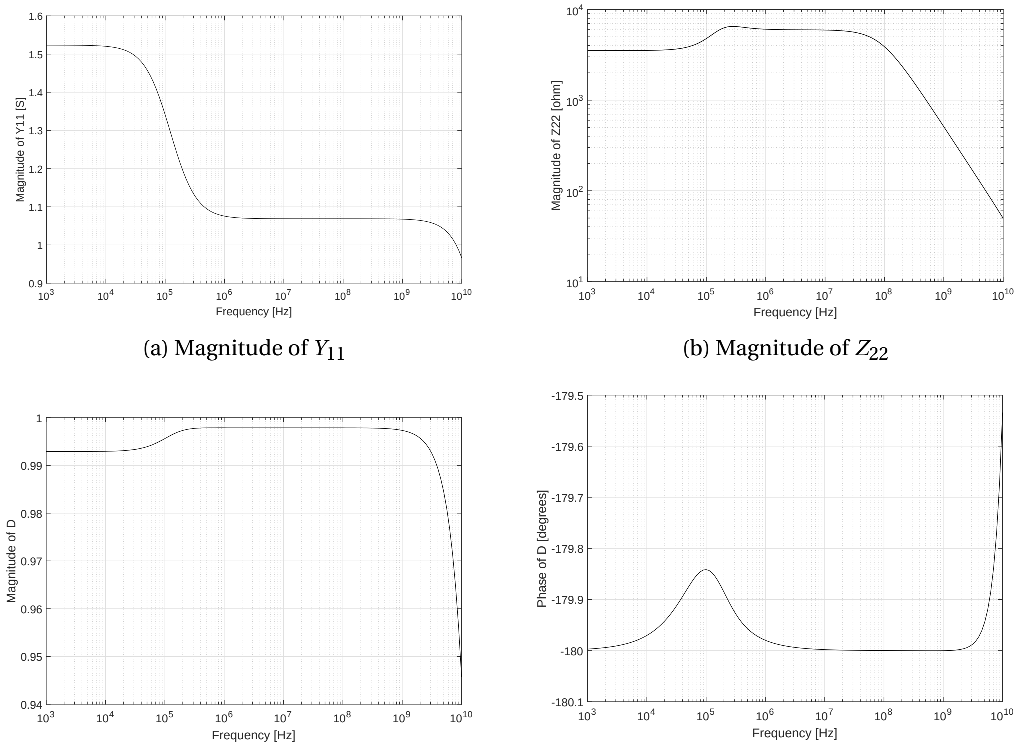

(a) Magnitude of Y_{11} (b) Magnitude of Z_{22}

(c) Magnitude of D (d) Phase of D

Figure 7.27: The simulation results of the four-transistor Wilson current mirror implementation of the CCCS

the CB-stage work. In an essence, the Q3 and Q2 transistor apply the required voltage swing for Q1 on the base, while in normal CB-stages this voltage swing will manifest itself at the emitter of the CB-stage. Q2 is a voltage follower. Without the voltage follower, the pole of Q1 is more dominant and therefore the input admittance would drop at much lower frequencies.

The required currents for low-ohmic operation are I_{bias1} =3mA, I_{bias2} =1mA and the bias current through Q3 is 9mA, making the total current 13mA, the lowest current consumption seen so far. Biasing is done using the 3.3V supply of the amplifier. The DC feed represents the output balun of the differential amplifier. R_{bias} is 120Ω. Q1 and Q2 are QUBiC4Xi HV BNA 0.5μm x 20.7μ x 1 devices, Q3 is a QUBiC4Xi HV BNA 0.5μm x 20.7μm x 5 device. The simulation results are given in Figure 7.31.

As can be seen, the input admittance is above 1S for the whole frequency range. The output impedance stays

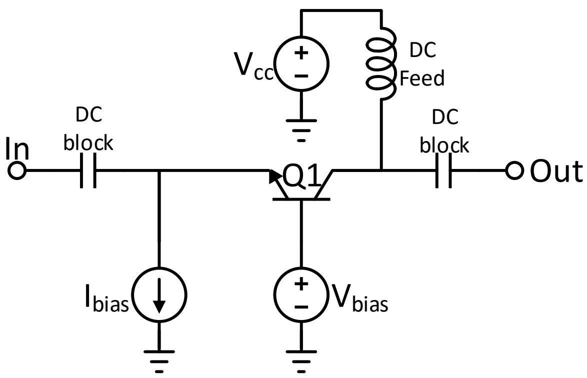

Figure 7.28: The CB-stage

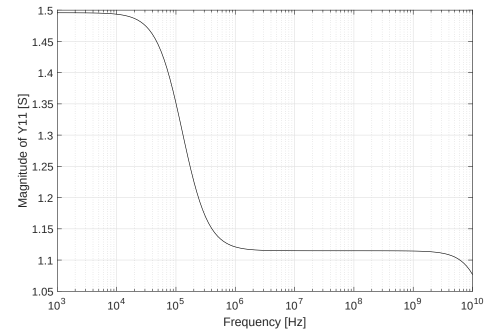

(a) Magnitude of Y_{11}

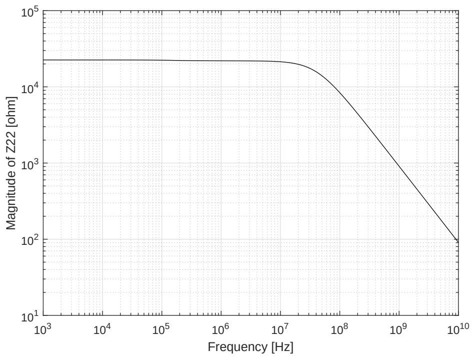

(b) Magnitude of Z_{22}

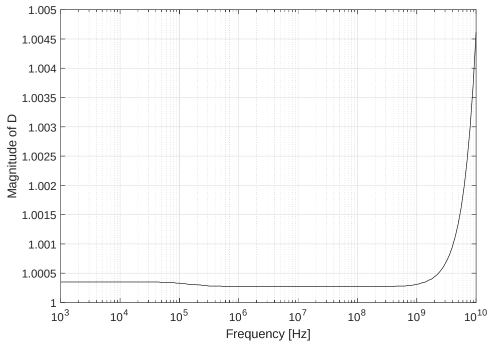

(c) Magnitude of D

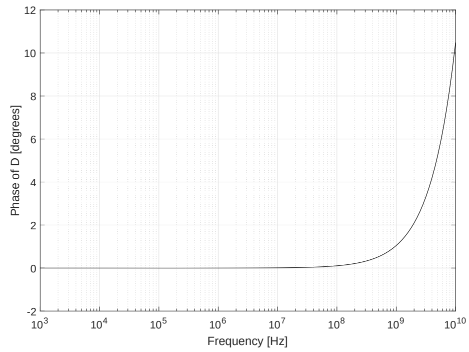

(d) Phase of D

Figure 7.29: The simulation results of the CB-stage implementation of the CCCS

well above 1kΩ. The magnitude of D doesn't show a 1% deviation up to 3.6GHz and the phase deviation does not exceed 5 degrees up to 3GHz. Therefore, this CCCS has the best specifications seen so far. Its current consumption is low, its input admittance and output impedance high, and the current amplification meets the requirements.

Whether these current controlled current sources work for active C_{bc} compensation has not been decided. First of all, only the IM3 contributions of the CB-stage has been considered: the IM3 contributions of CCCSs haven't been considered. Also the stability hasn't been taken into account. Finally the exact current amplification needed is still unsure, as shown in Section 7.2, 7.3 and 7.4.

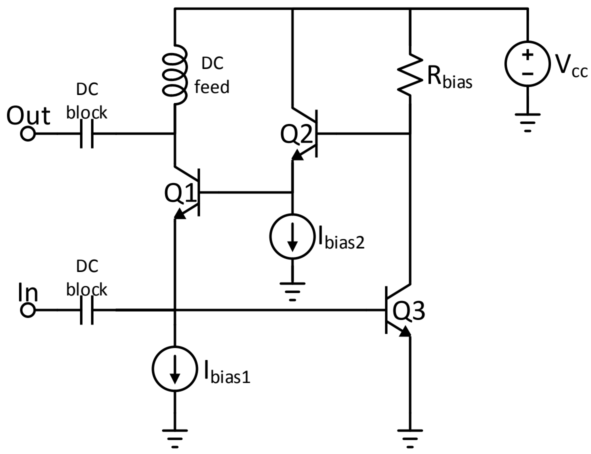

Figure 7.30: The low-ohmic CB-stage

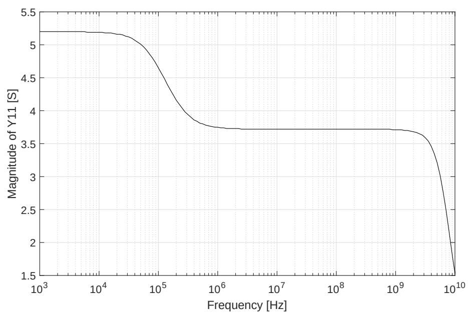

(a) Magnitude of Y_{11}

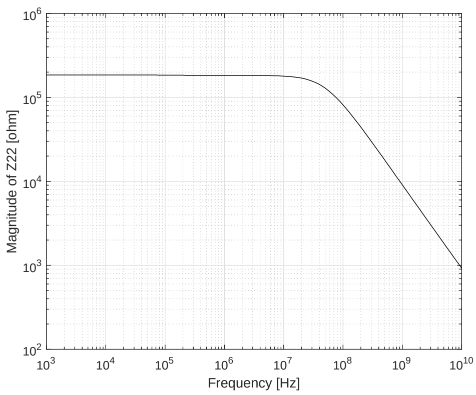

(b) Magnitude of Z_{22}

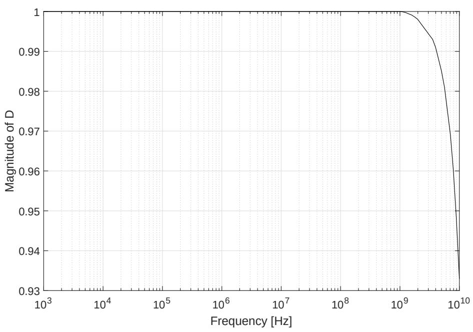

(c) Magnitude of D

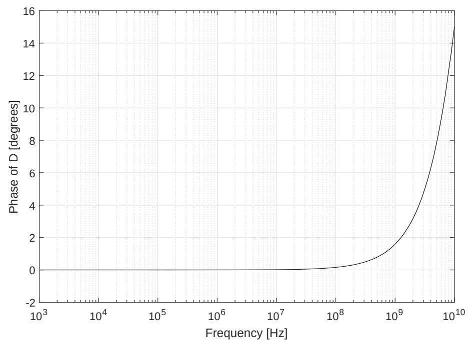

(d) Phase of D

Figure 7.31: The simulation results of the low-ohmic CB-stage implementation of the CCCS

7.6. CONCLUSION

This chapter has covered the principle of active C_{bc} compensation. In Section 7.1 the basic principle of active C_{bc} compensation has been demonstrated. Using a current controlled current source with a current amplification of 1, the IM3 currents could be perfectly canceled.

In Section 7.2 this concept has been tested in a Gummel-Poon modeled amplifier. It demonstrated that with a CCCS in the base of the CB-stage, perfect compensation is possible. Adding components like C_{je} and τ_f to the Gummel-Poon model of the CB-stage does not affect the active C_{bc} compensation. However, in the CE-stage these parameters do play a role. When adding τ_f, the OIP3 drops, since the exponential distortion is not perfectly canceled anymore. When the C_{je} is added, the τ_f distortion seems to decrease. However, C_{je} also introduces nonlinearities. These nonlinearities are weak and can be canceled in part by the active compensation, making the current amplification of the CCCS larger than 1. The C_{jc} of the CE-stage also lowers the OIP3, by introducing more nonlinearities.

In Section 7.3 the same has been done, with second order shorts at the collector of the CE-stage and second order opens at the emitter of the CB-stage. In this analysis, the influence of the CB-stage has remained the same. Also the influence of the C_{je} and τ_f of the CE-stage remained roughly the same. However, the C_{jc} influence of the CE-stage has highly increased when the second order shorts have been added. This is partly due to the feedback effect, since cross-coupling the CE-stage reduces this effect. More investigation has to be done on the influence of the feedback and the influence of the second order shorts on the phases and magnitudes of the IM3 currents in the CE-stage.

In Section 7.4 the transistors have been modeled with the Mextram model. First, the CB-stage has been transformed to the Mextram model. This lowers the OIP3, but the compensation is still working. However, once the CE-stage is converted to the Mextram model, the compensation does not work. Also when cross-coupling the CE-stage, the compensation doesn't work. The exact reason for this effect is unknown at the moment. Section 7.4 also contains a short examination of the stability of the amplifier. That analysis has shown that the amplifier needs a stabilization network at the differential output of the amplifier.

In Section 7.5 different implementations for the current controlled current source have been considered. Four parameters have been taken in consideration: the magnitudes of Y_{11}, Z_{22} and D and the phase of D, where D is from the ABCD- or chain-matrix. The current mirror has a high Y_{11} and a high Z_{22}. However, D is not accurate enough. Also the current consumption is rather high. Therefore, the current mirror is considered not to be a good implementation of the CCCS. The four-transistor Wilson current mirror has a lower phase deviation of D, but the current consumption is higher. The CB-stage has a high current consumption. However, the magnitudes of Y_{11} and Z_{22} are high and D is also accurate enough. Due to the high current consumption and the predictable IM3 effects, the CB stage is not a suitable implementation of the CCCS. The low-ohmic CB-stage is the best CCCS with a current amplification of 1. D is accurate, Y_{11} is high and Z_{22} is also high. The current consumption is low.

7.6.1. FUTURE RESEARCH

Since the active C_{bc} compensation doesn't work when the CE-stage is modeled in Mextram, future research has to rule out whether this problem can also be detected with Gummel-Poon models. Therefore it is advisable to model the QUBiC4Xi HV BNA devices in Gummel-Poon, so the effect of each Gummel-Poon variable can be understood better. Although the Gummel-Poon model has a lower accuracy than the Mextram model, the equations are in general more simplistic, making it easier to understand why the CE-stage interferes with the active C_{bc} compensation. Also the phase of IM3 currents for the Gummel-Poon model and the Mextram model should be examined, to see whether there are major differences that can cause the OIP3 deviations.

When the active C_{bc} compensation works when using the Mextram model, the wideband behavior should be investigated. The expectation is that this compensation gives wideband behavior. Simulations have to prove this claim. Also attention needs to be given to the stability of the amplifier.

Also the current controlled current sources need more investigation. The IM3 contribution of these components are unknown at the moment. Also their effect on stability is unknown. Therefore, more investigation on good high frequency current controlled current sources is needed. Also the option of combining certain CCCS topologies should be investigated. For instance, by using the low-ohmic CB-stage to achieve a low input impedance, the input impedance of a four-transistor Wilson current mirror can be higher. A four-transistor Wilson current mirror gives more flexibility in current amplification, making this option interesting for investigation.

8
CONCLUSIONS AND RECOMMENDATIONS

In this thesis report, the linearity issues concerning the base-collector capacitance C_{bc} in bipolar amplifiers have been presented. When implemented in SiGe, the C_{bc} induced distortion tends to limit the linearity of bipolar amplifiers used for base station purposes [1]. Due to this C_{bc} induced distortion, the linearity of SiGe bipolar amplifiers is lower compared to bipolar amplifiers implemented in GaAs. However, since SiGe technology offers cost and integration advantages compared to GaAs technology, this thesis report has focused on improving the linearity of the base station LNAs by finding new compensation schemes for the C_{bc} induced distortion.

In this chapter, the conclusions and recommendations of this thesis report will be discussed. In Section 8.1 the general findings of this thesis report are discussed. A comparison of the different compensation schemes for the C_{bc} induced distortion will be given. In Section 8.2 recommendations for future research are given.

8.1. GENERAL FINDINGS

In Chapter 2 the definitions and figures of merit to quantify distortion have been discussed. Also cascaded circuits and differential circuits have been discussed. Using cascaded circuits, a more orthogonal design can be used with respect to noise and linearity. Although cascaded circuits have not been used, the properties of cascaded circuits justify the aim at linearity in this thesis report. By using a differential circuit, more control of the impedances present at the baseband and second order frequencies could be gained. By using differential structures, design orthogonality between the impedances at the fundamental frequency and the impedances for the second order frequencies could be obtained. Throughout this report, this orthogonality has been used to gain better control of the C_{bc} induced distortion.

In Chapter 3 the linearity of the differential CE-stage has been studied using the Gummel-Poon model. Using the theory of out-of-band matching for exponential distortion as discussed by [6], the main linearity constraints have been studied. It demonstrates that with this theory, the exponential distortion and the distortion introduced by the transit time τ_f can be canceled. However, since [6] assumes linear depletion capacitances, the addition of depletion capacitances lowers the OIP3 of the amplifier. Since the voltage swing on the base-emitter junction is relatively small compared to the voltage swing on the base-collector junction, the C_{bc} depletion capacitance induced distortion tends to limit the OIP3. Using cross-coupled design, the influence of the C_{bc} on linearity has been canceled when all other transistor properties are close to ideal. However, once the transit time τ_f and depletion capacitance C_{je} have been added to the transistor model, the OIP3 improvement vanishes.

Another method commonly used to overcome C_{bc} related constraints in the CE-stage is moving to a cascode configuration. However, Chapter 4 shows that in a cascode configuration the C_{bc} induced distortion in the CB-stage tends to limit the linearity. The cascode configuration does decrease the voltage swing on the collector nodes of the CE-stage, which significantly decreases the influence of the C_{bc} of the CE-stage. Since the CB-stage is current driven in the cascode configuration, the exponential distortion of the CB-stage does not add a serious constraint on the linearity performance.

Chapter 5 has examined out-of-band matching as a technique for cancellation of C_{bc} distortion in bipolar differential cascode amplifiers. When studying a CB-stage, an inductor for the out-of-band components gives cancellation for grading coefficients of the base-collector junction lower than 0.5, while for values between 0.5 and 1, a capacitor gives cancellation. From these options, a capacitor would give a more wideband compensation, although implementation is difficult due to biasing constraints. However, the QUBiC4Xi process has grading coefficients of the base-collector junction lower than 0.5, indicating that an inductor should be used to achieve IM3 compensation. When the CE-stage is added, the IM2 and HD2 components of this CE-stage interrupt the cancellation of the C_{bc} distortion in the CB-stage. This can be solved by placing an intermediate transformer between the CE-stage and CB-stage. Due to the differential structure of the circuit, this would provide cancellation of the IM2 and HD2 components on the center tap, without cancellation of the signals present at the fundamental frequency. However, that would lead to many transformers and coils on-chip, increasing the likelihood of unwanted coupling.

In Chapter 6 a passive in-band C_{bc} compensation technique has been proposed to compensate for C_{bc} induced distortion in bipolar differential cascode amplifiers. It has been shown that passive in-band C_{bc} compensation could deliver a narrowband cancellation of the C_{bc} distortion in a CB-stage. A design for a test chip has been proposed. By using layout extraction, it has been demonstrated that this compensation technique is very sensitive to parasitic components. Measurements on the test chip have confirmed this sensitivity. Further recommendations have been done concerning the second harmonic shorts needed for passive in-band C_{bc} compensation and the testability and improvement of this compensation technique.

To overcome the problems related to the passive in-band and out-of-band C_{bc} compensation techniques, Chapter 7 has proposed an active C_{bc} compensation technique. Using the Gummel-Poon model, the different nonlinear elements of the cascode amplifier have been enabled or disabled. Doing this, the influence of the different nonlinear elements of the cascode amplifier on the active C_{bc} capacitance have been discussed. It has been demonstrated that the distortion induced by τ_f and C_{je} in the CB-stage do not influence the active C_{bc} compensation. However, once the C_{bc} and C_{je} capacitance of the CE-stage has been enabled, the active C_{bc} compensation starts to be less effective. Since active C_{bc} compensation poses a problem for output stability, a stabilization network has been added. This stabilization network decreases the influence of the C_{bc} of the CB-stage on nonlinearity. Therefore, the C_{bc} and C_{je} capacitances of the CE-stage become more important to the overall linearity performance. If the phase of the IM3 current of the CE-stage is in line with that of the IM3 currents from the C_{bc} capacitance of the CB-stage, active compensation can still provide an improved OIP3. However, once these are not in phase, the OIP3 improvement is limited when the Gummel-Poon model has been used and even nonexistent when the Mextram model has been used.

8.1.1. OVERVIEW OF THE DIFFERENT C_{bc} TECHNIQUES

Many different techniques have been described in this thesis report for canceling C_{bc} distortion. Table 8.1 provides a total overview of the different cancellation methods discussed in this thesis report.

Table 8.1: The different techniques for C_{bc} distortion cancellation

CE-stage amplifier	Cascode amplifier		
Cross-coupling	**Out-of-band matching**	**Passive in-band compensation**	**Active compensation**
+ Unilaterization + Prevents feedback of IM3 currents - No cancellation when C_{be} capacitances are present - Only possible in CE-stages	+ IM3 cancellation + No effect on the fundamental signal + Wideband when capacitor can be used (0.5<m<1) - Difficult to bias when capacitor can be used - Narrowband when inductor should be used (m<0.5 or 1<m) - Requires IM2 and IM3 cancellation of the CE-stage	+ IM3 cancellation - Requires resonator at fundamental - Very sensitive to parasitics - Narrowband - Area consuming	+ IM3 cancellation + Wideband - Requires current-controlled current source - Higher power consumption - Risk of positive feedback - Does not provide IM3 cancellation when the Mextram model has been used

As can be seen, the different techniques all have major disadvantages, which is why no definitive solution for C_{bc} solution has been found. Improvements are still needed to come to more practical, robust and product proven linearity enhancement techniques.

8.2. RECOMMENDATIONS

The linearity issues concerning the C_{bc} capacitance have not been solved yet. Important steps have been presented in this report. For each method discussed so far, suggestions for further research have been given.

For out-of-band matching it has been recommended to work on further analysis of the transformer based solution, in which a transformer cancels the IM2 and HD2 currents of the CE-stage. Another way forward is to look for simultaneous IM2, HD2 and IM3 cancellation in the CE-stage without transformers, to reduce the amount of coils on the chip. As a last option, IM2 and HD2 currents from the CE-stage could be manipulated using common-mode feedback or feedforward, to induce a new sweet spot for IM3 cancellation.

When using passive in-band C_{bc} compensation it has been recommended to investigate the addition of anti-parallel capacitances to fully eliminate the IM2 and HD2 currents or the indirect mixing products that result from them. Although this would cancel the IM2 and HD2 currents produced by the C_{bc} capacitances, a transformer is still needed to cancel the IM2 and HD2 currents produced by the exponential distortion in the CE-stage.

For active C_{bc} compensation, it has been recommended to model the QUBiC4Xi BNA HV devices in Gummel-Poon, so the different effects influencing the active C_{bc} compensation can be studied. Also the phase of the IM3 currents should be studied, to see whether phase differences between the IM3 currents from the CE-stage and the IM3 currents from the C_{bc} in the CB-stage can explain the OIP3 deviations between the Gummel-Poon model and Mextram model.

There are also other techniques possible that have not been studied in this report. Therefore, some general recommendations will be given in this section.

8.2.1. MATCHED INTERNAL COMPENSATION

During the study of active C_{bc} compensation, cancellation points have been found when loading the CB-stage with particular loads. In these compensation points, the IM3 currents from the CE-stage seemed to cancel the IM3 currents of the CB-stage. Since a lot of different variables are involved in this cancellation, no simple explanation can be given for these kind of cancellation points at the moment. Therefore, in the future, more investigation needs to be done to these kind of compensation techniques, in which internal IM3 currents cancel the IM3 current of the C_{bc} in the CB-stage. Since the amplitude and phase of the IM3 current of the C_{bc} capacitance is dependent on its loading, the load should be fully included in this analysis. In Figure 8.1 the concept of matched internal compensation is shown schematically.

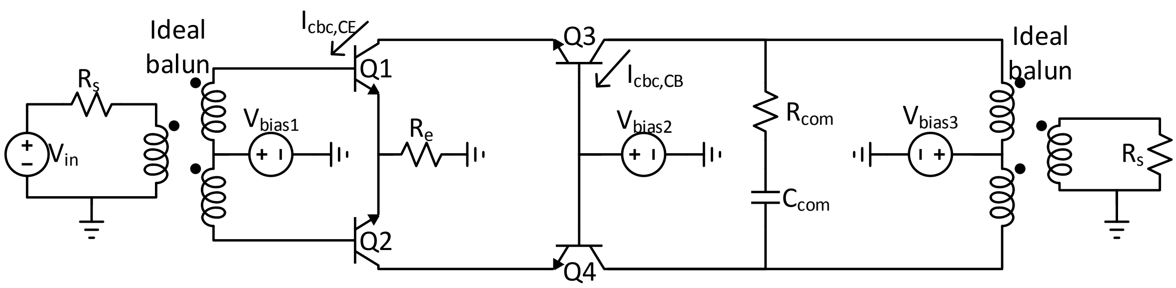

Figure 8.1: Matched internal compensation for C_{bc} distortion

A

VOLTERRA ANALYSES

In this appendix, the different Volterra analyses that are discussed in the report will be described. The method used for Volterra analyses is the method descibed by [12]. Four Volterra analyses will be discussed.

Appendix A.1 will discuss the OIP3 of the C_{bc} capacitance including a load resistance. This analysis will show that on lower frequencies, the load resistance is very important in determining the OIP3. For the lower frequency region, the OIP3 will drop when swept over frequency. In the higher frequency region, the OIP3 will rise when swept over frequency.

In Appendix A.2 the Volterra analysis of out-of-band matching for C_{bc} will be discussed. The analysis will show that an inductor or a capacitor can provide cancellation, depending on the doping profile of the C_{bc} capacitance.

Finally, in Appendix A.3 the IM3 currents producted by the C_{bc} and the compensation circuit used in passive in-band C_{bc} compensation will be discussed. These currents have to cancel each other. With this knowledge, the cancellation condition for the passive in-band C_{bc} compensation circuit will be determined.

A.1. C_{bc} DISTORTION

In Figure A.1 the circuit used for Volterra analysis of the C_{bc} is shown.

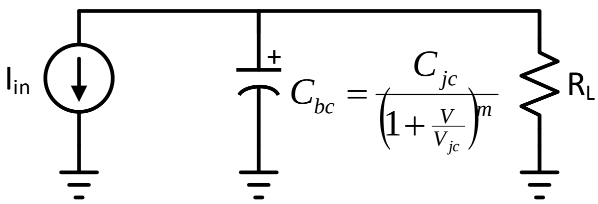

Figure A.1: Circuit used for Volterra analysis of the C_{bc} capacitance

The AC current running through the C_{bc} can be described as [12]:

$$i_{cb} = C_{bc}(V)\frac{dv}{dt} + K_{2C_{bc}}\frac{d}{dt}(v^2) + K_{3C_{bc}}\frac{d}{dt}(v^3) + \ldots [A] \tag{A.1}$$

where v is the AC collector-base voltage, and where:

$$K_{2C_{bc}} = -\frac{1}{2}\cdot\frac{m}{V_{jc}+V}\cdot C_{bc}[F/V] \quad K_{3C_{bc}} = \frac{1}{6}\cdot\frac{(m+1)m}{(V_{jc}+V)^2}\cdot C_{bc}[F/V^2] \tag{A.2}$$

The linear transfer from input current to voltage is:

$$H(s) = \frac{V(s)}{I_{in}(s)} = -\frac{R_L}{sC_{bc}R_L+1}[V/A] \tag{A.3}$$

From [12], the second-order nonlinear current source related to the C_{bc} capacitance can be found:

$$i_{NL2C_{bc}}(s_1,s_2) = (s_1+s_2)K_{2C_{bc}}H(s_1)H(s_2)[1/A] \tag{A.4}$$

where $s_1 = j2\pi f_1$ and $s_2 = j2\pi f_2$, with f_1 and f_2 being the fundamental frequencies.

Since the transfer from second-order nonlinear current to second-order nonlinear voltage is the same as the linear transfer from Equation (A.3), the total second-order nonlinear transfer $H_2(s_1,s_2)$ relating I_{in} with the second-order nonlinear voltage $V(s_1,s_2)$:

$$H_2(s_1,s_2) = i_{NL2C_{bc}}(s_1,s_2)H(s_1+s_2) = (s_1+s_2)K_{2C_{bc}}H(s_1)H(s_2)H(s_1+s_2)[V/A^2] \tag{A.5}$$

The third-order nonlinear current source related to the C_{bc} capacitance is then given by:

$$\begin{gathered} i_{NL3C_{bc}}(s_1,s_2,s_3) = (s_1+s_2+s_3)\Bigg[K_{3C_{bc}}H(s_1)H(s_2)H(s_3) + \\ \frac{2}{3}K_{2C_{bc}}(H(s_1)H_2(s_2,s_3)+H(s_2)H_2(s_1,s_3)+H(s_3)H_2(s_1,s_2))\Bigg][1/A^2] \end{gathered} \tag{A.6}$$

Again, the transfer from the third-order nonlinear current to third-order nonlinear voltage is the same as the linear transfer from Equation (A.3), so the total third-order nonlinear transfer $H_3(s_1,s_2,s_3)$ relating I_{in} with the third-order nonlinear voltage $V_(s_1,s_2,s_3)$ is:

$$H_3(s_1,s_2,s_3) = i_{NL3C_{bc}}(s_1,s_2,s_3)\cdot H(s_1+s_2+s_3)[V/A^3] \tag{A.7}$$

where $s_1 = j2\pi f_1$, $s_2 = j2\pi f_2$ and $s_3 = j2\pi f_3$, with f_1, f_2 and f_3 being the fundamental frequencies.

Now the OIP3$_{low}$ and OIP3$_{high}$ are determined as:

$$OIP3_{low} = \sqrt{\frac{4}{3}\left|\frac{H(s_1)}{H_3(s_1,s_1,-s_2)}\right|}[A] \tag{A.8}$$

$$OIP3_{high} = \sqrt{\frac{4}{3}\left|\frac{H(s_2)}{H_3(s_2,s_2,-s_1)}\right|}[A] \tag{A.9}$$

where $s_1 = j2\pi f_1$ and $s_2 = j2\pi f_2$ with f_1 and f_2 being the fundamental frequencies where $f_1 < f_2$.

If Equation (A.5), (A.6) and (A.7) are filled in, this leads to the following expressions:

$$OIP3_{low} = 2\sqrt{\left|\frac{1}{(2s_1-s_2)H(2s_1-s_2)H(s_1)H(-s2)\left[3K_{3C_{bc}}+2K^2_{2C_{bc}}(2s_1H(2s_1)+2(s_1-s_2)H(s_1-s_2))\right]}\right|}[A] \tag{A.10}$$

$$OIP3_{high} = 2\sqrt{\left|\frac{1}{(2s_2-s_1)H(2s_2-s_1)H(s_2)H(-s1)\left[3K_{3C_{bc}}+2K^2_{2C_{bc}}(2s_2H(2s_2)+2(s_2-s_1)H(s_2-s_1))\right]}\right|}[A] \tag{A.11}$$

The expressions for OIP3 are very complex and do not provide an intuitive result for the OIP3 of the C_{bc}. However, one important fact is ignored in this analysis. In most situations, $R_L \ll \frac{1}{s\cdot C_{bc}}$, so the most current will go through the load resistance. This means that $H(s)$ simplifies to:

$$OIP3_{low} \approx 2\sqrt{\left|\frac{1}{(2s_1-s_2)R_L^3\left[3K_{3C_{bc}}-2K^2_{2C_{bc}}(R_L(3s_1-s_2))\right]}\right|}[A] \tag{A.12}$$

$$OIP3_{high} \approx 2\sqrt{\left|\frac{1}{(2s_2-s_1)R_L^3\left[3K_{3C_{bc}}-2K^2_{2C_{bc}}(R_L(3s_2-s_1))\right]}\right|}[A] \tag{A.13}$$

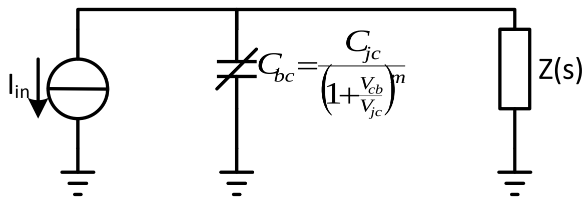

Figure A.2: Circuit used for Volterra analysis of out-of-band matching for the C_{bc} capacitance

A.2. OUT-OF-BAND MATCHING FOR C_{bc} DISTORTION

The circuit used for Volterra analysis of out-of-band matching for C_{bc} distortion is given in Figure A.2.

This circuit is very similar to the one used in Appendix A.1. In fact, the only difference is in $H(s)$:

$$H(s) = -\frac{Z(s)}{sC_{bc}Z(s)+1} \tag{A.14}$$

For the rest of the analysis, Equation (A.4) up to (A.11) are still valid. In the formulas for the OIP3, an asymptote can be found, at which the OIP3 becomes infinite. These asymptotes are at the point where the following equations are true:

$$-\frac{3}{2}\frac{K_{3C_{bc}}}{K_{2C_{bc}}^2} = 2s_1H(2s_1)+2(s_1-s_2)H(s_1-s_2) \tag{A.15}$$

$$-\frac{3}{2}\frac{K_{3C_{bc}}}{K_{2C_{bc}}^2} = 2s_2H(2s_2)+2(s_2-s_1)H(s_2-s_1) \tag{A.16}$$

Using the new definition for $H(s)$ and the $K_{2C_{bc}}$ and $K_{3C_{bc}}$ as given in Equation (A.2), the cancellation equations become:

$$\frac{m+1}{mC_{bc}} = 2s_1\frac{Z(2s_1)}{2s_1C_{bc}Z(2s_1)+1}+2(s_1-s_2)\frac{Z(s_1-s_2)}{(s_1-s_2)C_{bc}Z(s_1-s_2)+1} \tag{A.17}$$

$$\frac{m+1}{mC_{bc}} = 2s_2\frac{Z(2s_2)}{2s_2C_{bc}Z(2s_2)+1}+2(s_2-s_1)\frac{Z(s_2-s_1)}{(s_2-s_1)C_{bc}Z(s_2-s_1)+1} \tag{A.18}$$

For narrowband systems, it can be assumed that: $s_1-s_2 \approx s_2-s_1 \approx \Delta s$ and $s_1 \approx s_2 \approx s$. Then the equations for cancellation simplify to 1 equation:

$$\frac{m+1}{mC_{bc}} = 2s\frac{Z(2s)}{2sC_{bc}Z(2s)+1}+2\Delta s\frac{Z(\Delta s)}{\Delta sC_{bc}Z(\Delta s)+1} \tag{A.19}$$

When the tone spacing Δs is changed, the $2s$ term barely changes, while the Δs term can change several decades. Therefore, this term needs to be canceled.
The first option for canceling the Δs term is by making $Z(\Delta s)$ zero. Then the cancellation equation becomes:

$$\frac{m+1}{mC_{bc}} = 2s\frac{Z(2s)}{2sC_{bc}Z(2s)+1} \tag{A.20}$$

Solving this equation for $Z(2s)$ results in the following cancellation condition:

$$Z(2s) = j\cdot\frac{m+1}{4\pi fC_{bc}}[\Omega] \tag{A.21}$$

where f is the fundamental frequency. This solution is inductive, since it results in a positive imaginary impedance.
The second option for canceling the Δs term is by making $\Delta sC_{bc}Z(\Delta s) \gg 1$. The cancellation equation becomes:

$$\frac{m+1}{mC_{bc}} = 2s\frac{Z(2s)}{2sC_{bc}Z(2s)+1}+2\frac{1}{C_{bc}} \tag{A.22}$$

Solving this equation for $Z(2s)$ results in the following cancellation condition:

$$Z(2s) = j \cdot \frac{m-1}{2m-1} \frac{1}{4\pi f C_{bc}} [\Omega] \tag{A.23}$$

This equation is imaginary and positive for $m > 1$ and $m < 0.5$, giving a solution that is inductive. The solution is capacitive when $0.5 < m < 1$, since the solution then gives a negative imaginary impedance, which can be wideband in nature considering the frequency dependency.

A.3. PASSIVE IN-BAND C_{bc} COMPENSATION

In Figure A.3 the circuit for Volterra analysis for passive in-band C_{bc} compensation is given. Since the

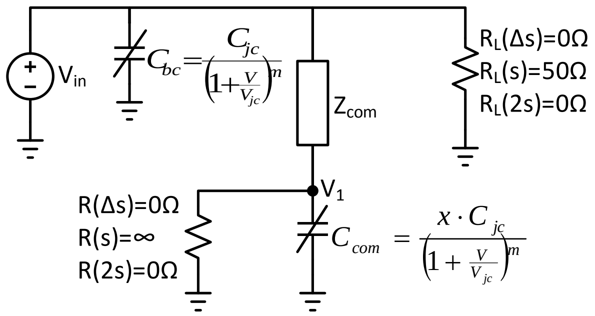

Figure A.3: Circuit used for Volterra analysis for passive in-band C_{bc} compensation

output is voltage driven, no IM3 voltages are present at the output node. However, there are IM3 currents. These currents can be calculated separately for each different branch. There are two important branches for calculation of the IM3:

1. The C_{bc} branch, consisting of the C_{bc} capacitance.
2. The compensation branch, consisting of Z_{com}, R and C_{com}.

THE C_{bc} BRANCH

For the C_{bc} branch the linear transfer from V_{in} to the voltage on the capacitance V_{cb} is:

$$H(s) = \frac{V_{cb}}{V_{in}} = 1 \tag{A.24}$$

Since the second-order currents are shorted, no second-order voltages will arise, making the transfer from V_{in} to second-order voltage:

$$H_2(s_1, s_2) = 0[V^{-1}] \tag{A.25}$$

The third-order current source related to the C_{bc} capacitance can now be determined as:

$$i_{NL3_{C_{bc}}} = (s_1+s_2+s_3) \cdot K_{3C_{bc}} H(s_1)H(s_2)H(s_3) = (s_1+s_2+s_3) \cdot K_{3C_{bc}} [A/V^3] \tag{A.26}$$

THE COMPENSATION BRANCH

In the compensation branch, the capacitance C_{com} is x times larger than C_{bc}. Therefore:

$$K_{2C_{com}} = x \cdot K_{2C_{bc}} [F/V] \quad K_{3C_{com}} = x \cdot K_{3C_{bc}} [F/V^2] \tag{A.27}$$

The linear response from V_{in} to V_1 is given by:

$$H(s) = \frac{1}{1 + sC_{com}Z_{com}(s)} \tag{A.28}$$

Since the second-order currents are shorted, the transfer from V_{in} to the second-order voltage on V_1 is:

$$H_2(s_1, s_2) = 0[V^{-1}] \tag{A.29}$$

The third-order current source related to the C_{com} capacitance can now be determined as:

$$i_{NL3_{Ccom}} = (s_1+s_2+s_3)\cdot K_{3C_{com}} H(s_1)H(s_2)H(s_3)[A/V^3] \tag{A.30}$$

The current injected in the output node can now be determined as:

$$i_{NL3_{com}} = i_{NL3_{Ccom}} \cdot \frac{1}{1+(s_1+s_2+s_3)C_{com}Z_{com}(s_1+s_2+s_3)}[A/V^3] \tag{A.31}$$

CANCELLATION

For cancellation, the IM3 currents created need to be in opposite phase. Using Equation (A.26) and (A.31), the following equation can be found for cancellation:

$$(s_1+s_2+s_3)\cdot K_{3C_{bc}} = -i_{NL3_{Ccom}} \cdot \frac{1}{1+(s_1+s_2+s_3)C_{com}Z_{com}(s_1+s_2+s_3)} \tag{A.32}$$

For IM3, the two IM3 frequencies need to be chosen. For the IM3$_{low}$, $s_1 = s_1$, $s_2 = s_1$ and $s_3 = -s_2$. For the IM3$_{high}$, $s_1 = s_2$, $s_2 = s_2$ and $s_3 = -s_1$. Combining this knowledge with Equation (A.32) and (A.30 gives the following cancellation equations for the IM3$_{low}$ and IM3$_{high}$:

$$(2s_1-s_2)\cdot K_{3C_{bc}} = -(2s_1-s_2)\cdot K_{3C_{com}} H(s_1)^2 H(-s_2)\cdot \frac{1}{1+(2s_1-s_2)C_{com}Z_{com}(2s_1-s_2)} \tag{A.33}$$

$$(2s_2-s_1)\cdot K_{3C_{bc}} = -(2s_2-s_1)\cdot K_{3C_{com}} H(s_2)^2 H(-s_1)\cdot \frac{1}{1+(2s_2-s_1)C_{com}Z_{com}(2s_2-s_1)} \tag{A.34}$$

For narrowband behavior, $s_1 \approx s_2 \approx s$, giving the following cancellation equation:

$$s\cdot K_{3C_{bc}} = -s\cdot K_{3C_{com}} H(s)^2 H(-s)\cdot \frac{1}{1+sC_{com}Z_{com}(s)} \tag{A.35}$$

Using Equation (A.27) and (A.28), this equation can be simplified:

$$1 = -x\cdot\left(\frac{1}{1+sC_{com}Z_{com}(s)}\right)^3 \cdot \frac{1}{1-sC_{com}Z_{com}(-s)} \tag{A.36}$$

This equation can be made valid, if $Z_{com}(s)$ is a combination of a resistor and an inductor $R_{com}+sL_{com}$. Then the inductor L_{com} and compensation capacitance C_{com} are put in resonance. This results in the following $H(s)$:

$$H(s) = \frac{1}{1+sC_{com}Z_{com}(s)} = \frac{1}{1+sC_{com}(R_{com}+sL_{com})} = \frac{1}{1+sC_{com}R_{com}-1} = \frac{1}{sC_{com}R_{com}} \tag{A.37}$$

This results in the following cancellation equation:

$$1 = x\cdot\left(\frac{1}{sC_{com}R_{com}}\right)^4 \tag{A.38}$$

This equation can be solved for R_{com}. Bearing in mind that the inductor L_{com} needs to be in resonance with C_{com}, the following conditions for cancellation can be derived:

$$L_{com} = \frac{1}{(2\pi f)^2\cdot x\cdot C_{bc}}[H] \tag{A.39}$$

$$R_{com} = \frac{1}{x^{3/4}\cdot C_{bc}\cdot 2\pi f}[\Omega] \tag{A.40}$$

where f is the fundamental frequency.

B

SIMULATING SEPARATE DEPLETION CAPACITANCES IN ADS

Sometimes it is useful for analysis to study the depletion capacitance seperately. For instance, in Section 7.1, the compensation has been tested first with only C_{bc} capacitances. This is only possible if a model is made for the depletion capacitances, since in the Gummel-Poon model the exponential distortion is always present.

There are two methods in which ADS can model the depletion capacitance:

1. Using the diode model
2. Using an equation based SDD

The first method is the easiest to implement. However, the diode model incorporates multiple effects [33]. Even when the diode has only the necessary parameters for modeling a depletion capacitance, the exponential characteristic is still present. For SDD models this is not the case. However, SDD models don't work when the capacitance is put in forward, making this option less suited for large-signal analysis.

DIODE MODEL

In ADS, the diode model can be found by using the drop down menu in the schematic-window and selecting 'Device-Diodes'. Here, the diode can be added and the diode model can be added. The diode model is shown in Figure B.1. In this model, Cj0 represents the zero-bias capacitance, Vj0 represents the built-in voltage and M represents the grading coefficient of the doping profile.

SDD MODEL

The SDD-model uses an SDD component, that can be found by using the drop down menu in the schematic-window and selecting 'Eqn Based-Nonlinear'. Here, the SDD block can be found. The one-port SDD block is used. With an SDD block, the currents can be described by a function of the voltages on the device. By applying a weighting number, the integral of the current, the charge, can be determined: "I[1,1]".

For a voltage-dependent capacitance, the charge can be described as the integral of the capacitance over voltage:

$$Q = \int C(v)dV \tag{B.1}$$

For the C_{bc} capacitance this is:

$$Q = \int C(v)dV = \int \frac{C_{jc}}{\left(1+\frac{V}{V_{jc}}\right)^m} = -\frac{\left(V_{jc}+V\right)^{-m+1}\cdot C_{jc}V_{jc}^m}{m-1}[C] \tag{B.2}$$

where, C_{jc} represents the zero bias capacitance, V_{jc} represents the built-in voltage and m represents the grading coefficient of the dopingprofile. With this equation, the depletion capacitance can be implemented. The SDD-model is shown in Figure B.2.

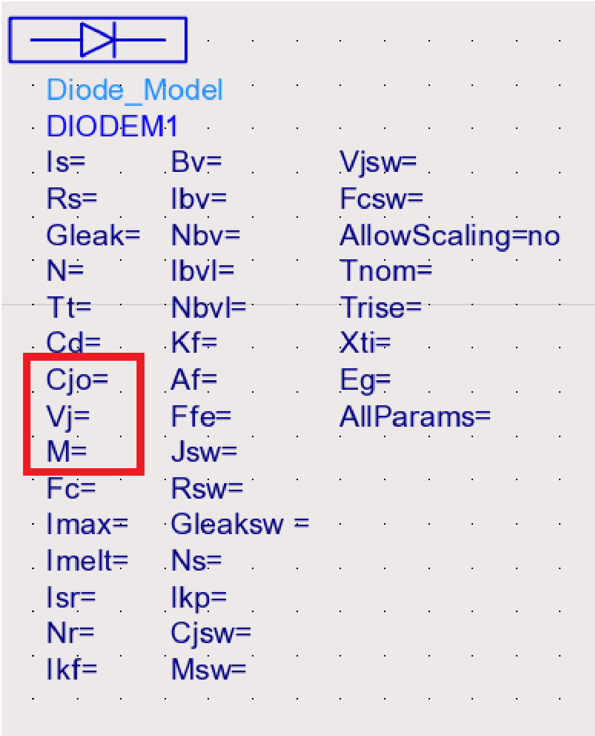

Figure B.1: The diode model in ADS

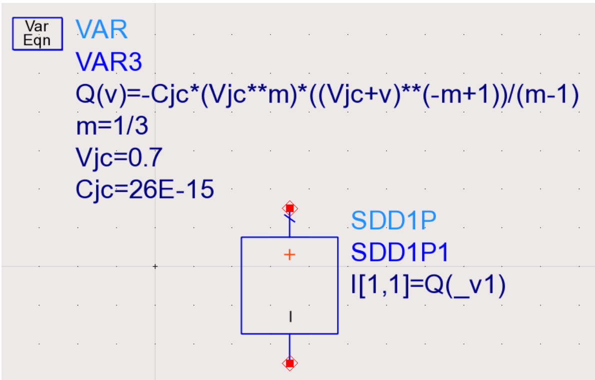

Figure B.2: The SDD model of a depletion capacitance in ADS

C

MAPLE SCRIPTS

In this appendix, the Maple script used for IM2 and HD2 cancellation using common-mode impedances is given.

File description

This file contains a Volterra analysis for the common-mode impedance IM2 and HD2 cancellation in a CE-stage.

Initialize script

```
> restart;
> with(linalg): with(plots): with(ArrayTools):
```

Definition of the admittance matrix

```
> Y:=matrix(2,2,[[1/Z1(s)+gm/beta+s*(Cde), -(gm/beta+s*(Cde))],[-(gm/beta + gm +s*(Cde)), 1/Z2(s)+gm/beta+gm+s*(Cde)]]);
```

$$Y := \begin{bmatrix} \frac{1}{Z1(s)} + \frac{gm}{\beta} + s\,Cde & -\frac{gm}{\beta} - s\,Cde \\ -\frac{gm}{\beta} - gm - s\,Cde & \frac{1}{Z2(s)} + \frac{gm}{\beta} + gm + s\,Cde \end{bmatrix} \tag{3.1}$$

Calculate the first order kernel

```
> IN1:=vector([1/Z1(s), 0]);
```

$$IN1 := \begin{bmatrix} \frac{1}{Z1(s)} & 0 \end{bmatrix} \tag{4.1}$$

```
> Y1:=eval(Y, [s=s1]);
```

$$Y1 := \begin{bmatrix} \frac{1}{Z1(s1)} + \frac{gm}{\beta} + s1\,Cde & -\frac{gm}{\beta} - s1\,Cde \\ -\frac{gm}{\beta} - gm - s1\,Cde & \frac{1}{Z2(s1)} + \frac{gm}{\beta} + gm + s1\,Cde \end{bmatrix} \tag{4.2}$$

```
> H1:=linsolve(Y1,IN1):
> h1[1]:=unapply(factor(H1[1]),s1);
  h1[2]:=unapply(factor(H1[2]),s1);
```

$$h1_1 := s1 \rightarrow \big((s1\,Cde\,Z2(s1)\,\beta + gm\,Z2(s1)\,\beta + gm\,Z2(s1) + \beta)\,Z1(s1) \big) \Big/ \big(Z1(s)\,(s1\,Cde\,Z2(s1)\,\beta + s1\,Cde\,Z1(s1)\,\beta + gm\,Z2(s1)\,\beta + gm\,Z2(s1) + gm\,Z1(s1) + \beta) \big)$$

$$h1_2 := s1 \rightarrow \big(Z2(s1)\,(Cde\,\beta\,s1 + gm\,\beta + gm)\,Z1(s1) \big) \Big/ \big(Z1(s)\,(s1\,Cde\,Z2(s1)\,\beta + s1\,Cde\,Z1(s1)\,\beta + gm\,Z2(s1)\,\beta + gm\,Z2(s1) + gm\,Z1(s1) + \beta) \big) \tag{4.3}$$

Calculate the second order kernel

```
> INL2Cde:=(s1+s2)*tau*INL2gm;
```

$$INL2Cde := (s1 + s2)\ \tau\ INL2gm \tag{5.1}$$

```
> INL2gpi:=INL2gm/beta;
```

$$INL2gpi := \frac{INL2gm}{\beta} \tag{5.2}$$

```
> Y2:=eval(Y, s=s1+s2);
```

$$Y2 := \left[\left[\frac{1}{Z1(s1+s2)} + \frac{gm}{\beta} + (s1+s2)\ Cde, -\frac{gm}{\beta} - (s1+s2)\ Cde\right], \left[-\frac{gm}{\beta} - gm - (s1+s2)\ Cde, \frac{1}{Z2(s1+s2)} + \frac{gm}{\beta} + gm + (s1+s2)\ Cde\right]\right] \tag{5.3}$$

```
> IN2:=vector([-INL2Cde-INL2gpi, INL2Cde+INL2gpi+INL2gm]);
```

$$IN2 := \left[-(s1+s2)\ \tau\ INL2gm - \frac{INL2gm}{\beta}, (s1+s2)\ \tau\ INL2gm + \frac{INL2gm}{\beta} + INL2gm\right] \tag{5.4}$$

```
> H2:=linsolve(Y2,IN2):
> h2[1]:=unapply(factor(H2[1]), (s1, s2));
  h2[2]:=unapply(factor(H2[2]), (s1, s2));
```

$$h2_1 := (s1, s2) \rightarrow \big(Z1(s1+s2)\ INL2gm\ (-Z2(s1+s2)\ \beta\ gm\ s1\ \tau - Z2(s1+s2)\ \beta\ gm\ s2\ \tau + Cde\ Z2(s1+s2)\ \beta\ s1 + Cde\ Z2(s1+s2)\ \beta\ s2 - \beta\ s1\ \tau - \beta\ s2\ \tau - 1)\big) \Big/ \big(Cde\ Z1(s1+s2)\ \beta\ s1 + Cde\ Z1(s1+s2)\ \beta\ s2 + Cde\ Z2(s1+s2)\ \beta\ s1 + Cde\ Z2(s1+s2)\ \beta\ s2 + gm\ Z2(s1+s2)\ \beta + gm\ Z1(s1+s2) + gm\ Z2(s1+s2) + \beta\big)$$

$$h2_2 := (s1, s2) \rightarrow \big((-Z1(s1+s2)\ \beta\ gm\ s1\ \tau - Z1(s1+s2)\ \beta\ gm\ s2\ \tau + Cde\ Z1(s1+s2)\ \beta\ s1 + Cde\ Z1(s1+s2)\ \beta\ s2 + \beta\ s1\ \tau + \beta\ s2\ \tau + \beta + 1)\ INL2gm\ Z2(s1+s2)\big) \Big/ \big(Cde\ Z1(s1+s2)\ \beta\ s1 + Cde\ Z1(s1+s2)\ \beta\ s2 + Cde\ Z2(s1+s2)\ \beta\ s1 + Cde\ Z2(s1+s2)\ \beta\ s2 + gm\ Z2(s1+s2)\ \beta + gm\ Z1(s1+s2) + gm\ Z2(s1+s2) + \beta\big) \tag{5.5}$$

Making the total zero

```
> compensation:=factor((h2[1](s1,s2)-h2[2](s1,s2))*gm);
```

$$compensation := -\big(INL2gm\ (Z1(s1+s2)\ \beta\ s1\ \tau + Z1(s1+s2)\ \beta\ s2\ \tau + \tau\ Z2(s1+s2)\ \beta\ s1 + \tau\ Z2(s1+s2)\ \beta\ s2 + Z2(s1+s2)\ \beta + Z1(s1+s2) + Z2(s1+s2))\ gm\big) \Big/ \big(Cde\ Z1(s1+s2)\ \beta\ s1 + Cde\ Z1(s1+s2)\ \beta\ s2 + Cde\ Z2(s1+s2)\ \beta\ s1 + Cde\ Z2(s1+s2)\ \beta\ s2 + gm\ Z2(s1+s2)\ \beta + gm\ Z1(s1+s2) + gm\ Z2(s1+s2) + \beta\big) \tag{6.1}$$

```
> compensation1:=factor(eval(compensation, [Cde=tau*gm]));
```

$$compensation1 := -\left(INL2gm\left(Z1(s1+s2)\,\beta\,s1\,\tau + Z1(s1+s2)\,\beta\,s2\,\tau + \tau\,Z2(s1+s2)\,\beta\,s1 + \tau\,Z2(s1+s2)\,\beta\,s2 + Z2(s1+s2)\,\beta + Z1(s1+s2) + Z2(s1+s2)\right)gm\right) \Big/ \left(Z1(s1+s2)\,\beta\,gm\,s1\,\tau + Z1(s1+s2)\,\beta\,gm\,s2\,\tau + Z2(s1+s2)\,\beta\,gm\,s1\,\tau + Z2(s1+s2)\,\beta\,gm\,s2\,\tau + gm\,Z2(s1+s2)\,\beta + gm\,Z1(s1+s2) + gm\,Z2(s1+s2) + \beta\right) \tag{6.2}$$

BIBLIOGRAPHY

[1] S. B. Patil, "An Ultra-Linear LNA for Base stations," Master's thesis, Delft University of Technology, November 2013.

[2] F. Ali and A. Gupta, *HEMTs and HBTs: Devices, Fabrication, and Circuits.* Artech House Publishers, 1991.

[3] D. A. Neamen, *Semiconductor physics and devices*, 4th ed. McGraw-Hill Higher Education, 2012.

[4] B. Gilbert, "The multi-tanh principle: a tutorial overview," *Solid-State Circuits, IEEE Journal of*, vol. 33, no. 1, pp. 2–17, Jan 1998.

[5] K. L. Fong and R. G. Meyer, "High-frequency nonlinearity analysis of common-emitter and differential-pair transconductance stages," *Solid-State Circuits, IEEE Journal of*, vol. 33, no. 4, pp. 548–555, Apr 1998.

[6] M. P. van der Heijden, "RF Amplifier Design Techniques for Linearity and Dynamic Range," Ph.D. dissertation, Delft University of Technology, 2005.

[7] S. A. Maas, *Nonlinear Microwave and RF Circuits*, 2nd ed. Artech House Publishers, 2003.

[8] C. J. M. Verhoeven, A. Van Staveren, G. L. E. Monna, M. H. L. Kouwenhoven, and E. Yildiz, *Structured Electronic Design.* Kluwer Academic Publishers, 2003.

[9] J. Vuolevi and T. Rahkonen, *Distortion in RF Power Amplifiers.* Artech House Publishers, 2003.

[10] J. Stewart, *Calculus: early transcendentals.* Cengage Learning, 2008.

[11] B. Razavi, *RF microelectronics.* Prentice Hall New Jersey, 1998, vol. 1.

[12] P. Wambacq and W. Sansen, *Distortion Analysis of Analog Integrated Circuits.* Kluwer Academic Publishers, 1998.

[13] L. C. N. de Vreede, "Large Signal Operation," Course notes Chapter 4, ET4294 Microwave Circuit Design, 2013.

[14] H. T. Friis, "Noise Figures of Radio Receivers," *Proceedings of the IRE*, vol. 32, no. 7, pp. 419–422, July 1944.

[15] L. C. N. de Vreede, H. C. de Graaff, J. A. Willemen, W. van Noort, R. Jos, L. E. Larson, J. W. Slotboom, and J. L. Tauritz, "Bipolar transistor epilayer design using the MAIDS mixed-level simulator," *Solid-State Circuits, IEEE Journal of*, vol. 34, no. 9, pp. 1331–1338, Sep 1999.

[16] *QUBiC4 Platform Design Manual*, 4th ed., NXP Semiconductors, November 2014.

[17] H. K. Gummel and H. C. Poon, "An integral charge control model of bipolar transistors," *Bell System Technical Journal, The*, vol. 49, no. 5, pp. 827–852, May 1970.

[18] G. Haines, J. Mataya, and S. Marshall, "IF amplifier using Cc compensated transistors," in *Solid-State Circuits Conference. Digest of Technical Papers. 1968 IEEE International*, vol. XI, Feb 1968, pp. 120–121.

[19] M. Spirito, M. J. Pelk, F. van Rijs, S. J. C. H. Theeuwen, D. Hartskeerl, and L. C. N. de Vreede, "Active Harmonic Load-Pull for On-Wafer Out-of-Band Device Linearity Optimization," *Microwave Theory and Techniques, IEEE Transactions on*, vol. 54, no. 12, pp. 4225–4236, Dec 2006.

[20] H. C. de Graaf and F. M. Klaassen, *Compact Transistor Modelling for Circuit Design.* Springer-Verlag Wien New York, 1990.

[21] R. G. Meyer and M. L. Stephens, "Distortion in variable-capacitance diodes," *Solid-State Circuits, IEEE Journal of*, vol. 10, no. 1, pp. 47–54, Feb 1975.

[22] K. Buisman, L. C. N. de Vreede, L. E. Larson, M. Spirito, A. Akhnoukh, T. L. M. Scholtes, and L. K. Nanver, "Distortion-free varactor diode topologies for RF adaptivity," in *Microwave Symposium Digest, 2005 IEEE MTT-S International*, June 2005, pp. 4 pp.–.

[23] R. van der Toorn, J. C. J. Paasschens, and W. J. Kloosterman, *The Mextram Bipolar Transistor Model*, Delft University of Technology, March 2008.

[24] J. R. Long, "Small-Signal Analysis of Amplifiers," Course notes ET4254 RF Integrated circuit design, 2013.

[25] J. D. Cressler, *Silicon Heterostructure Handbook*. CRC Press, 2006.

[26] J. W. M. Rogers and C. Plett, *Radio Frequency Integrated Circuit Design*, 2nd ed. Artech House Publishers, 2010.

[27] M. Willemsen, R. Pijper, D. Stephens, D. Klaassen, L. Tiemeijer, and A. Scholten, "IP3 modeling - MEXTRAM, status update," NXP Company confidential presentation, 2014.

[28] G. R. Wilson, "A monolithic junction FET-n-p-n operational amplifier," *Solid-State Circuits, IEEE Journal of*, vol. 3, no. 4, pp. 341–348, Dec 1968.

[29] B. A. Minch, "Low-Voltage Wilson Current Mirrors in CMOS," in *Circuits and Systems, 2007. ISCAS 2007. IEEE International Symposium on*, May 2007, pp. 2220–2223.

[30] B. L. Hart and R. W. J. Barker, "D.C. matching errors in the Wilson current source," *Electronics Letters*, vol. 12, no. 15, pp. 389–390, July 1976.

[31] I. Lattenberg and K. Vrba, "Low Input-Impedance Current-Mirror for High-Speed Data Communication," in *Networking, 2007. ICN '07. Sixth International Conference on*, April 2007, pp. 72–72.

[32] K. Bult and G. J. G. M. Geelen, "A fast-settling CMOS op amp for SC circuits with 90-dB DC gain," *Solid-State Circuits, IEEE Journal of*, vol. 25, no. 6, pp. 1379–1384, Dec 1990.

[33] *Advanced Design System (ADS) 2014 Documentation*, Agilent Technologies, 2014.